

INORGANIC CARBON DISTRIBUTION AND DYNAMICS IN THE MISSISSIPPI RIVER
PLUME ON THE NORTHERN GULF OF MEXICO

by

WEI-JEN HUANG

(Under the Direction of Wei-Jun Cai)

ABSTRACT

The continental shelf, especially the river-dominated shelf, plays an important role in the global carbon cycle. Thirteen cruises were conducted to measure sea surface salinity, temperature, and partial pressure of carbon dioxide ($p\text{CO}_2$) on the Louisiana (LA) shelf, a shelf great influenced by the Mississippi and Atchafalaya River System (MARS) from 2004 to 2010. The result showed that the LA shelf was a sink of atmospheric CO_2 , particularly strong on the eastern shelf, with a seasonal variation: strong in spring, weak during summer; shifting to a weak source in fall and back to near equilibrium in winter. In terms of salinity sub-divisions, the small low salinity region ($S = 0$ to 17) acted as a strong CO_2 source to the atmosphere, the wide middle salinity region ($17 < S < 33$) acted as a CO_2 sink, and middle-to-high salinity region ($33 < S < 35$) was near neutral to the atmosphere.

The MARS plume was subjected to local wind forcing, thus the $p\text{CO}_2$ spatial variation on the LA shelf was mostly dominated by this varied plume trajectory. The plume associated processes, including mixing, autotrophic and heterotrophic activities, and gas exchanges, further controlled the CO_2 dynamics in the plume. A widespread plume in March 2010 induced by northerly wind forcing provided a clear example illustrating that the MARS plume was affected

by wind forcing and transition from autotrophy to heterotrophy along the plume trajectory. The altered shelf circulation in July 2009 further demonstrated that not only surface water but also the bottom water conditions were affected, such as the extent of hypoxia (dissolved oxygen less than 2 mg L^{-1}). This study also revealed that the Mississippi riverine nitrate plus nitrite fluxes were positively correlated with the magnitude of the CO_2 sink in the Louisiana Bight, providing the first quantitative estimation of the relationship between the anthropogenic export nitrogen and air-sea CO_2 fluxes. To sum up, this dissertation describes the CO_2 dynamics under river-to-sea interaction and also air-to-sea interaction, i.e. the local wind forcing dominated the river plume trajectory while the transition from autotrophic to heterotrophic activities and the compensatory gas exchanges along the trajectory were largely responsible the CO_2 variation in the plume.

INDEX WORDS: carbon dioxide, CO_2 flux, $p\text{CO}_2$, nutrient, mixing, air-sea exchange, hypoxia, Gulf of Mexico, Mississippi River, alkalinity, dissolved inorganic carbon, DIC, net community production, eutrophication, river-to-sea, river plume, nitrogen flux, shelf circulation, anthropogenic export, biogeochemistry

INORGANIC CARBON DISTRIBUTION AND DYNAMICS IN THE MISSISSIPPI RIVER
PLUME ON THE NORTHERN GULF OF MEXICO

by

WEI-JEN HUANG

B.S., National Cheng Kung University, Taiwan, 2001

M.S., National Taiwan University, Taiwan, 2003

A Dissertation Submitted to the Graduate Faculty of The University of Georgia in Partial

Fulfillment of the Requirements for the Degree

DOCTOR OF PHILOSOPHY

ATHENS, GEORGIA

2013

© 2013

Wei-Jen Huang

All Rights Reserved

INORGANIC CARBON DISTRIBUTION AND DYNAMICS IN THE MISSISSIPPI RIVER
PLUME ON THE NORTHERN GULF OF MEXICO

by

WEI-JEN HUANG

Major Professor: Wei-Jun Cai

Committee: Steven E. Lohrenz
Charles S. Hopkinson
Patricia L. Yager
Christof Meile

Electronic Version Approved:

Maureen Grasso
Dean of the Graduate School
The University of Georgia
May 2013

DEDICATION

To my lovely wife,

Fang-Er Lin

ACKNOWLEDGEMENTS

First, I want to thank my major advisor, Dr. Wei-Jun Cai, who gave me abundant resources and freedom on research. I would also like to thank my committee members, who pushed me in the correct direction and gave me critical comments. Thank Dr. Renato Castelao for your valuable discussion.

Many thanks to Dr. Michael Murrell, Dr. Alan Shiller, and Dr. Steve DiMarco for your valuable ship time. Thank the crews on R/V Cape Hatteras and R/V Pelican for your supports during the cruises.

Thank Dr. Xinping Hu and all lab members in these years, especially Feizhou Chen, Li-Qing Jiang, Baoshan Chen, Qi Lin, Liang Xue, and Chenhua Han for their help during the cruises and during experiment. I also would like to thank Eric King for your walking.

Special thanks to Dr. Yongchen Wang and Guirong Han, who supported me in various aspects. Finally, I would like to thank my father and mother for their support in these years.

TABLE OF CONTENTS

	Page
ACKNOWLEDGEMENTS	v
LIST OF TABLES	viii
LIST OF FIGURES	ix
CHAPTER	
1 INTRODUCTION AND LITERATURE REVIEW	1
2 EFFECTS OF A WIND-DRIVEN CROSS-SHELF LARGE RIVER PLUME ON BIOLOGICAL PRODUCTION AND CO ₂ UPTAKE ON THE GULF OF MEXICO DURING SPRING.....	14
3 IMPACTS OF WEATHER EVENTS ON SHELF CIRCULATION AND CO ₂ AND O ₂ DYNAMICS ON THE LOUISIAN SHELF DURING SUMMER	43
4 THE CARBON DIOXIDE (CO ₂) SYSTEM IN THE MISSISSIPPI RIVER DOMINATED CONTINENTAL SHELF, NORTHERN GULF OF MEXICO—I: DISTRIBUTION AND AIR-SEA FLUX.....	77
5 THE CARBON DIOXIDE (CO ₂) SYSTEM IN THE MISSISSIPPI RIVER DOMINATED CONTINENTAL SHELF, NORTHERN GULF OF MEXICO—II: THE DYNAMICS OF SURFACE CO ₂ AND OXYGEN.....	127
6 SUMMARY	166

APPENDIX

A ASSESSMENT OF SAMPLE STORAGE TECHNIQUES FOR TOTAL
ALKALINITY AND DISSOLVED INORGANIC CARBON IN SEWATER.....173

LIST OF TABLES

	Page
Table 2.1: Plume and non-plume areas and air-sea CO ₂ fluxes in April 2009 and March 2010 ...	33
Table 2.2: The area-averaged mole fraction concentration of CO ₂ in the dried sample gas flow for surface seawater and atmosphere in the survey area	34
Table 3.1: Average <i>p</i> CO ₂ (μatm) and air-sea CO ₂ fluxes in the reference area and western and eastern areas	66
Table 4.1: Summary of survey cruises.....	107
Table 4.2: Surface water <i>p</i> CO ₂ values from bays along the coast of the LA shelf and from the lower Mississippi River	108
Table 4.3: Seasonal air-sea CO ₂ flux in the northern Gulf of Mexico.....	109
Table 4.4: Average CO ₂ flux, temperature, <i>p</i> CO ₂ , and area in the LA shelf of each cruise.....	110
Table 4.5: End-members for the mixing model	111
Table 5.1: Summary of the cruises information.....	151
Table 5.2: Initial conditions for each simulation	152
Table A.1: Summary of the five types of containers	188
Table A.2: Mean ΔTA for each type of bottle over time in each experiment.....	189
Table A.3: Mean ΔDIC concentration and its standard deviation (SD) for each type of containers over 148 day.....	190

LIST OF FIGURES

	Page
Figure 2.1: SeaWiFS Chl-a distributions on the Gulf of Mexico under normal conditions.	35
Figure 2.2: Spatial and temporal wind patterns in the Gulf of Mexico	36
Figure 2.3: The MARS monthly average discharge and standard deviation from water year 1998 to 2010	37
Figure 2.4: SeaWiFS Chl-a distributions in 2010.....	38
Figure 2.5: Anomalies of (A) SeaWiFS Chl-a concentration and (B) surface temperature from northern to southern Gulf of Mexico	39
Figure 2.6: Distribution of in situ (A, B) SSS and (C, D) $p\text{CO}_2$	40
Figure 2.7: The correlation between air-sea CO_2 flux and SeaWiFS Chl-a concentration to the west of 91.2°W	41
Figure 2.8: A conceptual model illustrates the differing plume dynamics between normal spring conditions and March 2010.....	42
Figure 3.1: Conceptual shelf circulations	67
Figure 3.2: Distribution of surface seawater salinity and satellite monthly Chl-a.....	69
Figure 3.3: Temperature to salinity diagram during August 2007 and July 2009	70
Figure 3.4: Distributions of sea surface $p\text{CO}_2$	71
Figure 3.5: Spatial distributions of bottom-water DO (mg L^{-1}) and DIC (μM) concentrations on the Louisiana Shelf	72
Figure 3.6: Distributions of HYCOM simulated surface currents and wind forcing.....	73

Figure 3.7: Conceptual shelf circulation in July 2009	74
Figure 3.8: Mixing process (blue arrows) and respiration (red arrows) dominated the variations of DO and DIC concentrations in August 2007	75
Figure 3.9: Mixing process (blue arrows) and respiration (red arrows) dominated the variations of DO and DIC concentrations in July 2009	76
Figure 4.1: The survey area	112
Figure 4.2: The variations of monthly freshwater discharge (black line), and nitrate plus nitrite (NN) fluxes (red line) from the MARS from 2004 to May 2010	113
Figure 4.3: Distributions of sea surface salinity along cruise tracks in each cruise	114
Figure 4.4: Distributions of sea surface temperature in each cruise.	115
Figure 4.5: Distributions of sea surface $p\text{CO}_2$	116
Figure 4.6: Cross-shelf gradients of sea surface $p\text{CO}_2$	117
Figure 4.7: Relationship between the average of areal-integrated $p\text{CO}_2$ values and areal- integrated salinity unity.....	118
Figure 4.8: Relationships between sea surface $p\text{CO}_2$ and its temperature.....	120
Figure 4.9: Seasonal variations of the average of areal-averaged values in the reference area...	121
Figure 4.10: Conceptual diagrams for two unusual MARS plumes	122
Figure 4.11: The correlation between air-sea CO_2 fluxes and riverine NN fluxes on the LA Bight	123
Figure 4.12: The correlation between coverage of enhanced PP and riverine NN fluxes on the LA shelf.....	124
Figure 4.13: The relationship between the lag-time to the riverine NN fluxes and the coefficient of determination (R^2)	125

Figure 4.14: The conceptual model. Blue dash lines separate the plume into four salinity divisions: 0-17, 17-25, 25-33, and 33-35	126
Figure 5.1: Site maps	153
Figure 5.2: The distribution of sea surface dissolved oxygen (DO).....	154
Figure 5.3: $p\text{CO}_2$ -to-DO relationship for low salinity ($S < 17$) waters.....	155
Figure 5.4: $p\text{CO}_2$ -to-DO relationship for all waters.....	156
Figure 5.5: $p\text{CO}_2$ -to-DO relationship for high salinity ($S > 35$) waters.....	157
Figure 5.6: Distributions of Quadrants of DO% and $p\text{CO}_2\%$	158
Figure 5.7: Theoretical $p\text{CO}_2$ -to-DO relationship under plume processes.	159
Figure 5.8: $p\text{CO}_2$ -to-DO relationship in March 2010	160
Figure 5.9: $p\text{CO}_2$ -to-DO relationship in July 2009.....	161
Figure 5.10: $p\text{CO}_2$ -to-DO relationship in September 2006	162
Figure 5.11: $p\text{CO}_2$ -to-Chl-a relationship during 2006 and 2007	163
Figure 5.12: $p\text{CO}_2$ -to-DO relationship in November 2009.....	164
Figure 5.13: $p\text{CO}_2$ -to-DO relationship in January 2009	165
Figure 6.1: Synthesize conceptual model for the interactions between effects of river-to-sea associated processes and effects of air-to-sea related processes.....	172
Figure A.1: Summary of measurements for TA and DIC during each experiment along the timeline	191
Figure A.2: ΔTA variations for the borosilicate glass bottle samples in TA Exp. 1, 2, and 3 over 95 days	192
Figure A.3: ΔTA variations for the soda-lime glass bottles used in TA Exp. 1 and 2 over 95 days	193

Figure A.4: ΔTA variation for the PP or HDPE bottles in TA Exp. 3 over 47 days194

Figure A.5: ΔDIC variations for borosilicate glass bottles, soda-lime glass bottles, and the small
volume borosilicate glass vials over 148 days195

CHAPTER 1

INTRODUCTION AND LITERATURE REVIEW

1. The role of continental shelves in the air-sea CO₂ fluxes

Ocean takes up approximately 50% of the carbon dioxide (CO₂) released through the burning of fossil fuel and deforestation, and acts as an important sink of atmospheric CO₂ (Sabine et al. 2004). This increasing atmospheric CO₂ thus leads to reducing oceanic pH, a process called ocean acidification (Orr et al. 2005). The continental shelf acts as a critical region for this atmosphere-ocean interaction because it accounts for 17-30% of the net annual CO₂ sink of global ocean and 33% of oceanic net ecosystem production even though it only covers about 7% of the seafloor in area (Cai 2011; Borges 2011; Chen and Borges, 2009; Ducklow and McCallister, 2005). Though quickly improved in the past decade, the role that the continental shelf plays in the global ocean carbon cycle remain imprecise and poorly constrained (Cai 2011; Ducklow and McCallister 2005). This is because the spatial and temporal heterogeneity of air-sea CO₂ fluxes on continental shelves was usually large compared to that of the open ocean (Takahashi et al. 2009) but the associated data were not abundant enough to cover these variations, especially in winter. This is particularly true for the river-dominated continental shelf for such shelves usually receive large freshwater and nutrient discharge, which is often an important factor dominating the variations of partial pressure of CO₂ ($p\text{CO}_2$) values in its plume and surrounding areas through biological activities (Cai 2003; Cooley et al. 2007; Kortzinger 2003; Terson et al. 2000; Tseng et al. 2011; Tsunogai et al. 1997; Zhai and Dai 2009; Zhai et al.

2007). This effect from riverine exports has been suggested to be particularly strong when eutrophication was observed in these large river plumes (Borges and Gypens 2010; Cai et al. 2011; Chou et al. 2011). Moreover, these $p\text{CO}_2$ variations are usually large and are often difficult to quantify as river-dominated shelves are characterized by intense mixing processes and complex coastal currents, which are highly related to local wind forcing (Lentz and Fewings 2012). As such, a better understanding of air-sea CO_2 fluxes in river-dominated continental shelves is needed.

Previous studies have shown that large river plumes strongly influence air-sea CO_2 exchange with enhanced biological productivity contributing to a net uptake of CO_2 in river-influenced regions (Cooley and Yager 2006; Lohrenz et al. 2010; Tseng et al. 2011). The Amazon River plume has been associated with reduced surface $p\text{CO}_2$ even though the Western North Atlantic Ocean has oversaturated $p\text{CO}_2$ values with respect to the atmosphere (Cooley and Yager 2006; Takahashi et al. 2002). The plume impacts on CO_2 fluxes in surrounding marginal seas could be more pronounced for large-river plumes located in semi-enclosed marginal seas due to the relatively constrained nature of the receiving waters, such as the Mississippi River plume, the Changjiang River plume, and the Pearl River plume (Tseng et al. 2011; Tsunogai et al. 1999; Zhai and Dai 2009).

In addition to the estimation of air-sea CO_2 fluxes, previous studies also discussed the dynamics of the CO_2 system by considering the effect of air-sea CO_2 exchanges on the water carbonate system along with air-sea oxygen exchanges (Carrillo et al. 2004; Degrandpre et al. 1998; Zhai et al. 2009). Degrandpre et al. (1998) have considered the fact of a more rapid gas exchange rate of DO than CO_2 , and suggested these characteristics have a significant effect on the $p\text{CO}_2$ and DO relationship. Carrillo et al. (2004) have demonstrated the effect of air-sea gas exchanges on sea

surface waters during equilibration through this characteristics on the $p\text{CO}_2$ and DO diagram, and they also discussed other influences from photosynthesis/respiration and cooling/heating separately. In addition, Zhai et al. (2009) have examined the biological effects on surface $p\text{CO}_2$ and DO relationship by coupling through the Redfield ratio (Redfield 1958) and the Revelle factor in a coastal plume and upwelling system. To sum up, the surface water $p\text{CO}_2$ and DO values could be affected by river-ocean mixing and biological activities and be further compensated by air-sea gas exchanges to equilibrium. This alteration-compensation process can be observed through the $p\text{CO}_2$ and DO diagram due to a more rapid gas exchange rate of DO relative to CO_2 . However, though DeGrandpre et al. (1998) have touched upon the effect of mixing on $p\text{CO}_2$ and DO, mixing effects are not further discussed in other related studies but are important in a river-dominated shelf.

2. The Mississippi and Atchafalaya River System

The Mississippi and Atchafalaya River system (MARS) is one of the world's largest rivers ranking 4th in length (6300 km) and 6th in freshwater discharge ($18400 \text{ m}^3 \text{ s}^{-1}$) (Milliman and Meade 1983). The MARS also delivers a mean annual nitrogen flux of $1.5 \times 10^{12} \text{ g}$ (or Tg) with 61% as nitrate N (Goolsby et al. 2000) and an annual mean of 13-17 Tg bicarbonate to the northern Gulf of Mexico (Raymond et al. 2008) and thus is the major freshwater and nutrient source for the Louisiana (LA) shelf (Cochrane and Kelly 1986; Rabalais et al. 1996). This riverine nitrogen flux has increased significantly from the 1950s to 1990s through evidence from paleoindicators of eutrophication and oxygen condition in the sediments cores (Rabalais et al. 2007).

In previous studies, surface $p\text{CO}_2$ variation has been implied to be related to the riverine nitrogen fluxes on the LA Bight. The riverine nitrogen flux stimulates high rates of primary production (PP) (Dagg et al. 2007; Lohrenz et al. 1990; Rabalais et al. 2002), and has also suggested to induce a strong uptake of atmospheric CO_2 at the sea surface in a limited area of the Mississippi river plume (Cai 2003; Green et al. 2008; John et al. 2007). Additionally, those measured sea surface $p\text{CO}_2$ values have showed to be under-saturated with respect to atmospheric CO_2 with a cross-shelf $p\text{CO}_2$ gradient near the Mississippi River mouth (Lohrenz and Cai 2006; Lohrenz et al. 2010). This anthropogenic riverine nitrogen export and its associated eutrophication have also been known to be largely responsible for the bottom water hypoxia (dissolved oxygen $[\text{DO}] < 2 \text{ mg O L}^{-1}$) on the LA shelf during summer (Rabalais et al. 2010; Rabouille et al. 2008). However, this conceptual relationship between riverine nitrogen fluxes and air-sea CO_2 fluxes on the LA shelf is still not quantified and examined by in-situ measurements.

In addition to biological effects, the shelf circulation could further complicate the spatial distribution of $p\text{CO}_2$ on the LA shelf because the trajectory of the MARS plume has been known to be related to wind forcing (Cochrane and Kelly 1986; Schiller et al. 2011; Walker 1996; Walker et al. 1996; Walker et al. 2005; Zhang et al. 2012) and upwelling favorable winds can alter the trajectory of river plumes leading to transport of low salinity waters offshore (Castelao et al. 2008; Fong and Geyer 2001; Lentz 2004). The majority of MARS plume is generally confined alongshore to the Louisiana-Texas shelf, but has also been observed to extend to the Mississippi-Alabama-Florida shelf regions in some cases (Castillo et al. 2001; Morey et al. 2003b) and to the west Florida shelf and even beyond (Ortner et al. 1995). The trajectory of this plume shows seasonal variations on the LA shelf: the predominant surface current is westward

driven by northerly winds from autumn to spring; southerly winds tend to reverse the plume circulation in summer and to promote eastward transport of plume water (Morey et al. 2003a; Walker et al. 2005). Shelf circulations have been suggested to affect the distribution of surface PP on the LA shelf (Chen et al. 2000). But the variation of this plume trajectory and $p\text{CO}_2$ variation on the LA shelf is still not clear.

3. The purpose and the structure of the dissertation

The purpose of this study is to survey the temporal and spatial $p\text{CO}_2$ variations on the LA shelf, and to discuss the relationship between “river-to-sea interaction” and “air-sea CO_2 exchange” on this river-dominated continental shelf. We first start from discussing the effect of local wind forcing on the location of river plume (Chapters 2 and 3); and show $p\text{CO}_2$ variations and its correlation with the river nitrogen fluxes in chapter 4; and finally demonstrate the compensatory effects of air-sea gas exchanges on these river-to-sea associated processes (Chapter 5). Detailed structures for each chapter are as follow:

Chapter 2 describes the distribution of the MARS plume under a northerly wind forcing, which resulted from extreme weather conditions in March 2010 in North America. We use a combination of *in situ* sea surface salinity (SSS) and surface $p\text{CO}_2$ data as well as satellite Chl-a data to demonstrate the plume was extended southward across 28°N to pelagic Gulf of Mexico. A systematic analysis of remote sensing observations of the plume extent was also applied for the climatological mean condition. The widespread plume was compared to this mean condition to evaluate its effect on air-sea CO_2 flux in pelagic Gulf of Mexico. This chapter displays important information contributing to the knowledge of the interactions between the atmosphere

and the ocean; and demonstrates an interesting example of the response of coastal ocean biogeochemistry, such as air-sea CO₂ exchange, to extreme weather events.

Chapter 3 describes how the MARS plume distribution and its biogeochemical impact on the water column CO₂ properties and dissolved oxygen (DO) distributions under an unusual shelf circulation. This unusual shelf circulation in July 2009 was compared to the circulation in August 2007, which was close to the mean condition during the past 10 years, to show the biogeochemical impacts of the shelf circulation on variation of CO₂ and DO concentrations in the LA shelf. Furthermore, the relationship between dissolved inorganic carbon (DIC) and DO in the bottom water is applied to identify the distinct water masses, and its slopes on the Louisiana shelf is also discussed to demonstrate the importance of biological activities in these shelf bottom waters.

In Chapter 4, first, I present a complete summary of the surface water *p*CO₂ distribution and quantified air-sea CO₂ fluxes over the LA shelf. I also summarize the distribution of *p*CO₂ values and air-sea CO₂ fluxes along the salinity sub-regions in this river plume, and discuss the spatial distribution of *p*CO₂ affected by the variation of river plume. Second, the relationship between riverine nitrogen fluxes and air-sea CO₂ fluxes is discussed, and the response time of the surface air-sea CO₂ fluxes to the riverine nitrogen flux on the LA Bight and on the enhanced primary production area (region of low *p*CO₂ values < 300 μatm) are systematically determined, respectively. Finally, I provide an inorganic carbon budget and conceptual model to synthesize our understanding of the interactions between the river export and the estimates of net CO₂ flux in the MARS plume.

To show the dynamic of CO₂ in the MARS plume, Chapter 5 applies a model to describe the simultaneous relationship between sea surface *p*CO₂ and DO relationships from ten cruises

over the LA shelf from four seasons. I consider combination effects of the transition of net ecosystem production (NCP) from autotrophy to heterotrophy and air-sea gas exchanges on the CO₂ system and DO concentration, and simulate their dynamic relationship. This modeled relationship is compared with our measurements to discuss the seasonal and spatial effects of the controlling factors on *p*CO₂ variations over the LA shelf. The methods to measure these DIC concentrations in Chapter 3, and total alkalinity and DIC values as river and seawater end-members for the simulations in Chapter 4 and 5 are described in the Appendix A.

To synthesize the characteristics of quantity and dynamics of *p*CO₂ variations in the LA shelf, Chapter 6 combines a conceptual model to integrate the various concepts and conclusion derived in the previous chapters. In this chapter, I conclude how several processes associated with river-ocean interaction would affect sea surface *p*CO₂ variation and air-sea CO₂ exchanges, and further conclude how the weather affect the river plume and its associated biogeochemical processes.

References

- Borges, A. V. 2011. Present Day Carbon Dioxide Fluxes in the Coastal Ocean and Possible Feedbacks Under Global Change Oceans and the Atmospheric Carbon Content, p. 47-77. *In* P. Duarte and J. M. Santana-Casiano [eds.]. Springer Netherlands.
- Borges, A. V., and N. Gypens. 2010. Carbonate chemistry in the coastal zone responds more strongly to eutrophication than to ocean acidification. *Limnology and Oceanography* **55**: 346-353.
- Cai, W.-J. 2003. Riverine inorganic carbon flux and rate of biological uptake in the Mississippi River plume. *Geophysical Research Letters* **30**: 1032.
- . 2011. Estuarine and Coastal Ocean Carbon Paradox: CO₂ Sinks or Sites of Terrestrial Carbon Incineration? *Annual Review of Marine Science* **3**: 123-145.
- Cai, W.-J. and others 2011. Acidification of subsurface coastal waters enhanced by eutrophication. *Nature Geosci* **4**: 766-770.
- Carrillo, C. J., R. C. Smith, and D. M. Karl. 2004. Processes regulating oxygen and carbon dioxide in surface waters west of the Antarctic Peninsula. *Marine Chemistry* **84**: 161-179.
- Castelao, R., O. Schofield, S. Glenn, R. Chant, and J. Kohut. 2008. Cross-shelf transport of freshwater on the New Jersey shelf. *J. Geophys. Res.* **113**: C07017.
- Castillo, D. and others 2001. Multispectral in situ measurements of organic matter and chlorophyll fluorescence in seawater: Documenting the intrusion of the Mississippi River Plume in the West Florida Shelf. *Limnology and Oceanography* **46**: 1836-1843.
- Chen, C.-T. A., and A. V. Borges. 2009. Reconciling opposing views on carbon cycling in the coastal ocean: Continental shelves as sinks and near-shore ecosystems as sources of atmospheric CO₂. *Deep Sea Research Part II: Topical Studies in Oceanography* **56**: 578-590.
- Chen, X., S. E. Lohrenz, and D. A. Wiesenburg. 2000. Distribution and controlling mechanisms of primary production on the Louisiana-Texas continental shelf. *Journal of Marine Systems* **25**: 179-207.

- Chou, W.-C. and others 2011. The carbonate system in the East China Sea in winter. *Marine Chemistry* **123**: 44-55.
- Cochrane, J. D., and F. J. Kelly. 1986. Low-frequency circulation on the Texas-Louisiana continental shelf. *Journal of geophysical research. Part C, Oceans and atmospheres* **91(9)**: 10645-10659.
- Cooley, S. R., V. J. Coles, A. Subramaniam, and P. L. Yager. 2007. Seasonal variations in the Amazon plume-related atmospheric carbon sink. *Global Biogeochem. Cycles* **21**: GB3014.
- Cooley, S. R., and P. L. Yager. 2006. Physical and biological contributions to the western tropical North Atlantic Ocean carbon sink formed by the Amazon River plume. *Journal of Geophysical Research* **111**: C08018.
- Dagg, M. J., J. Ammerman, R. Amon, W. Gardner, R. Green, and S. Lohrenz. 2007. A review of water column processes influencing hypoxia in the northern Gulf of Mexico. *Estuaries and Coasts* **30**: 735-752.
- Degrandpre, M. D., T. R. Hammar, and C. D. Wirick. 1998. Short-term $p\text{CO}_2$ and O_2 dynamics in California coastal waters. *Deep Sea Research Part II: Topical Studies in Oceanography* **45**: 1557-1575.
- Ducklow, H. W., and S. L. McCallister. 2005. The biogeochemistry of carbon dioxide in the coastal oceans, p. 269-315. *In* A. R. Robinson and K. H. Brink [eds.], *The global coastal ocean. Multiscale interdisciplinary processes. The sea: ideas and observations on progress in the study of the seas*. Harvard University Press.
- Fong, D. A., and W. R. Geyer. 2001. Response of a river plume during an upwelling favorable wind event. *J. Geophys. Res.* **106**: 1067-1084.
- Goolsby, D. A., W. A. Battaglin, B. T. Aulenbach, and R. P. Hooper. 2000. Nitrogen flux and sources in the Mississippi River Basin. *The Science of The Total Environment* **248**: 75-86.
- Green, R. E., G. A. Breed, M. J. Dagg, and S. E. Lohrenz. 2008. Modeling the response of primary production and sedimentation to variable nitrate loading in the Mississippi River plume. *Continental Shelf Research* **28**: 1451-1465.

- John, D. E. and others 2007. Phytoplankton carbon fixation gene (RuBisCO) transcripts and air-sea CO₂ flux in the Mississippi River plume. *ISME J* **1**: 517-531.
- Kortzinger, A. 2003. A significant CO₂ sink in the tropical Atlantic Ocean associated with the Amazon River plume. *Geophysical Research Letters* **30**: 4.
- Lentz, S. 2004. The response of buoyant coastal plumes to upwelling-favorable winds. *J. Phys. Oceanogr.* **34**: 2458-2469.
- Lentz, S. J., and M. R. Fewings. 2012. The wind- and wave-driven inner-shelf circulation. *Annu. Rev. Mar. Sci.* **4**: 317-343.
- Lohrenz, S. E., and W.-J. Cai. 2006. Satellite ocean color assessment of air-sea fluxes of CO₂ in a river-dominated coastal margin. *Geophysical Research Letters* **33**: L01601.
- Lohrenz, S. E., W.-J. Cai, F. Chen, X. Chen, and M. Tuel. 2010. Seasonal variability in air-sea fluxes of CO₂ in a river-influenced coastal margin. *J. Geophys. Res.* **115**: C10034.
- Lohrenz, S. E., M. J. Dagg, and T. E. Whitledge. 1990. Enhanced primary production at the plume/oceanic interface of the Mississippi River. *Continental Shelf Research* **10**: 639-664.
- Milliman, J. D., and R. H. Meade. 1983. World-Wide Delivery of River Sediment to the Oceans. *The Journal of Geology* **91**: 1-21.
- Morey, S. L., P. J. Martin, J. J. O'brien, A. A. Wallcraft, and J. Zavala-Hidalgo. 2003a. Export pathways for river discharged fresh water in the northern Gulf of Mexico. *Journal of Geophysical Research* **108**: 3303.
- Morey, S. L., W. W. Schroeder, J. J. O'brien, and J. Zavala-Hidalgo. 2003b. The annual cycle of riverine influence in the eastern Gulf of Mexico basin. *Geophys. Res. Lett.* **30**: 1867.
- Orr, J. C., Fabry, V. J., Aumont, O., Bopp, L., Doney, S. C., Feely, R. A., Gnanadesikan, A., Gruber, N., Ishida, A., Joos, F., Key, R. M., Lindsay, K., Maier-Reimer, E., Matear, R., Monfray, P., Mouchet, A., Najjar, R. G., Plattner, G.-K., Rodgers, K. B., Sabine, C. L., Sarmiento, J. L., Schlitzer, R., Slater, R. D., Totterdell, I. J., Weirig, M.-F., Yamanaka, Y., and Yool, A.:

- Anthropogenic ocean acidification over the twenty-first century and its impact on calcifying organisms, *Nature*, **437**, 681-686, 2005.
- Ortner, P. B. and others 1995. Mississippi River flood waters that reached the Gulf Stream. *J. Geophys. Res.* **100(C7)**: 13,595-513,601.
- Rabalais, N. N., R. J. Diaz, L. A. Levin, R. E. Turner, D. Gilbert, and J. Zhang. 2010. Dynamics and distribution of natural and human-caused hypoxia. *Biogeosciences* **7**: 585-619.
- Rabalais, N. N., R. E. Turner, Q. Dortch, D. Justic, V. Bierman, and W. Wiseman. 2002. Nutrient-enhanced productivity in the northern Gulf of Mexico: past, present and future. *Hydrobiologia* **475-476**: 39-63.
- Rabalais, N. N., R. E. Turner, B. K. S. Gupta, E. Platon, and M. L. Parsons. 2007. Sediments tell the history of eutrophication and hypoxia in the northern Gulf of Mexico. *Ecological Applications* **17**: S129-S143.
- Rabalais, N. N., R. E. Turner, D. Justic, Q. Dortch, W. Wiseman, and B. Sen Gupta. 1996. Nutrient changes in the Mississippi River and system responses on the adjacent continental shelf. *Estuaries and Coasts* **19**: 386-407.
- Rabouille, C. and others 2008. Comparison of hypoxia among four river-dominated ocean margins: The Changjiang (Yangtze), Mississippi, Pearl, and Rhône rivers. *Continental Shelf Research* **28**: 1527-1537.
- Raymond, P. A., N.-H. Oh, R. E. Turner, and W. Broussard. 2008. Anthropogenically enhanced fluxes of water and carbon from the Mississippi River. *Nature* **451**: 449-452.
- Redfield, A. C. 1958. The biological control of chemical factors in the environment. *American Scientist* **46**: 205-221.
- Sabine, C. L., Feely, R. A., Gruber, N., Key, R. M., Lee, K., Bullister, J. L., Wanninkhof, R., Wong, C. S., Wallace, D. W. R., Tilbrook, B., Millero, F. J., Peng, T.-H., Kozyr, A., Ono, T., and Rios, A. F.: The Oceanic Sink for Anthropogenic CO₂, *Science*, **305**, 367-371, 10.1126/science.1097403, 2004.

- Schiller, R. V., V. H. Kourafalou, P. Hogan, and N. D. Walker. 2011. The dynamics of the Mississippi River plume: Impact of topography, wind and offshore forcing on the fate of plume waters. *J. Geophys. Res.* **116**: C06029.
- Takahashi, T. and others 2002. Global sea-air CO₂ flux based on climatological surface ocean pCO₂, and seasonal biological and temperature effects. *Deep Sea Research Part II: Topical Studies in Oceanography* **49**: 1601-1622.
- Takahashi, T. and others 2009. Climatological mean and decadal change in surface ocean pCO₂, and net sea-air CO₂ flux over the global oceans. *Deep Sea Research Part II: Topical Studies in Oceanography* **56**: 554-577.
- Ternon, J. F., C. Oudot, A. Dessier, and D. Diverres. 2000. A seasonal tropical sink for atmospheric CO₂ in the Atlantic ocean: the role of the Amazon River discharge. *Marine Chemistry* **68**: 183-201.
- Tseng, C.-M., K. K. Liu, G. C. Gong, P. Y. Shen, and W. J. Cai. 2011. CO₂ uptake in the East China Sea relying on Changjiang runoff is prone to change. *Geophys. Res. Lett.* **38**: L24609.
- Tsunogai, S., S. Watanabe, J. Nakamura, T. Ono, and T. Sato. 1997. A preliminary study of carbon system in the East China Sea. *Journal of Oceanography* **53**: 9-17.
- Tsunogai, S., S. Watanabe, and T. Sato. 1999. Is there a "continental shelf pump" for the absorption of atmospheric CO₂? *Tellus Series B-Chemical and Physical Meteorology* **51**: 701-712.
- Walker, N. D. 1996. Satellite assessment of Mississippi River plume variability: Causes and predictability. *Remote Sensing of Environment* **58**: 21-35.
- Walker, N. D., O. K. Huh, L. J. Rouse Jr., and S. P. Murray. 1996. Evolution and structure of a coastal squirt off the Mississippi River delta: Northern Gulf of Mexico. *J. Geophys. Res.* **101**: 20643-20655.
- Walker, N. D., W. J. Wiseman, L. J. Rouse, and A. Babin. 2005. Effects of river discharge, wind stress, and slope eddies on circulation and the satellite-observed structure of the Mississippi River plume. *Journal of Coastal Research* **21**: 1228-1244.

- Zhai, W., and M. Dai. 2009. On the seasonal variation of air - sea CO₂ fluxes in the outer Changjiang (Yangtze River) Estuary, East China Sea. *Marine Chemistry* **117**: 2-10.
- Zhai, W., M. Dai, and W.-J. Cai. 2009. Coupling of surface *p*CO₂ and dissolved oxygen in the northern South China Sea: impacts of contrasting coastal processes. *Biogeosciences* **6**: 2589-2598.
- Zhai, W., M. Dai, and X. Guo. 2007. Carbonate system and CO₂ degassing fluxes in the inner estuary of Changjiang (Yangtze) River, China. *Marine Chemistry* **107**: 342-356.
- Zhang, X., R. D. Hetland, M. Marta-Almeida, and S. F. Dimarco. 2012. A numerical investigation of the Mississippi and Atchafalaya freshwater transport, filling and flushing times on the Texas-Louisiana Shelf. *J. Geophys. Res.* **117**: C11009.

CHAPTER 2

EFFECTS OF A WIND-DRIVEN CROSS-SHELF LARGE RIVER PLUME ON
BIOLOGICAL PRODUCTION AND CO₂ UPTAKE ON THE GULF OF MEXICO DURING
SPRING¹

¹Wei-Jen Huang, Wei-Jun Cai, Renato M. Castelao, Yongchen Wang, and Steven E. Lohrenz.
Submitted to *Limnology and Oceanography*, 9/17/2012

Abstract

The plume of Mississippi and Atchafalaya River system (MARS) is normally confined to the continental shelf and extends westward. During March 2010, while weather in North America was dominated by unusually low temperatures and winter storms in conjunction with large low-pressure systems, we observed an unusually broad extension of the MARS plume. Winds favorable for offshore transport along with high freshwater discharge contributed to a widespread MARS plume, which was statistically different from those normally occurring in spring. A strong relationship was observed between the location of this widespread plume and a reduced partial pressure of carbon dioxide (P_{CO_2}) and elevated satellite-derived chlorophyll *a*. Furthermore, P_{CO_2} in the plume was reduced by 6.3 Pa (62 ppm) in March 2010 in contrast to a reduction of only 2.4 Pa (24 ppm) in April 2009, thus exhibiting a greater CO_2 uptake capacity in March 2010. This wide plume also covered at least twice the area and was a stronger CO_2 sink by a factor of five when compared to more typical plume conditions in April 2009. Extending across the Louisiana shelf to the pelagic ocean, this widespread MARS plume encompassed regions that would normally exhibit nearly net zero air-sea CO_2 exchange, and resulted instead in a strong net sink for atmospheric CO_2 . Our findings demonstrate that regional weather-associated variations in wind forcing and river discharge may be important in influencing air-sea CO_2 fluxes in marginal sea environments.

1. Introduction

Large river plumes are known to influence air-sea exchange of carbon dioxide (CO_2) strongly with enhanced biological productivity contributing to a net uptake of CO_2 in river-influenced regions (Cooley and Yager 2006; Lohrenz et al. 2010; Tseng et al. 2011). Consequently, large river plumes can be expected to affect air-sea CO_2 exchange in their open ocean surroundings depending on their spatial variability. For example, the Amazon River plume, which extends into the Western North Atlantic Ocean, has been associated with reduced surface partial pressure of CO_2 (P_{CO_2}) even though the surrounding ocean areas are CO_2 sources (Takahashi et al. 2002; Cooley and Yager 2006). For large-river systems emptying into semi-enclosed marginal seas, such as the Mississippi River, the Changjiang River, and the Pearl River, river plume influences on CO_2 fluxes in surrounding waters may be more pronounced due to the relatively constrained nature of the receiving waters. However, to our knowledge, the influence of wind-driven variations on large river plumes and its relationship to air-sea exchange of CO_2 has not been reported.

The Mississippi River basin is the largest freshwater basin in the North America and also serves as the major freshwater and nutrient source for the Gulf of Mexico (Cochrane and Kelly 1986; Rabalais et al. 1996). Three successive large low-pressure systems were observed to cross North America in March 2010 when the atmospheric temperature in North America during early 2010 was unusually low (Lecomte 2011). These winter storms and low-pressure systems resulted in several decadal or centennial record-setting snowfall events in northeastern and southeastern America (Lecomte 2011; Robinson 2011). The unusual weather had dramatic effects on precipitation and run-off in the Mississippi River basin. The trajectory of the Mississippi and Atchafalaya River System (MARS) plume is subject to wind forcing (Cochrane and Kelly 1986;

Walker et al. 2005; Zhang et al. 2012) and is generally confined along the shelf regions; for example, on the Louisiana-Texas shelf, on the Mississippi-Alabama-Florida shelf, to the west Florida shelf in some cases (Castillo et al. 2001; Zhang et al. 2012). Upwelling favorable winds can alter the trajectory of river plumes leading to transport of low salinity waters offshore (Fong and Geyer 2001; Lentz 2004; Castelao et al. 2008). Thus, the unusual weather in March 2010 provided a unique opportunity to study physical and biogeochemical responses of the MARS plume and the surface Gulf of Mexico to these winter storms.

In this study, we examine the MARS plume response to extreme weather conditions in North America. The MARS plume in March 2010 was documented using a combination of in situ sea surface salinity (SSS) and surface P_{CO_2} data as well as satellite chlorophyll *a* (Chl *a*) data. Using these data, we assess the regional effect of this widespread cross-shelf plume on air-sea CO_2 flux in pelagic Gulf of Mexico waters and compare it to climatological mean conditions determined from a systematic analysis of remote sensing observations of wind forcing and plume extent. This study provides important information contributing to the understanding of atmosphere-ocean interactions, and provides an illustration of how coastal ocean biogeochemistry, such as air-sea CO_2 exchange, responds to extreme weather events.

2. Methods

2.1 Analytical methods and data processing

In situ observations were from two cruises conducted on board R/V *Cape Hatteras* during 22-30 April 2009 and during 09-21 March 2010 in the northern Gulf of Mexico. Samples for SSS, sea surface temperature (SST) and surface P_{CO_2} were acquired from the ship's seawater system supplied by an inlet located at an approximate depth of 1.5- 2 m. Measurements of P_{CO_2}

were made using a flow-through system with a shower head equilibrator plus a CO₂ and H₂O detector (LI-7000) with a precision of ±0.1 Pa (±1 ppm) (Jiang et al. 2008). The LI-7000 detector was calibrated automatically every 3.5 to 6 h using five certified gas standards, which had dry CO₂ values of 0, 20.01, 40.59, 60.25, and 98.82 Pa (or 0, 197.45, 400.57, and 594.65, and 975.26 ppm, respectively) referenced against standards traceable to those of the National Institute of Standards and Technology (NIST).

Areal average values of P_{CO₂} were gridded to a resolution of 0.1° × 0.1° using Matlab® software and these gridded fields were used to calculate the air-sea CO₂ flux by the following equation:

$$\text{CO}_2 \text{ flux} = k \times K_0 \times (P_{\text{CO}_2\text{sw}} - P_{\text{CO}_2\text{air}}) \quad (1)$$

where k is the gas transfer velocity, K_0 is the solubility of CO₂ (Weiss 1974), $P_{\text{CO}_2\text{sw}}$ and $P_{\text{CO}_2\text{air}}$ represent the partial pressure of CO₂ in surface seawater and overlying air, respectively. The difference between $P_{\text{CO}_2\text{sw}}$ and $P_{\text{CO}_2\text{air}}$ represents the CO₂ gradient (ΔP_{CO_2}) across the air-sea interface. Calculations of air-sea CO₂ fluxes (positive values represented a source to the atmosphere) were made following the approaches given by Jiang et al. (2008). Ocean surface winds with a resolution of 0.25° were acquired from the Quick Scatterometer (QuikSCAT) and the air-sea gas transfer coefficient was estimated by following Ho et al. (2006). As QuikSCAT has a limited time resolution, we supplemented it by obtaining hourly wind climatology data from a buoy (No.42040, the National Data Buoy Center of National Oceanic and Atmospheric Administration [NOAA]) at the Mississippi River Southwest Pass (*see* the justification and method described by Jiang et al. [2008]).

Sea-viewing Wide Field-of-view Sensor (SeaWiFS), which represents ocean surface Chl a data with a resolution of 0.1°, and the QuikSCAT wind data were downloaded from the

Science-Quality Satellite Data on the Ocean Watch Live Access Server

(<http://las.pfeg.noaa.gov/oceanWatch/oceanwatch.php>) of NOAA. Additionally, to supplement the salinity data from our ship-based surveys, we used salinity estimated with the ‘1/25° Gulf of Mexico Hybrid Coordinate Ocean Model (HYCOM)’ (Chassignet et al. 2007) from the Naval Research Laboratory (<http://www7320.nrlssc.navy.mil/>).

2.2 Plume width calculation from Ekman transport model

A two-dimensional model developed by Lentz (2004) was used to compute the width of the MARS plume. The primary model assumption is that competition between wind-driven vertical mixing and geostrophic adjustment associated with buoyancy forcing at the offshore edge of the plume results in continual entrainment. If the plume buoyancy anomaly is conserved as it is advected offshore, the time-varying plume thickness can be computed assuming that wind-driven vertical mixing satisfies a bulk Richardson criterion. The cross-shelf position of the offshore edge of the plume is then estimated by integrating over time the Ekman transport divided by the plume thickness.

3. Results

The distribution of the MARS plume in spring was generally along the Louisiana-Texas shelf from 1999 to 2009. This is reflected by high Chl *a* concentrations ($\geq 0.3 \mu\text{g L}^{-1}$) derived from satellite along the shelf to the north of latitude 28°N and between longitudes 88 and 94°W (Fig. 2.1A-C). Conditions during spring 2009 were similar to the climatological mean conditions for the period 1999-2009 (Fig. 2.1D-F). We thus used our observations during April 2009 (e.g., SST, Chl *a* and P_{CO_2}) to represent the typical spring conditions.

3.1 Winter storms and the wind forcing over the Gulf of Mexico

Three winter storms were documented on the U.S. east coast in February 2010 (05-06, 09-10, and 25-26 February <http://www.erh.noaa.gov/er/phi/archives.html#2010>) and three successive large low-pressure systems were observed to cross North America in March 2010 (during 21-24 and 27-31 March 2010 (*see* http://www.nasa.gov/multimedia/videogallery/index.html?media_id=12287707, NASA)). These weather events in February resulted in a higher than normal snowfall in the central U.S. For example, 78 mm snow was recorded in Muscle Shoals, Alabama, and record snowfalls were reported for February 2010 in many northeastern areas (Lecomte 2011). Although snow was less in March 2010, several regional areas still set snowfall records (Lecomte 2011; Robinson 2011). These historical snow events were indicative of extreme weather conditions prevalent in North America in February and March 2010.

While these three low-pressure systems dominated North American weather in March 2010, offshore winds with an upwelling-favorable component (from the north-northwest) were prevalent in the Gulf of Mexico in March 2010 (Fig. 2.2A). Wind observations from NOAA buoy No.42040 near the Mississippi River delta from February to April 2010 revealed a wind direction consistent with this wind circulation (Fig. 2.2B). This pattern of wind circulation in 2010 was different from that in April 2009, which was more representative of typical spring conditions, i.e., the wind circulation over the Gulf of Mexico dominated by easterly winds in April 2009 (Fig. 2.2C). Wind directions recorded by the buoy at the Mississippi River delta in April 2009 were characterized by downwelling-favorable onshore wind conditions (from the southeast, Fig. 2.2D).

Prior to March 2010, unusually high MARS river discharge was also observed in February 2010 ($38,400 \text{ m}^3 \text{ s}^{-1}$, U.S. Geological Survey [USGS] data), which was above one standard deviation of the average for the past ten years ($26,000 \text{ m}^3 \text{ s}^{-1}$, Fig. 2.3). In contrast, discharge in February and March 2009 ($19,300$ and $23,300 \text{ m}^3 \text{ s}^{-1}$) was slightly below average conditions, but within one standard deviation of the recent ten year average (Fig. 2.3).

Furthermore, nitrate plus nitrite fluxes from the MARS were higher in February to March 2010 ($103 \times 10^9 \text{ g N}$ and $121 \times 10^9 \text{ g N}$) than for the same period in 2009 ($76 \times 10^9 \text{ g N}$ to $124 \times 10^9 \text{ g N}$, USGS data).

3.2 SeaWiFS Chl *a* distribution

The low-pressure systems that passed through North America during spring 2010 significantly affected the Chl *a* distribution in the Gulf of Mexico as evidenced by anomalously high values extending offshore in March 2010. This was attributed to the influence of the widespread MARS plume extending southward across 28°N (Fig. 2.4), which was particularly significant in March 2010. In March 2010, high Chl *a* concentrations were not only distributed along the shelf, but also extended from the immediate vicinity of the river outflow to the pelagic Gulf of Mexico near 26°N (Fig. 2.4B). Intermittent regions of high Chl *a* concentration were also observed in pelagic waters one month before or after March 2010 (Fig. 2.4A, C), showing that this widespread plume feature persisted for at least one month. This widespread cross-shelf MARS plume, evident in SeaWiFS Chl *a* imagery in March 2010, was in dramatic contrast to average conditions over the past ten years, with values during March 2010 two standard deviations above the climatological mean in pelagic waters (Fig. 2.5A). Other satellite data also exhibited atypical patterns in March 2010 in this region, including multiple-satellite blended products of sea surface temperature available from the Ocean Watch Live Access Server, which

were characterized by an anomalously low temperatures associated with the plume feature in March 2010 as compared to other years from 2002 to 2011 (Fig. 2.5B). The area of the plume within the region from 88 to 94°W and north of 24°N in March 2010 was twice as large as that in April 2009 based on SeaWiFS Chl *a* concentrations $\geq 0.3 \mu\text{g L}^{-1}$ as the delineation of the plume boundary (Table 2.1).

3.3 Sea surface salinity distribution

Distributions of SSS were characterized by a narrow along-shore plume of low salinity water in April 2009, in contrast to a widespread cross-shelf plume in March 2010. During April 2009, low salinity water (SSS ≤ 35) was confined to the Louisiana shelf (Fig. 2.6A). In March 2010, the low salinity water crossed the shelf and extended beyond the southern limit of our survey area (i.e., the 35 salinity contour line was not found during our survey between 91.5 to 94°W and north of 27.6°N, Fig. 2.6B). Particularly at the southernmost station in March 2010, we observed a thin low salinity surface layer as evidenced by the comparison of the salinity of 36.3 at depth 2.4 m from the vertical profile vs. 34.7 determined with the underway system from the inlet at a depth of 1.5-2 m.

To better represent the extent of the low salinity feature, salinity contour lines of 35 and 35.5 from data generated from the HYCOM model were overlaid on a composite SeaWiFS chlorophyll image. The widespread plume was evident south of the river delta in March 2010, as an extension of the 35 salinity contour to near latitude 28°N and the 35.5 contour to 26 to 27°N (Fig. 2.4B). In contrast, the MARS plume in April 2009 was confined to the shelf, and the 35 and 35.5 salinity contour lines were confined to the region near 28°N near the river delta (Fig. 2.1F).

3.4 Sea surface P_{CO₂} distribution

The in situ sea surface P_{CO₂} values were generally lower on the inner shelf than on the outer shelf for both the April 2009 and March 2010 cruise periods (Fig. 2.6C, D). A strong cross-shelf P_{CO₂} gradient was evident in April 2009 with surface water values below atmospheric values in inner shelf waters and near or above atmospheric values in outer shelf waters, especially for those transects on the western portion of the study region (91-94°W). In the same region during March 2010, surface water P_{CO₂} values below the atmospheric value extended across the shelf, and corresponded to the low salinity surface layer. The mean area-averaged P_{CO₂} value for the area of salinity less than 35 (i.e., the plume) was 36.8 Pa (or 371.7 ppm before water vapor correction) in April 2009 and 33.6 Pa (or 337.8 ppm before water vapor correction) in March 2010 (Table 2.2). While both were significantly lower than the corresponding atmospheric levels (40.1 Pa or 396.1 ppm in 2009, and 40.6 Pa or 400.3 ppm in 2010), the air-sea P_{CO₂} difference (-6.3 Pa or -62 ppm vs. -2.4 Pa or -24 ppm) was much greater in 2010 than in 2009. For areas with surface salinity greater than 35 (here designated as non-plume), the mean area-averaged surface water P_{CO₂} was close to the atmospheric CO₂ level in April 2009 (38.5 Pa or 388.9 ppm, or within 1.0 Pa or 10 ppm), but was significantly below the atmospheric level in March 2010 (36.3 Pa or 371.7 ppm, or 2.9 Pa or 28.6 ppm).

3.5 Air-sea CO₂ fluxes for the plume area

As the area with SSS < 35 was twice as large and ΔP_{CO_2} (P_{CO₂} in water – P_{CO₂} in atmosphere) was more than twice as large in March 2010 as in April 2009, the wide plume region in March 2010 was also a much stronger sink for atmospheric CO₂. In March 2010, because the plume extended beyond the survey area, in addition to using measured air-sea CO₂ flux for the region within survey area, we also estimated air-sea CO₂ flux for areas beyond that

surveyed. The latter estimation was based on a strong correlation between measured CO₂ fluxes and the SeaWiFS Chl *a* concentrations in the survey area to the west of 91°W (Fig. 2.7). By combining these two sets of results, the total CO₂ uptake in the wide plume in March 2010 was estimated as 25.1×10^9 g C d⁻¹, which was five times greater than the uptake fluxes in April 2009 (4.5×10^9 g C d⁻¹, Table 2.1). Even taking into account the potentially large uncertainties in these air-sea CO₂ flux estimates, < 30% (Jiang et al. 2008), it is unequivocal that CO₂ uptake flux in March 2010 was much higher than that in April 2009.

4. Discussion

4.1 Formation of this widespread cross-shelf plume

Wind patterns and intensity were key factors in the unusually large extent of the MARS plume in March 2010. Wind patterns over the Gulf of Mexico were different between April 2009 and March 2010 (Fig. 2.2), and we also found that northerly wind speeds along the Louisiana coast in March 2010 were significantly higher than those during February, March, and April in the past ten years, including specifically in April 2009. Such wind forcing was largely due to the atmospheric conditions on the order of 1000 km horizontal space scales (Wang et al. 1998). In order to compute changes in the width of the MARS plume in response to variable winds during 2009 and 2010, we used a two-dimensional Ekman transport model developed by Lentz (2004) (*see* Methods section). Based on surface Ekman transport alone, the calculated plume of salinity < 35 would have been 80-130 km-wide in April 2009 (Fig. 2.2A), in contrast to 180-250 km in March 2010 (Fig. 2.2B). This result was consistent with observations of higher SeaWiFS Chl *a* and broader extent of low salinity waters evident in HYCOM model output for March 2010 (Fig. 2.4B). Furthermore, this result was also consistent with previous studies that have described

coastal currents on the Louisiana shelf dominated by local wind forcing (Cochrane and Kelly 1986; Walker et al. 2005; Zhang et al. 2012).

In addition to wind forcing, high MARS river discharge in February 2010 ($38,400 \text{ m}^3 \text{ s}^{-1}$ in Fig. 2.3) was also a contributing factor to the extensive plume in March 2010. We noted that the high river discharge alone was not sufficient to result in a wide plume. For example, April to July 2008 was a flood season ($10,000$ to $20,000 \text{ m}^3 \text{ s}^{-1}$), but the MARS plume was confined primarily to a narrow alongshore feature in the northern Gulf inside of 28°N latitude although the plume coverage was large that year (Shi and Wang 2009). Thus, we concluded that both discharge and wind direction were important in contributing to the expansive plume in March 2010. Simultaneous conditions of upwelling-favorable winds and high river discharge have been reported to be factors in increased width of low salinity plumes in the MARS and other river systems (Kourafalou et al. 1996; Fong and Geyer 2001), which supports our findings. As noted in other studies, however, additional factors such as topography and coastal circulation patterns can further influence the behavior of river outflow in a complex system such as the Gulf of Mexico (Schiller et al. 2011).

4.2 How does this cross-shelf plume affect air-sea CO_2 fluxes in the pelagic Gulf of Mexico?

In contrast to the normal spring plume in the northern Gulf of Mexico, which is characterized by a strong cross-shelf gradient in surface water Pco_2 (Lohrenz et al. 2010), the extensive plume in March 2010 affected biological uptake across the shelf and contributed to a drawdown of Pco_2 (relative to the atmosphere) over a substantial portion of the pelagic Gulf of Mexico. To illustrate the effect on regional air-sea CO_2 flux, we calculated CO_2 fluxes by partitioning the MARS outflow region into plume and non-plume areas (Table 2.1). For the non-plume area in March 2010, as the surveyed area was quite limited, we used a range of estimates

that included the observed flux as the upper estimation ($-4.20 \text{ mmol m}^{-2} \text{ d}^{-1}$) as well as the April 2009 flux as the lower estimation ($-0.74 \text{ mmol m}^{-2} \text{ d}^{-1}$), assuming there were similar conditions in the pelagic ocean further south for those two years (Table 2.1). We found that the extensive plume in March 2010 encompassed a large area in pelagic waters, and was associated with enhanced CO_2 uptake in offshore areas that were ordinarily near neutral to CO_2 exchange (Fig. 2.8). Thus, our assessment supports the view that this cross-shelf plume significantly altered air-sea CO_2 fluxes in the pelagic area of Gulf of Mexico by shifting it from a weak sink to a strong sink for the atmospheric CO_2 at this season (Table 2.1), presumably through riverine nutrient-enhanced primary production (Green et al. 2006; Lohrenz et al. 2008).

4.3 The biogeochemical dynamics of this widespread plume

The major nitrogen source to support biological production in this large river plume was from the MARS. The strong CO_2 sink of this plume was supported by high nitrogen flux during February 2010 ($103 \times 10^9 \text{ g N}$), which was 25% higher than in February 2009 ($76 \times 10^9 \text{ g N}$, USGS data). Comparisons of riverine nutrient loading to DIC removal (Guo et al. 2012) or direct primary production measurements (Lohrenz et al. 1999) in the plume both suggested that during springtime only a small fraction of riverine nutrients are used by biological production in the low to middle salinity plume zones and a significant amount of riverine nutrient is available for potential biological production in high salinity plume edge areas. A wider and thinner plume would also be associated with higher light availability in the water column thereby contributing to higher biomass and productivity (Lohrenz et al. 1999). Furthermore, the strong CO_2 sink in the plume, was also promoted by lower temperature (Takahashi et al. 1993), which leads to a 10 to 15% decrease in P_{CO_2} when temperature decreased 2 to 3°C in March 2010.

Satellite Chl *a* concentrations were generally consistent with the concentrations measured during contemporaneous cruises, i.e., Chl *a* concentrations on the middle shelf and continental slope in March 2010 (1.68 and 1.58 mg m⁻³) were much higher than in April 2009 (0.22 and 0.15 mg m⁻³) (Chakraborty 2013). Although SeaWiFS-derived Chl *a* may be sensitive to the relatively high colored dissolved organic matter (CDOM) concentrations (Castillo et al. 2001), we surmise that such effects should be minor in offshore waters.

In addition, for surface waters with salinities higher than 35, the nitrate and nitrite concentrations were higher in March 2010 (0.27 to 2.23 μM) than in April 2009 (0.16 to 0.58 μM) (S. E. Lohrenz, unpubl.), supporting higher Chl *a* in the non-plume area in March 2010 than April 2009 (Fig. 2.1E, 4B). In addition to the river source, higher nitrogen on the salinity >~35 waters might also come from subsurface upwelling between the offshore to pelagic Gulf in March 2010 (however, stratification was strong for areas with salinity less than ~35 water). Thus, in contrast to that biological nitrogen fixation was observed at the outer extent of the Amazon plume (Subramaniam et al. 2008), we consider that biological nitrogen fixation was a minor fraction of the total nitrogen input in the MARS plume. Although various taxa were present, no significant N-fixation species were observed in March 2010 as the dominant phytoplankton group was diatom (Chakraborty 2013).

4.4 Potential relevance to paleoceanographic research

The plume in March 2010 had several characteristics similar to the paleoceanographic signals reported for the Mississippi plume during glacial periods, i.e., low water temperature (< 24°C), widespread plume trajectory, and reduced Loop Current interaction (Nürnberg et al. 2008). Our results demonstrate that weather-associated wind variation can alter the width and trajectory of the plume and the associated carbon biogeochemistry. Thus, colder and stronger wind

conditions may be an important potential mechanism for explaining the distribution of the MARS plume and its biogeochemical properties during glacial periods in addition to apparent differences in freshwater discharge, shelf area and bottom topography.

5. Conclusion

In conclusion, we observed a greatly enhanced CO₂ uptake flux in the northern Gulf of Mexico in March 2010 due to an unusually widespread MARS plume. This feature was not evident during any other year over the period 1999-2010. The widespread plume was induced by the combination of a high MARS river discharge and the northerly winds driven by a large low-pressure system over the North America continent. A conceptual diagram in Fig. 2.8 provides a comparative illustration of plume processes during normal conditions and those corresponding to the anomalous conditions in March 2010. In normal conditions, a narrow-alongshore plume is confined to the shelf due to alongshore winds, resulting in a CO₂ sink on the shelf and a nearly neutral status for CO₂ air-sea exchange in the pelagic region (Fig. 2.8A). In March 2010, offshore winds and high MARS discharge contributed to the large extent of the cross-shelf MARS plume. This widespread plume enhanced the pelagic sea surface Chl *a* concentrations and decreased the pelagic surface water P_{CO₂} values (Fig. 2.8B). As a result, air-sea CO₂ fluxes in pelagic Gulf of Mexico waters influenced by this cross-shelf plume were shifted from being largely neutral to being a strong net sink for atmospheric CO₂. We suggest that weather-related variation in river discharge and wind forcing may have a substantial influence on coastal carbon air-sea fluxes.

References

- Castelao, R., O. Schofield, S. Glenn, R. Chant, and J. Kohut. 2008. Cross-shelf transport of freshwater on the New Jersey shelf. *J. Geophys. Res.* **113**: C07017, doi:10.1029/2007JC004241
- Castillo, D., E. Carlos, P. G. Coble, R. N. Conmy, F. E. Müller-Karger, L. Vanderbloemen, and G. A. Vargo. 2001. Multispectral in situ measurements of organic matter and chlorophyll fluorescence in seawater: documenting the intrusion of the Mississippi River plume in the west Florida Shelf. *Limnol. Oceanogr.* **46**: 1836-1843, doi: 10.4319/lo.2001.46.7.1836
- Chakraborty, S. 2013. Phytoplankton community distribution and light absorption properties in the northern Gulf of Mexico. Ph.D. thesis. Univ. of Southern Mississippi.
- Chassignet, E. P., H. E. Hurlburt, O. M. Smedstad, G. R. Halliwell, P. J. Hogan, A. J. Wallcraft, R. Baraille, and R. Bleck. 2007. The HYCOM (HYbrid Coordinate Ocean Model) data assimilative system. *J. Marine Syst.* **65**: 60-83, doi:10.1016/j.jmarsys.2005.09.016
- Cochrane, J. D., and F. J. Kelly. 1986. Low-frequency circulation on the Texas-Louisiana continental shelf. *J. Geophys. Res.* **91**: 10645-10659, doi: 10.1029/JC091iC09p10645
- Cooley, S. R., and P. L. Yager. 2006. Physical and biological contributions to the western tropical North Atlantic Ocean carbon sink formed by the Amazon River plume. *J. Geophys. Res.* **111**: C08018, doi:10.1029/2005jc002954
- Fong, D. A., and W. R. Geyer. 2001. Response of a river plume during an upwelling favorable wind event. *J. Geophys. Res.* **106**: 1067-1084, doi:10.1029/2000JC900134
- Green, R. E., T. S. Bianchi, M. J. Dagg, N. D. Walker, and G. A. Breed. 2006. An organic carbon budget for the Mississippi River turbidity plume and plume contributions to air-sea CO₂ fluxes and bottom water hypoxia. *Estuaries Coasts* **29**: 579-597

- Guo, X., W.-J. Cai, W.-J. Huang, Y. Wang, F. Chen, M. C. Murrell, S. E. Lohrenz, L.-Q. Jiang, M. Dai, J. Hartmann, Q. Lin, and R. Culp. Carbon dynamics and community production in the Mississippi River plume. *Limnol. Oceanogr.* **57**: 1-17
- Ho, D. T., C. S. Law, M. J. Smith, P. Schlosser, M. Harvey, and P. Hill. 2006. Measurements of air-sea gas exchange at high wind speeds in the Southern Ocean: Implications for global parameterizations. *Geophys. Res. Lett.* **33**: L16611, doi:10.1029/2006GL026817
- Jiang, L.-Q., W.-J. Cai, Y. Wang, R. Wanninkhof, and H. Lüger. 2008. Air-sea CO₂ fluxes on the U.S. South Atlantic Bight: spatial and seasonal variability. *J. Geophys. Res.* **113**: C07019, doi:10.1029/2007JC004366
- Kourafalou, V. H., L.-Y. Oey, J. D. Wang, and T. N. Lee. 1996. The fate of river discharge on the continental shelf 1. Modeling the river plume and the inner shelf coastal current. *J. Geophys. Res.* **101**: 3415-3434, doi:10.1029/95JC03024
- Lecomte, D. 2011. U.S. weather highlights 2010: A year of extremes. *Weatherwise* **64**: 13-20, doi: 10.1080/00431672.2011.566815
- Lentz, S. 2004. The response of buoyant coastal plumes to upwelling-favorable winds. *J. Phys. Oceanogr.* **34**: 2458-2469, doi:10.1175/JPO2647.1
- Lohrenz, S. E. G. L. Fahnenstiel, D. G. Redalje, G. A. Lang, M. J. Dagg, T. E. Whitledge, and Q. Dortch. 1999. Nutrients, irradiance, and mixing as factors regulating primary production in coastal waters impacted by the Mississippi River plume. *Cont. Shelf Res.* **19**: 1113-1141
- Lohrenz, S. E., D. G. Redalje, W.-J. Cai, J. Acker, and M. Dagg. 2008. A retrospective analysis of nutrients and phytoplankton productivity in the Mississippi River plume. *Cont. Shelf Res.* **28**: 1466-1475

- Lohrenz, S. E., W.-J. Cai, F. Chen, X. Chen, and M. Tuel. 2010. Seasonal variability in air-sea fluxes of CO₂ in a river-influenced coastal margin. *J. Geophys. Res.* **115**: C10034, doi:10.1029/2009JC005608
- Nürnberg, D., M. Ziegler, C. Karas, R. Tiedemann, and M. W. Schmidt. 2008. Interacting Loop Current variability and Mississippi River discharge over the past 400 kyr. *Earth Planet. Sc. Lett.* **272**: 278-289, doi:10.1016/j.epsl.2008.04.051
- Rabalais, N. N., R. E. Turner, D. Justić, Q. Dortch, W. Wiseman, and B. Sen Gupta. 1996. Nutrient changes in the Mississippi River and system responses on the adjacent continental shelf. *Estuaries Coasts* **19**: 386-407, doi:10.2307/1352458
- Robinson, D. A. 2011. An upside-down winter: The 2009–2010 snow report. *Weatherwise* **64**: 22-29, doi:10.1080/00431672.2011.536119
- Schiller, R. V., V. H. Kourafalou, P. Hogan, and N. D. Walker. 2011. The dynamics of the Mississippi River plume: Impact of topography, wind and offshore forcing on the fate of plume waters. *J. Geophys. Res.* **116**: C06029, doi:10.1029/2010JC006883
- Shi, W., and M. Wang. 2009. Satellite observations of flood-driven Mississippi River plume in the spring of 2008. *Geophys. Res. Lett.* **36**: L07607, doi:10.1029/2009GL037210
- Subramaniam, A., P. L. Yager, E. J. Carpenter, C. Mahaffey, K. Björkman, S. Cooley, A. B. Kustka, J. P. Montoya, S. A. Sanudo-Wilhelmy, R. Shipe, and D. G. Capone. 2008. Amazon River enhances diazotrophy and carbon sequestration in the tropical North Atlantic Ocean. *P. Natl. Acad. Sci.* **105**: 10460-10465
- Takahashi, T., J. Olafsson, J. G. Goddard, D. W. Chipman, and S. C. Sutherland. 1993. Seasonal Variation of CO₂ and Nutrients in the High-Latitude Surface Oceans: a Comparative Study. *Global Biogeochem. Cycles* **7**: 843-878

- Takahashi, T., S. C. Sutherland, C. Sweeney, A. Poisson, N. Metzl, B. Tilbrook, N. Bates, R. Wanninkhof, R. A. Feely, C. Sabine, J. Olafsson, and Y. Nojiri. 2002. Global sea-air CO₂ flux based on climatological surface ocean *p*CO₂, and seasonal biological and temperature effects. *Deep-Sea Res. II* **49**: 1601-1622, doi:10.1016/S0967-0645(02)00003-6
- Tseng, C.-M., K. K. Liu, G. C. Gong, P. Y. Shen, and W. J. Cai. 2011. CO₂ uptake in the East China Sea relying on Changjiang runoff is prone to change. *Geophys. Res. Lett.* **38**: L24609, doi: 10.1029/2011gl049774
- Vandemark, D., J. E. Salisbury, C. W. Hunt, S. M. Shellito, J. D. Irish, W. R. McGillis, C. L. Sabine, and S. M. Maenner. 2011. Temporal and spatial dynamics of CO₂ air-sea flux in the Gulf of Maine. *J. Geophys. Res.* **116**: C01012, doi:10.1029/2010JC006408
- Walker, N. D., W. J. Wiseman, L. J. Rouse, and A. Babin. 2005. Effects of river discharge, wind stress, and slope eddies on circulation and the satellite-observed structure of the Mississippi River plume. *J. Coastal Res.* **21**: 1228-1244
- Wang, W., W. D. Nowlin, and R. O. Reid. 1998. Analyzed surface meteorological fields over the northwestern Gulf of Mexico for 1992–94: Mean, seasonal, and monthly patterns. *Mon. Weather Rev.* **126**: 2864-2883.
- Weiss, R. F. 1974. Carbon dioxide in water and seawater: The solubility of a non-ideal gas. *Mar. Chem.* **2**: 203-215, doi:10.1016/0304-4203(74)90015-2
- Zhang, X., R. D. Hetland, M. Marta-Almeida, and S. F. Dimarco. 2012. A numerical investigation of the Mississippi and Atchafalaya freshwater transport, filling and flushing times on the Texas-Louisiana Shelf. *J. Geophys. Res.* **117**: C11009, doi:10.1029/2012jc008108

Table 2.1. Plume and non-plume areas and air-sea CO₂ fluxes in April 2009 and March 2010.

Cruise	April 2009	March 2010
MARS Plume in its dominant region ^a		
Chl <i>a</i> ^b Area (10 ³ km ²)	72	180
SSS ^b Area (10 ³ km ²)	60	150
Average area (10 ³ km ²)	66	165
CO ₂ flux (mmol m ⁻² d ⁻¹)	-5.2	-10.4 to -14.1
Total flux (10 ⁹ g C d ⁻¹)	-4.5 ± 1.4	-25.1 ± 7.5
Non-plume region of Gulf of Mexico		
Area (10 ³ km ²)	1434 ^c	1335 ^c
CO ₂ flux (mmol m ⁻² d ⁻¹)	-0.74	-0.74 to -4.20
Total flux (10 ⁹ g C d ⁻¹)	-12.7 ± 3.8	-11.9 ± 3.5 to -67.3 ± 20.2
Entire Gulf of Mexico		
Area (10 ³ km ²)	1500 ^c	1500 ^c
Total flux (10 ⁹ g C d ⁻¹)	-17.2 ± 5.2	-37.0 ± 11.1 to -92.4 ± 27.7

^a This dominant region refers to the area between Longitude 88 to 94°W and north of Latitude 26°N.

^b The plume boundary of Chl *a* = 0.3 μg L⁻¹ was adopted as it is higher than the average Chl *a* (0.19 μg L⁻¹) in March from 1998 to 2010 when water depth larger than 200 m. The boundary of SSS = 35 was estimated by a model based on Ekman dynamics.

^c The entire Gulf of Mexico was assumed to be 1500 × 10³ km². The non-plume area was calculated by subtracting the plume area from entire Gulf of Mexico area (e.g., 1500 - 66 = 1434 for April 2009).

Table 2.2. The area-averaged mole fraction concentration of CO₂ for surface seawater and atmosphere in the survey area. Unit: Pa (or ppm in the dried sample gas flow).

	April 2009	March 2010
Plume	36.8 (371.7)	33.6 (337.8)
Non-plume	38.5 (388.9)	36.3 (371.7)
Atmosphere	40.1 (396.1)	40.6 (400.3)

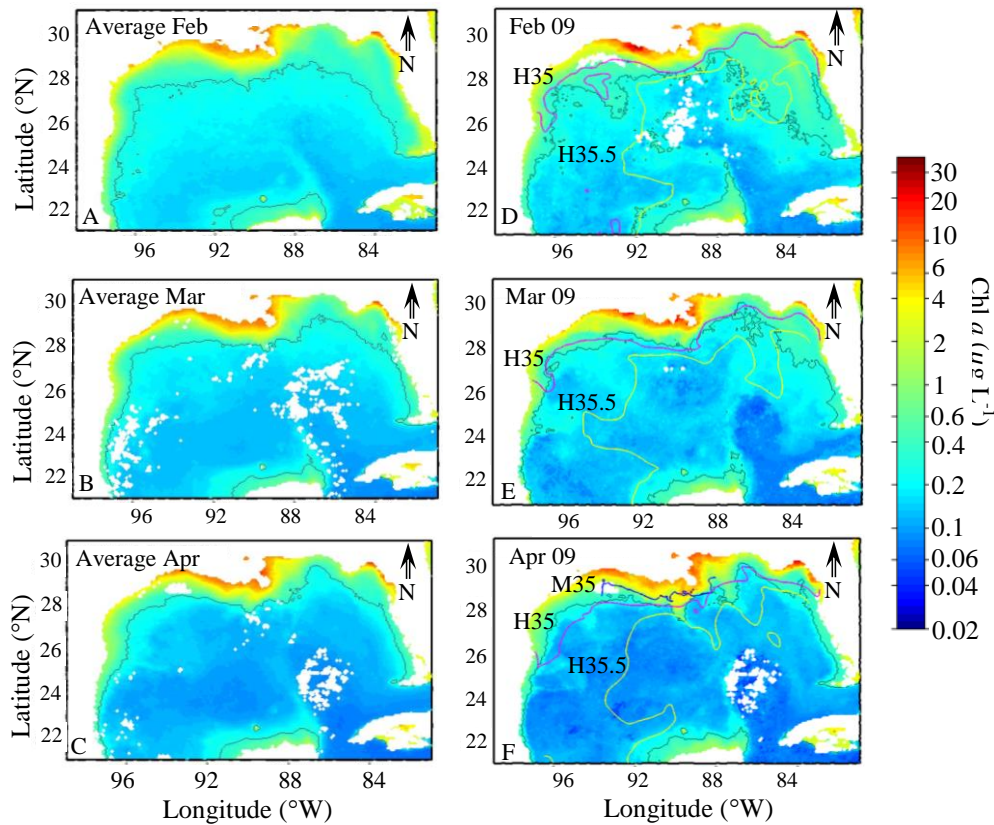


Figure 2.1. SeaWiFS Chl *a* distributions on the Gulf of Mexico under normal conditions. (A) February, (B) March, and (C) April showed monthly Chl *a* distribution from 1999 to 2009. (D) February, (E) March, and (F) April showed these distributions in 2010. Black lines represent Chl *a* of $0.3 \mu\text{g L}^{-1}$ contour line. (D - F) Magenta lines are the HYCOM model estimated salinity of 35 contour lines (H35) and yellow lines are the salinity 35.5 contour lines (H35.5). (F) The blue line represents in situ measurement SSS contour line of 35 (M35).

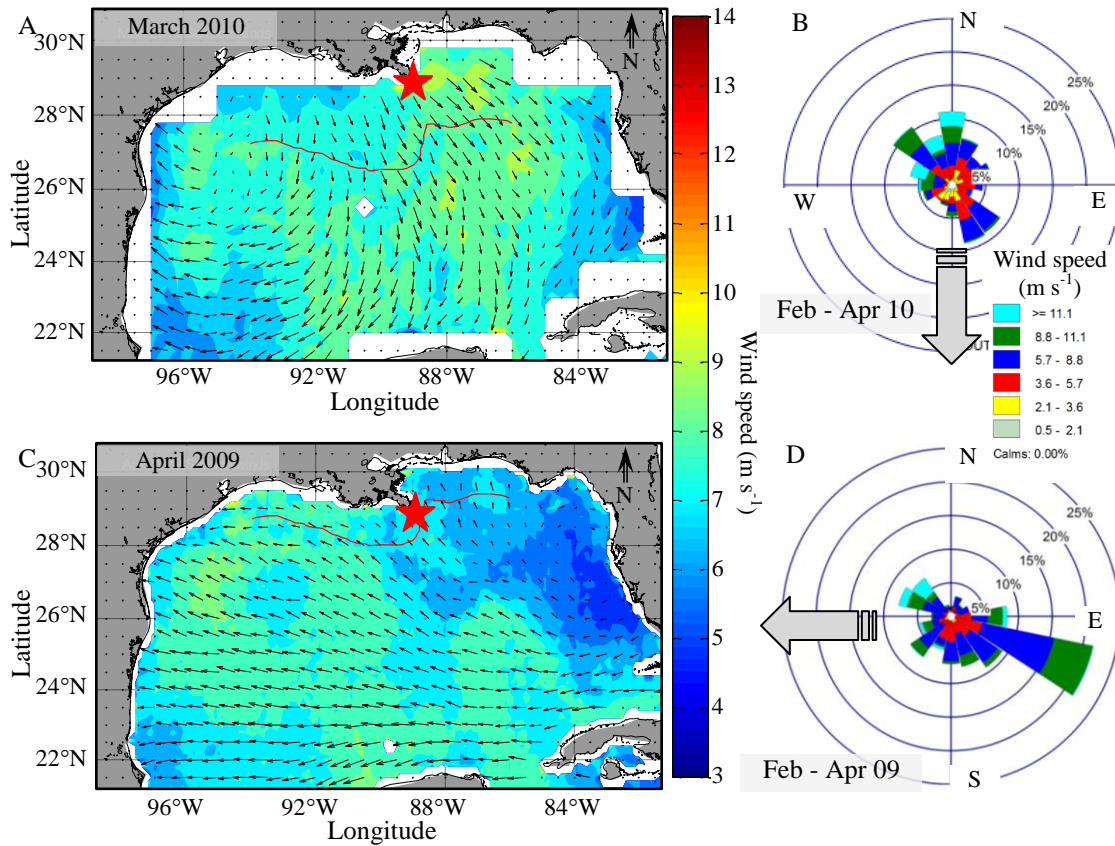


Figure 2.2. Spatial and temporal wind patterns in the Gulf of Mexico. (A) The QuikSCAT winds were predominantly northerly to northwesterly in March 2010 and (B) Continuous wind data from a NOAA meteorological buoy (No.42040, red stars in A) were characterized predominantly by northerly winds during February, March, and April in 2010. (C) The QuikSCAT winds were easterly to southeasterly in April 2009 and (D) Continuous wind data from the same buoy also showed easterly to southeasterly winds for three months in 2009. (A, C) The extent of the plume as estimated by the Ekman-transport model (red line) was substantially greater in March 2010. (B, D) The inserted grey arrows represent the drifting direction of MARS plumes.

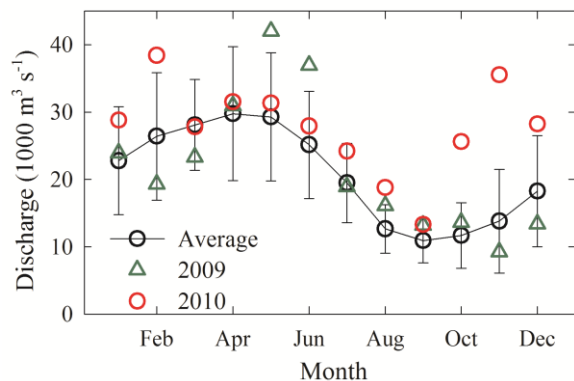


Figure 2.3. The MARS monthly average discharge (black circles) and standard deviation from water year 1998 to 2010 (USGS data, streamflow and nutrient delivery to the Gulf of Mexico, http://toxics.usgs.gov/hypoxia/mississippi/flux_estimates/delivery/index.html), showing that February discharge in 2010 (red circle) was higher than the standard deviation of average February discharge, and March discharge in 2009 (green triangle) was within the standard deviation of the average March discharge. (The water year of MARS begins from the October in one year in advance to the calendar year until the September of the calendar year, e.g., Oct 2010 to Sep 2011).

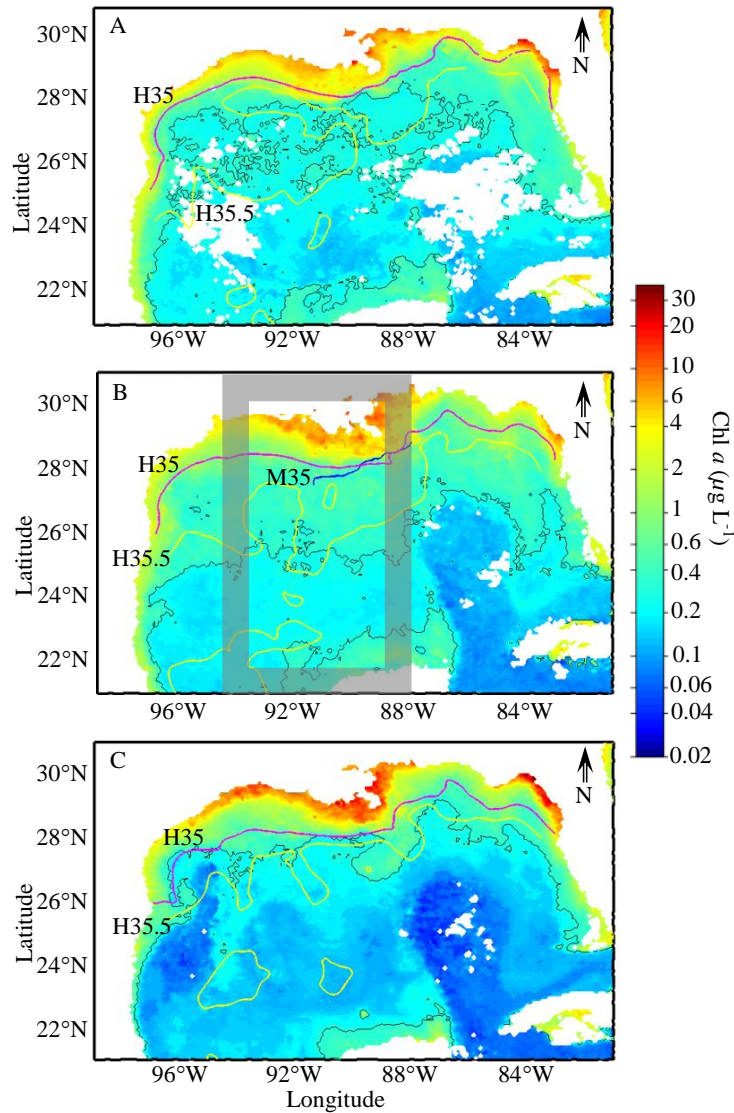


Figure 2.4. SeaWiFS Chl *a* distributions in 2010. (A) February, (B) March, and (C) April were characterized by extensive areas of relatively high Chl *a* concentrations in the northern Gulf of Mexico, particularly during March 2010 when concentrations of $0.3 \mu\text{g L}^{-1}$ (black contour lines) extended well beyond 28°N . The HYCOM modeled monthly averaged salinity distributions were also consistent with an extensive MARS plume, with salinities as low as 35 (magenta line, H35) extending to near 28°N and 35.5 (yellow line, H35.5) to between 26 to 28°N . The blue line was as in Fig. 2.1, M35.

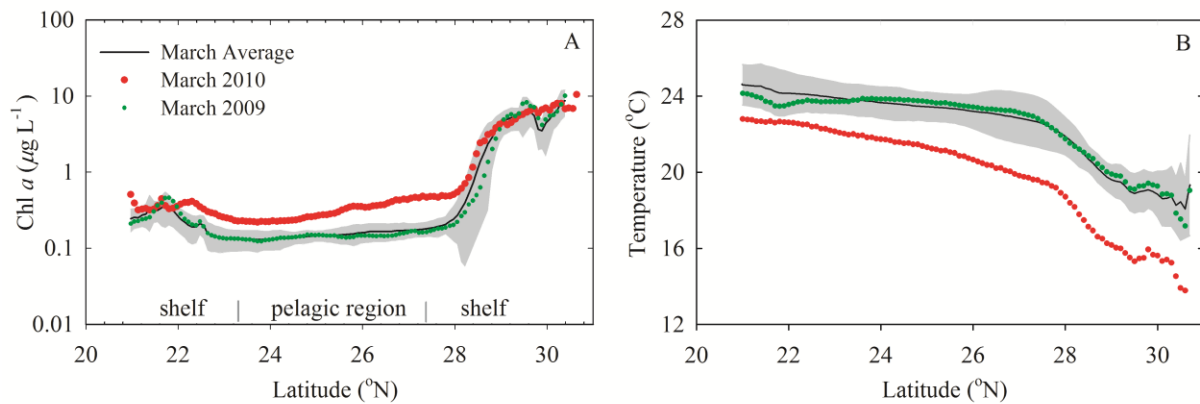


Figure 2.5. Anomalies of (A) SeaWiFS Chl *a* concentration and (B) surface temperature from northern to southern Gulf of Mexico. (A) For the pelagic regions, March SeaWiFS Chl *a* concentrations in 2010 (red dots) were higher than average March Chl *a* concentrations (black line) ± 2 standard deviation (SD, gray shading) from 1999 to 2009 (no data for 2008) between latitude 88 and 94°W (the area in the gray rectangular in Fig. 2.4B), and March SeaWiFS Chl *a* concentrations in 2009 (green dots) were within ± 2 SD of this average.

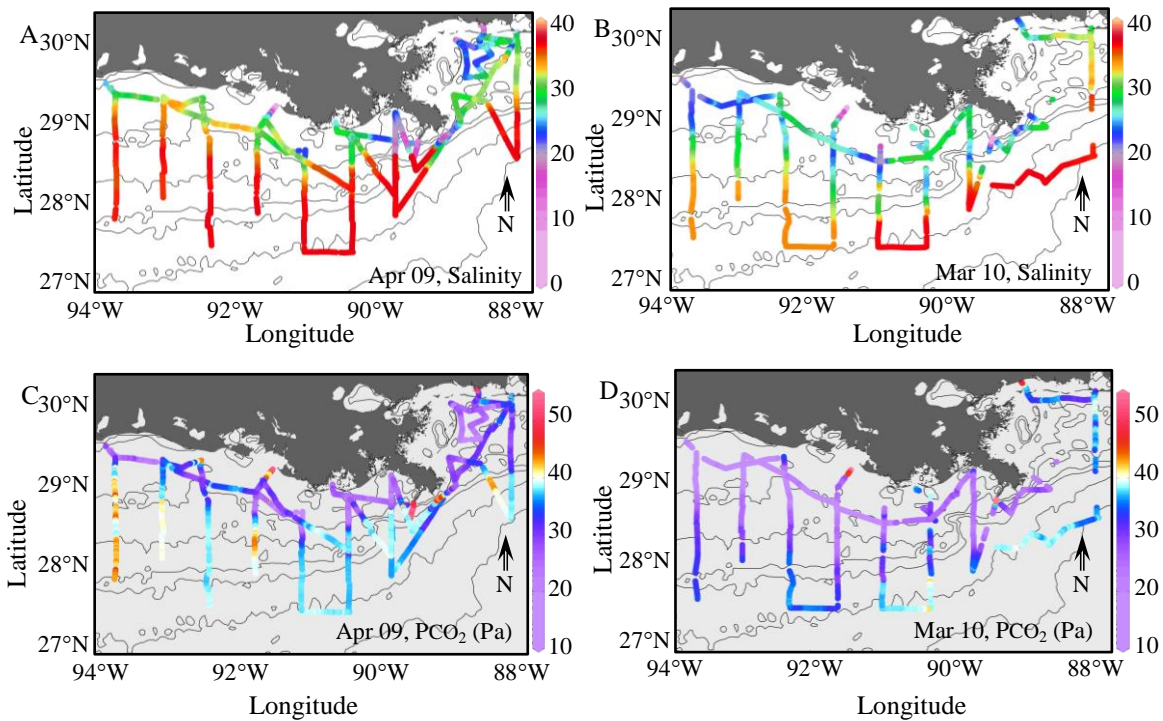


Figure 2.6. Distributions of in situ measured (A, B) SSS and (C, D) PCO₂. (A) Low salinity waters were confined to the inner shelf in April 2009 but (B) extending to outer shelf waters in March 2010. (C) Low sea surface PCO₂ was evident mainly in the inner shelf in April 2009 but (D) covered a much large area in March 2010. The sequence of the bathymetry is 20 m, 50 m, 100 m, 200 m, 1000 m, and 2000 m.

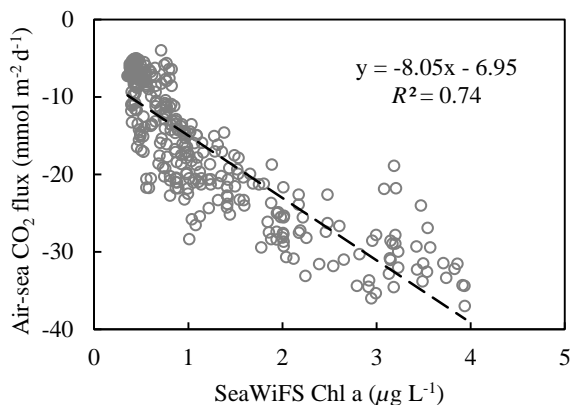


Figure 2.7. The correlation between air-sea CO₂ flux and SeaWiFS Chl *a* concentration to the west of 91.2°W is given. The data in the eastern area was excluded because they were affected by water with salinity higher than 35 and was not representative of the widespread plume. Based on the correlation, the estimated air-sea CO₂ flux was -10.4 mmol m⁻² d⁻¹ (-15.0×10⁹ g C d⁻¹) for plume out of the survey area in the MARS-influenced region (between 26 to 28°N and 88 to 94°W). By combining this estimated flux with the measured CO₂ flux of the plume in the survey area (-14.1 mmol m⁻² d⁻¹, -10.1×10⁹ g C d⁻¹), the total air-sea CO₂ flux of the plume was -25.1×10⁹ g C d⁻¹.

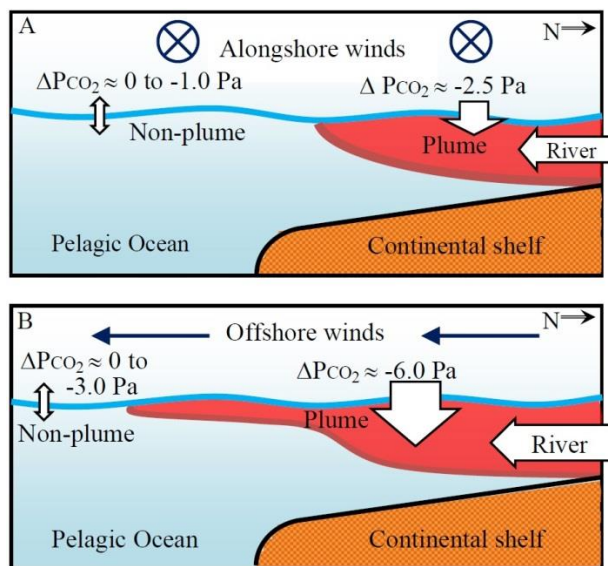


Figure 2.8. A conceptual model illustrates the differing plume dynamics between normal spring conditions and March 2010. (A) Under normal conditions, the narrow, alongshore plume was confined on the continental shelf due to alongshore winds. The plume acts as a sink to atmospheric CO_2 while the non-plume area is near neutral, resulting in a cross shelf Pco_2 gradient in normal years. (B) In March 2010, a widespread cross shelf river plume occurred due to offshore winds and high river discharge. This widespread plume encompassed a large area and acted as a strong CO_2 sink. The widespread plume therefore enhanced the CO_2 sink in the pelagic ocean. ($\Delta\text{Pco}_2 = \text{Pco}_2$ of water – Pco_2 of atmosphere).

CHAPTER 3

IMPACTS OF WEATHER EVENTS ON SHELF CIRCULATION AND CO₂ AND O₂ DYNAMICS ON THE LOUISIANA SHELF DURING SUMMER ¹

¹Wei-Jen Huang, Wei-Jun Cai, Yongchen Wang, and Charles S. Hopkins. To be submitted to *Biogeosciences*.

Abstract

While much is known of the physics of coastal currents, much less is known of the effects of coastal currents and mixing on shelf carbon dioxide (CO_2) and oxygen distribution and dynamics. On the Louisiana (LA) shelf, a typical alongshore plume generated by the Mississippi and Atchafalaya River System (M-ARS) and the easterly wind existed along the entire inner shelf in August 2007. Associated with this normal current pattern, we observed low salinity and low partial pressure of CO_2 ($p\text{CO}_2$), indicating high biological production, on the inner shelf and higher salinity and $p\text{CO}_2$ on the outer shelf. In contrast, the trajectory of the M-ARS plume was relocated to the eastern part of the LA shelf by the altered shelf circulation characterized by pelagic water signals on the western inner shelf in July 2009. Satellite wind distribution, chlorophyll pattern, and numerical model were all consistent with this altered shelf circulation. Associated with this altered coastal current pattern, we observed low salinity and low $p\text{CO}_2$ waters on the eastern inner shelf, but high salinity and high $p\text{CO}_2$ values on the western inner shelf. This altered circulation pattern and the associated wind strength shifted the LA shelf from normally a CO_2 sink (as in 2007) to a strong source for the atmosphere in 2009 during summer. As the M-ARS plume trajectory was relocated and the stratified area was reduced in July 2009, the bottom water hypoxia area was much smaller than previous prediction.

Our observation further showed that the relationships between bottom water dissolved oxygen (DO) and dissolved inorganic carbon (DIC) in typical summer time generally followed Redfield stoichiometry during organic matter decomposition in two separate water masses (brackish/nearshore vs. high salinity/offshore water). But the hypoxic DIC concentration in July 2009 was higher than the prediction from Redfield-type respiration. Such accumulation of DIC might be the product of repetition between stratification (Redfield-type respiration) and de-

stratification (a much rapid O₂ compensation than CO₂ due to a strong buffering effect of the marine carbonate system on CO₂). Thus, the wind-forcing related shelf circulation was a critical factor that influences the trajectory of plume and the associated biogeochemical properties on coastal waters.

1. Introduction

Despite its small geographic extent, the coastal ocean plays an important role in the global carbon cycle through the combined processes of net biological production, net carbon dioxide (CO₂) uptake from the atmosphere, and organic carbon export to the open ocean (Cai, 2011; Chen and Borges, 2009; Cai et al., 2006). Coastal oceans also face serious anthropogenic stresses that can alter shelf metabolism, for example, nitrogen enrichment or eutrophication and the associated surface algal blooms and bottom water hypoxia (dissolved oxygen [DO] < 2 mg O L⁻¹), especially on large-river-dominated continental shelves (Rabalais et al., 2010; Rabouille et al., 2008). Physically, coastal oceans are characterized by a complex shelf circulation that is driven by variations in freshwater discharge, upwelling along the shelf edge, and local wind forcing (Lentz and Fewings, 2012). Variations in shelf circulation can have a major impact on shelf carbon dynamics and the severity of eutrophication, such as through the formation of hypoxia (Bianchi et al., 2010). As coastal oceans are highly dynamic, the relationship between surface partial pressure of CO₂ (*p*CO₂) and bottom water hypoxia and their interactions with circulation are poorly understood.

For most of the year, circulation of the LA shelf is characterized as a westward drifting current, driven primarily by easterly winds and a pressure gradient established from freshwater inputs from the combined Mississippi - Atchafalaya Rivers (M-ARs), which are the major freshwater and nutrient sources for the Louisiana (LA) shelf (Cochrane and Kelly, 1986; Rabalais et al., 1996). The westward drifting current converges with a northward current from along the Mexican coast and turns eastward, where it may be entrained with the Loop Current eddy (Fig. 3.1a). During summer this general circulation pattern often reverses on the outer shelf and flows to the east. (Fig. 3.3.1b) (Cochrane and Kelly, 1986; Ohlmann and Niiler, 2005; Smith

and Jacobs, 2005; Zavala-Hidalgo et al., 2003; Chu et al., 2005). A portion of the northward flowing coastal current on the Texas (TX) shelf extends eastward along the outer LA shelf, further contributing to an eastward circulation pattern for the M-ARs plume (Zavala-Hidalgo et al. 2003) (Morey et al. 2003; Ohlmann and Niiler 2005). The summer pattern of LA shelf circulation is greatly dependent on local wind forcing (Cochrane and Kelly, 1986; Ohlmann and Niiler, 2005; Smith and Jacobs, 2005). Simulation modeling shows this summer pattern was usually common over the past decade (Zhang et al. 2012), including August 2007, which is a base year we use in this study.

The magnitude and spatial extent of plume algal production and bottom water hypoxia are primarily controlled by nitrogen mass export from the M-ARs and secondarily by freshwater flux and the strength of easterly winds on the LA shelf (Green et al., 2008; Scavia et al., 2003; Forrest et al., 2011; Turner et al., 2006). Hypoxic strength and areal extent were markedly different in July 2009 (Turner et al., 2012; Bianchi et al., 2010), however, and were only marginally related to the estimations (Forrest et al., 2011; Evans and Scavia, 2011).

Hydrodynamic modeling suggests that persistent southerly winds along the TX coast shifted coastal circulation patterns (Zhang et al. 2012). This unexpected smaller hypoxia event in July 2009 thus provides a good opportunity to understand how factors other than river freshwater and nutrient fluxes affect the biogeochemical and metabolic processes on the LA shelf.

In this study, we compare two summers with contrasting shelf circulation: August 2007, which we consider typical to July 2009, which we consider unusual. We describe how the biogeochemical processes were affected by shelf circulation using measured data on sea surface salinity and surface water $p\text{CO}_2$ distribution and satellite-derived data on chlorophyll-a concentrations. We discuss how this unusual physical condition affects air-sea CO_2 flux, the

coverage of bottom water hypoxia, and the relationship between dissolved inorganic carbon (DIC) and DO in the bottom water of the LA shelf.

2. Sampling area and methods

Two cruises were conducted during August 18-24, 2007 on board OSV *Bold*, and during July 19-29, 2009 on board R/V *Cape Hatteras* on the LA shelf. The monthly average M-ARs freshwater discharge from July to August was $15,800 \text{ m}^3 \text{ s}^{-1}$ and $17,500 \text{ m}^3 \text{ s}^{-1}$ in 2007 and 2009, respectively. The associated inorganic nitrogen flux in May (time best correlated with plume phytoplankton production) was $1.48 \times 10^{11} \text{ g N}$ in 2007 and $1.55 \times 10^{11} \text{ g N}$ in 2009 (USGS data).

Total alkalinity (TA) and DIC concentrations were determined on water samples collected either from Niskin bottles or from the ship's flow-through system from about 2-m depth. Niskin bottles were usually taken from surface waters and bottom waters on the continental shelf. DIC and TA samples were collected using 250 ml borosilicate glass bottles thoroughly flushed with sample with extensive overflow ($> 125 \text{ mL}$) and preserved with $100\text{-}\mu\text{L}$ HgCl_2 . DIC was measured shortly after the cruise by acidifying 0.5 mL of sample and quantifying the released CO_2 using an infrared gas analyzer (Li-Cor 6252). TA was determined by the Gran titration on a sample volume of 25 mL using a semi-automated system. DIC and TA measurements had a precision of 0.1% (Cai et al., 2010; Huang et al., 2012).

For sea surface salinity and $p\text{CO}_2$ measurements, seawater was sampled from the ship flow-through inlet at 2-m depth. $p\text{CO}_2$ was measured by a flow-through system with a "shower head equilibrator plus a CO_2 analyzer (LI-COR 7000)" (Jiang et al., 2008). The LI-COR[®] 7000 was calibrated every 3.5-6 h using five certified gas standards, which had dry CO_2 values of 0, 197.45, 400.57, and 594.65, and 975.26 ppm referenced against standards traceable to those of

the National Institute of Standards and Technology. Area average of $p\text{CO}_2$ values were gridded to a resolution of $0.1^\circ \times 0.1^\circ$ and were used to calculate the air-sea CO_2 flux by this equation:

$$\text{CO}_2 \text{ Flux} = k \times K_0 \times (p\text{CO}_{2\text{sw}} - \text{CO}_{2\text{air}}) \quad (1)$$

k represents the gas transfer velocity; K_0 is the solubility of CO_2 (Weiss, 1974); $p\text{CO}_{2\text{sw}}$ and $p\text{CO}_{2\text{air}}$ are the $p\text{CO}_2$ in surface seawater and overlying atmosphere, respectively. Their difference expresses the CO_2 gradient ($\Delta p\text{CO}_2$) across the air-sea interface. We applied the QuikSCAT (Quick Scatterometer) ocean surface winds data with a resolution of 0.25° and air-sea gas transfer coefficient estimated by Ho (2006) to calculate air-sea CO_2 fluxes with methods given by Jiang et al. (2008).

3. Results

3.1 Spatial distributions of sea surface salinity and SeaWiFS Chl-a

Distribution of sea surface salinity in August 2007 is typical for the summer season on the LA shelf (Fig 3.2a,b). Salinity is lowest immediately adjacent to southwest pass of the Mississippi river. Salinities less than 30 were found to the east and west of the river's birdfoot delta and extended along the inner shelf towards Texas. The outer shelf between the delta and TX has salinities greater than 30. Overall, lower salinity waters on the inner shelf and higher salinity waters on the outer shelf, demonstrating that the freshwater plume was distributed throughout the inner LA shelf in August 2007 and can be considered as a normal year (Fig. 3.2a). During July 2009, however, lower salinity waters (salinity less than 33) were confined mostly on the eastern shelf (east of 91.5°W) except small pocket areas immediately next to another freshwater source, Atchafalaya Bay. These lower salinity waters were also observed on the outer shelf to pelagic ocean to the east of 91.5°W . On the western shelf, salinity higher than 33 waters

were observed from inner to outer shelves (Fig. 3.2b), demonstrating that the M-ARs plume was promoted to the eastern shelf and offshore in July 2009.

Satellite Chl-a images broke the spatial limitation of ship surveys and also displayed distinct trajectories of the M-ARs plume in summer 2007 and 2009 (Fig. 3.2c, d). High Chl-a concentrations were observed along the coast in summer 2007 (Fig. 3.2c), demonstrating that the plume trajectory was narrow and extending westward along the shore from LA shelf to Texas coast. In contrast, Chl-a distribution was high and extended toward offshore on the eastern LA shelf in July 2009 (Fig. 3.2d), showing the plume trajectory was cross-shelf on the LA shelf and was less observed along Texas coast.

3.2 Water column temperature-salinity diagram

The impact of different circulation patterns between Aug 2007 and July 2009 was also evident in water column temperature to salinity (T-S) distributions. Typically we see low salinity / high temperature in shallow waters along the shelf and high salinity / high temperature in deeper waters just off the shelf (Fig. 3.3a). In contrast, in July 2009, temperature and salinity were both lower on the eastern shelf (indicating more freshwater) while temperature and salinity were both slightly higher on the western shelf. This east-to-west difference in T-S patterns was also consistent with the east-to-west contrast of sea surface salinity distributions in July 2009.

3.3 $p\text{CO}_2$ distributions and air-sea CO_2 fluxes

Surface $p\text{CO}_2$ distributions also differed greatly between August 2007 and July 2009. Typically surface $p\text{CO}_2$ values showed strong cross-shelf gradients (i.e. low in the inner shelf and high in the outer shelf) and a weak alongshore gradient as in August 2007 (Fig. 3.4a). In stark contrast, in July 2009, $p\text{CO}_2$ was high in the western inner shelf, resulting in a strong east-to-west alongshore gradient (i.e. low $p\text{CO}_2$ in the east and high in the west) (Fig. 3.4b). These

spatial patterns in surface $p\text{CO}_2$ and Chl-a in July 2009 were consistent with the distribution of T-S and sea surface salinity, showing that these biogeochemical contrasts were affected by the altered shelf circulation.

To systematically compare air-sea CO_2 fluxes on the LA shelf between the two cruises, the smaller survey area of August 2007 was adopted for reference. We find that the LA shelf acted as weak CO_2 sink to the atmosphere ($-0.98 \text{ mmol m}^{-2} \text{ d}^{-1}$) under normal summer conditions, as in August 2007, but acted as a strong source ($3.31 \text{ mmol m}^{-2} \text{ d}^{-1}$) in July 2009. In particular, the difference between August 2007 and July 2009 was greater in the western area (ΔCO_2 flux = $5.5 \text{ mmol m}^{-2} \text{ d}^{-1}$) than in the eastern area (ΔCO_2 flux = $2.8 \text{ mmol m}^{-2} \text{ d}^{-1}$). This large difference in behavior was mainly due to the difference in $p\text{CO}_2$ levels in the western area between years (Table 1).

3.4 Bottom water DO and DIC

Bottom water DO and DIC distributions also varied between August 2007 (alongshore) and July 2009 (Fig. 3.5). Typically, hypoxic bottom waters stretch alongshore following the 20-45 m isobaths on the LA shelf, as in August 2007. In August 2007 areal hypoxic water coverage was $\sim 20,000 \text{ km}^2$ (Fig. 3.5a). In contrast, bottom water hypoxia was only observed on the eastern shelf in July 2009, displaying a smaller hypoxic area of only $\sim 4,000 \text{ km}^2$ near the Mississippi River mouth (Fig. 3.5b). Consistent with the DO distribution, highest DIC concentrations were distributed in bottom waters along the 20-45 m isobaths with greatly reduced areal coverage in July 2009 (Fig. 3.5c, d). In summary, the distribution of hypoxia was consistent with the surface distribution of sea surface salinity and $p\text{CO}_2$, i.e. alongshore in August 2007 and confined to the eastern shelf in July 2009.

4. Discussion

4.1 Surface shelf circulation and wind forcing in summer

Wind forcing and shelf circulation differed greatly between August 2007 and July 2009. We used QuikSCAT wind fields (Fig. 3.6a, b) to demonstrate wind forcing, and applied the HYCOM (Hybrid Coordinate Ocean Model, the Naval Research Laboratory) modeled sea surface currents (Fig. 3.6c, d) to illustrate shelf circulation patterns in August 2007 and July 2009. The monthly average wind field was easterly and weak over the entire Gulf of Mexico in August 2007, which is typical (Fig. 3.6a). The modeled shelf circulation in August 2007 (Fig. 3.6c) was also typical of summer shelf circulation (Fig. 3.1d). The typically strong alongshore components tend to confine the M-ARs plume to the inner shelf (Fig. 3.1b). In contrast, this wind forcing was clockwise over the Gulf of Mexico in July 2009, showing mostly southerly winds along the TX and LA coasts (Fig. 3.6b). This wind forcing was favorable for the northward coastal current running up along Texas and over to LA and also for cross-shelf components near the Mississippi River delta (Fig. 3.6d) (Lentz and Fewings, 2012). The major difference in circulation between summer 09 and 07 were: 1) the strength of the eastward/westward current on the outer LA shelf, and 2) the strength of the northward coastal current from TX to LA (Fig. 3.6c, d).

We conceptualize shelf circulation for July 2009 (Fig. 3.7) with a particularly strong inner coastal current from the southern Texas coast to the inner western LA shelf (Fig. 3.7). By comparing this modeled shelf circulation (Fig. 3.6d) to the distribution of T-S (Fig. 3.3), we see high salinity waters on the western inner shelf were likely affected by the intrusion of the stronger coastal current up from the TX coast. This inner shelf coastal current turned off shelf and joined the Loop Current eddies on the outer shelf between longitude 91° to 92° W. These

cross-shelf components would have been favorable for the transport of M-ARs plume waters across the shelf (Fig. 3.7).

The HYCOM modeled cross-shelf circulation for July 2009 was consistent with the east-west contrasts in the distributions of sea surface salinity and $p\text{CO}_2$ (Fig. 3.2b, d). Both HYCOM and measurement distribution were consistent with the modeled distribution of M-ARs freshwater in July 2009 (Zhang et al. 2012). Relationship between this shelf circulation characterized by cross-shelf components and southerly wind forcing was also suggested by Zhang et al. (2012) and Chu et al. (2005).

4.2 The biogeochemical impact on plume and surface waters

Shelf circulation and the location and strength of river inputs obviously plays a major role in the resultant distributions of surface $p\text{CO}_2$ and the air-sea CO_2 fluxes in this region as well as the distribution of primary production (Chen et al., 2000). Net primary production in the plume draws down CO_2 (Williams and Follows, 2003), leaving under-saturated $p\text{CO}_2$ values with respect to the atmosphere. These under-saturated $p\text{CO}_2$ waters are typically distributed alongshore, as we observed in August 2007 and in previous summer studies (Lohrenz et al., 2010; John et al., 2007; Lohrenz and Cai, 2006). However, the relocated plume trajectory under the altered shelf circulation in July 2009 may have changed the location of enhanced primary production and organic carbon export (i.e. from locating westward along the LA shelf to locating offshore and around the Mississippi River birdfoot delta). In shifting the region of CO_2 drawdown (from net primary production), the more western shelf area shifted from being a weak CO_2 sink for the atmosphere to as a strong CO_2 source during summer. Obviously if shelf circulation controls the distribution of primary production (Chen et al., 2000) it will also control the distribution of sea surface $p\text{CO}_2$.

4.3 The impact of shifting biological production on bottom-water hypoxia

Bottom-water hypoxia coverage was different between these two summers and corresponded to surface under-saturated $p\text{CO}_2$ area, i.e. it was along LA shelf in August 2007 and was limited to the eastern shelf only in July 2009. The difference of hypoxia coverage was not only observed by this study but also observed by Rabalais et al. on the “Hypoxia in the Northern Gulf of Mexico” (<http://www.gulfhypoxia.net/>), i.e. 20,500 km² during 12-19 July 2007 and 8,000 km² during 12-19 July 2009. Based on the estimation made by the M-ARs riverine nitrogen flux in May, the summer hypoxia coverage was expected to be large (~23,500 km²) in July 2009 (Turner et al., 2012), implying there was enough riverine nutrient-driven supply of organic material, so called “hypoxic potential” (Hetland and DiMarco, 2008), to support a large hypoxic area in July 2009. However, the M-ARs plume path was shifted to the eastern shelf and offshore areas in July 2009 and thus changed the location of hypoxic potential. In addition, the stratification was stronger in the surface 20-m waters and the corresponding DO concentrations were mostly below 2 mg L⁻¹ in the bottom water in August 2007. This so called “stratification envelope” (Hetland and DiMarco, 2008) was evident on the eastern shelf. Since hypoxic potential was relocated and the coverage of stratification envelope was reduced due to the altered shelf circulation in July 2009, the coverage of hypoxia was only observed when the distribution of hypoxic potential and stratification envelope overlapped. Thus, the hypoxic potential was only effective when they overlapped with stratification envelope.

Based on the variation of M-ARs plumes between these two cruises, we suggest that the regional wind forcing induced shelf circulation was important to the hypoxia coverage. Our conclusion was consistent with earlier finding that hypoxia area was affected by large scale circulation (Wiseman et al., 1997), and was also consistent with the importance of easterly wind

in the estimation of hypoxia coverage in addition to river discharge and nitrogen concentration (Forrest et al., 2011; Feng et al., 2012).

4.4 Bottom water DO-to-DIC relationships

4.4.1 The association with shelf circulations

Bottom water distributions of DO- and-DIC reflect the combined results of circulation and mixing of water masses and the strength and location of primary production and community respiration. In August 2007, the bottom water DO-to-salinity and DIC-to-salinity relationships showed freshwater water - seawater mixing processes that mirrored each other (Fig. 3.8a, b). To better illustrate the effect of this mixing on DO and DIC, we analyze bottom waters along the 10 and 20 m isobaths, which parallels the trajectory of plume waters and encompasses much of hypoxic zone (Fig. 3.5a, c). Bottom waters inshore of this zone varied greatly in salinity and were biogeochemically similar in composition to the river end-member (low salinity, shallow depth, and high DO). We define these inner waters as “brackish waters”. Bottom waters offshore the 20 m isobath showed small variation of salinity (< 0.4) and were similar in composition to the open ocean end-member (high salinity, deeper depth and high DO). We define these waters as “high salinity waters”. During this river-to-sea mixing process, brackish waters and high salinity waters independently demonstrated strong DO and DIC relationships with slopes similar but opposite concentrations (Fig. 3.8c, d). In a previous study measuring $\delta^{13}\text{C}$ of DIC, two water masses have been distinguished as inshore (less than 10-m isobath) and offshore (more than 20-m isobaths) (Strauss et al. 2012) and are similar to our DO-to-DIC results.

While the mixing behavior and two water masses were still observed in July 2009 (Fig. 3.9), their locations were different from August 2007. Similar to August 2007 mixing behavior discussed above, O_2 consumption and DIC production appeared at various salinities, mostly one

group in high salinity waters and another group in low salinity waters (Fig. 3.9c). However, these two water masses were not separated by the alongshore isobath zone (10 to 20 m) as in August 2007. Instead, these two water masses were characterized by the shelf circulation mostly with a contrast between the eastern (brackish waters) and western (high salinity) shelf. Additionally, the association of the increasing DO from deeper waters (as observed in August 2007) was not so clear in July 2009 (Fig. 3.9d).

4.4.2 The DO and DIC relationships

In general, DO-to-DIC relationships are determined by the respiration of organic matter in the water when it is isolated from mixing and air-sea gas exchange. The ratios of DO-to-DIC relationships in August 2007 were close to the prediction of Redfield respiration, i.e. the C/O molar ratio is 106/138 (Redfield, 1958). Previous studies have showed that water column respiration and benthic respiration dominated bottom water oxygen consumption (Hetland and DiMarco, 2008; Quiñones-Rivera et al., 2010). For benthic respiration, sediment was also dominated by phytoplankton and zooplankton fecal exporting from the M-ARs plume (Quiñones-Rivera et al., 2007). Strauss et al. (2012) also observed Redfield stoichiometry respiration in their analysis of the $\delta^{13}\text{C}$ and DO relationship on the inner LA shelf. Furthermore, mixing of water masses could modify or even completely change the respiration signals. A large DIC variation (100 μM) was observed in the hypoxic area between isobaths 10 and 20 m in August 2007 (Fig. 3.8c). This was most likely due to the mixing between the brackish (lower DIC and low DO) and high salinity waters (higher DIC and low DO). On the Gulf of Trieste, Cantoni et al. (2012) also observed a large DIC variation (100 $\mu\text{mol L}^{-1}$) associated with a narrow DO range (30 $\mu\text{mol L}^{-1}$) in surface and subsurface waters, and suggested the DIC variation was mostly affected by mixing between water masses while DO concentrations were

similar for those two water masses. Furthermore, for the high salinity waters, the increasing DO or decreasing DIC concentrations were generally corresponded to increasing depths (Fig. 3.8d), suggesting that such respiration processes were occurred cross-shelf. To sum up, both water mass demonstrated that hypoxia was a source of DIC through Redfield-type respiration.

But the DIC concentration in hypoxic waters in July 2009 was higher than the prediction from Redfield-type respiration. The formation of such higher DIC might be a complex physical and biogeochemical process: first, DIC concentration increased through Redfield-type respiration under stratification; but second, when the water column was de-stratified, DIC could remained in water while DO could be compensated from air-sea exchanges rapidly. This is because a rapid gas transfer velocity for O₂ than carbonate system (Sarmiento and Gruber, 2006; Cai et al., 1999); and mostly importantly the carbon system has a strong buffering on CO₂ concentration. This allows O₂ to be resupplied rapidly and be CO₂ produced during the subsequent stratification and respiration. Thus, this high DIC concentration might be a result of accumulation through repetition between stratification (increase DIC and decrease DO) and de-stratification (slow DIC loss and rapid DO resupply).

4.4.3 Comparison with other coastal systems

In two other coastal systems, Gulf of Trieste and Gulf of California, AOU (Apparent Oxygen Utilization) and DIC relationships in subsurface waters have also been reported (Cantoni et al., 2012; Maske et al., 2010). The slopes of these AOU-DIC relationships were close to Redfield stoichiometry respiration in these two systems. Previous studies also revealed that about 70% of POC in the sedimentation was also converted to DIC through respiration and sediment remobilization on the LA shelf (Green et al., 2006; Rowe et al., 2002). Therefore, respiration was the major source of DIC in the bottom water, especially when hypoxia occurs. As the hypoxia

was occurred under stratification, these high DIC concentrations could be stored in these hypoxic bottom water (Taguchi and Fujiwara, 2010). The LA shelf system was unique to the others two systems because there were two bottom water DO-to-DIC relationships (i.e. two water masses) in this system. This is because the exist of brackish water between freshwater discharge and seawater also displayed a DO-to-DIC relationship. As these brackish waters had potential to accumulate DIC and thus resulted in low pH values to acidify the water and affect the ecosystem, these waters needs further investigation to better understand its relationship with other effects, such as respiration, mixing, remaining effects from air-sea gas exchange, and possible mobile muds (Allison et al., 2000; Corbett et al., 2006; Bianchi et al., 2010).

5. Summary

Shelf circulation plays a major role in the distribution of biological communities, community metabolism, and the biogeochemical properties, such as salinity, Chl-a, and $p\text{CO}_2$ and DIC values on the LA shelf. Deviations from normal climatology can have a profound influence on the typical distribution of these properties and processes in summer. Under typical summer conditions as in August 2007, the M-ARs plume is confined on the shelf, showing alongshore gradients. Under different climatological conditions however, we have seen that the M-ARs plume does not move westward but is confined to the eastern LA shelf, with significant cross-shelf exchange, as in July 2009. These shelf circulations were highly related to local wind forcing, e.g. typical easterly winds were observed in August 2007 and southerly winds were observed in July 2009. Changes in shelf circulation resulted in shifting the LA shelf from a neutral to a weak source of atmospheric CO_2 . The different circulation pattern also caused a shift in where the plume algal bloom sedimented out. In 2009 this resulted hypoxia being

confined just off the Mississippi River delta and a decrease in the areal extent of bottom water hypoxia. Therefore, we suggest that hypoxia potential was only effective when these hypoxia potential was overlapped with stratification envelope. Such shelf circulation altered effective hypoxia potential was the reason that the bottom water hypoxic area was smaller than predicted in July 2009.

Bottom water DO-to-DIC relationship also reflected shelf circulations, i.e. this relationship can be observed individually in brackish waters and in sea waters. Both of these two waters were distributed alongshore and were separated by a zone between isobath 10 and 20 m in August 2007. Such DO-to-DIC relationships were still observed in these two waters, respectively, in July 2009. However, the alongshore distribution in August 2007 was altered in July 2009. DO-to-DIC relationships were mostly dominated by river-sea mixing and respiration. The slopes of DO-to-DIC relationships were close to the prediction of Redfield respiration in August 2007. But accumulated high DIC concentration was observed in July 2009, probably through frequent repetition between stratification (Redfield-type respiration) and de-stratification (rapid DO compensatory than carbonate system).

We conclude that while the distribution and areal extent of shelf bottom water hypoxia are well predicted by river N flux under typical summer conditions, climatological events can shift both the magnitude and location of hypoxic waters. A shift in circulation regimes brought about by altered climatology can also alter the spatial distribution of air-sea CO₂ fluxes. Regional climate change will likely have a large impact on coastal biogeochemical processes in this region of the northern Gulf of Mexico brought about by altered wind regimes shelf circulation.

References

- Allison, M. A., Kineke, G. C., Gordon, E. S., and Goñi, M. A.: Development and reworking of a seasonal flood deposit on the inner continental shelf off the Atchafalaya River, *Cont. Shelf Res.*, 20, 2267-2294, 2000.
- Bianchi, T. S., DiMarco, S. F., Cowan, J. H. Jr., Hetland, R. D., Chapman, P., Day, J. W., and Allison, M. A.: The science of hypoxia in the Northern Gulf of Mexico: A review, *Sci. Total Environ.*, 408, 1471-1484, 2010.
- Cai, W.-J., Pomeroy, L. R., Moran, M. A., and Wang, Y.: Oxygen and carbon dioxide mass balance for the estuarine-intertidal marsh complex of five rivers in the southeastern U.S., *Limnol. Oceanogr.*, 44, 639-649, 1999.
- Cai, W.-J., Dai, M., and Wang, Y. C.: Air-sea exchange of carbon dioxide in ocean margins: A province-based synthesis, *Geophys. Res. Lett.*, 33, L12603, 2006.
- Cai, W.-J., Hu, X., Huang, W.-J., Jiang, L.-Q., Wang, Y., Peng, T.-H., and Zhang, X.: Alkalinity distribution in the western North Atlantic Ocean margins, *J. Geophys. Res.*, 115, C08014, 10.1029/2009jc005482, 2010.
- Cai, W.-J.: Estuarine and coastal ocean carbon paradox: CO₂ sinks or sites of terrestrial carbon incineration?, *Annu. Rev. Marine Sci.*, 3, 123-145, doi:10.1146/annurev-marine-120709-142723, 2011.
- Cantoni, C., Luchetta, A., Celio, M., Cozzi, S., Raicich, F., and Catalano, G.: Carbonate system variability in the Gulf of Trieste (North Adriatic Sea), *Estuar. Coast. Shelf S.*, doi: 10.1016/j.ecss.2012.07.006, 2012.

- Chen, C.-T. A., and Borges, A. V.: Reconciling opposing views on carbon cycling in the coastal ocean: Continental shelves as sinks and near-shore ecosystems as sources of atmospheric CO₂, *Deep-Sea Res. II*, 56, 578-590, 2009.
- Chen, X., Lohrenz, S. E., and Wiesenburg, D. A.: Distribution and controlling mechanisms of primary production on the LA-Texas continental shelf, *J. Marine Syst.*, 25, 179-207, 2000.
- Chu, P. P., Ivanov, L. M., and Melnichenko, O. V.: Fall–winter current reversals on the Texas–LA continental shelf, *J. Phys. Oceanogr.*, 35, 902-910, 10.1175/jpo2703.1, 2005.
- Cochrane, J. D., and Kelly, F. J.: Low-frequency circulation on the Texas-LA continental shelf, *J. Geophys. Res.-Oc. Atm.*, 91(9), 10645-10659, 10.1029/JC091iC09p10645, 1986.
- Corbett, D. R., McKee, B., and Allison, M.: Nature of decadal-scale sediment accumulation on the western shelf of the Mississippi River delta, *Cont. Shelf Res.*, 26, 2125-2140, 10.1016/j.csr.2006.07.012, 2006.
- Evans, M. A., and Scavia, D.: Forecasting hypoxia in the Chesapeake Bay and Gulf of Mexico: model accuracy, precision, and sensitivity to ecosystem change, *Environ. Res. Lett.*, 6, 015001, 2011.
- Feng, Y., DiMarco, S. F., and Jackson, G. A.: Relative role of wind forcing and riverine nutrient input on the extent of hypoxia in the northern Gulf of Mexico, *Geophys. Res. Lett.*, 39, L09601, 10.1029/2012gl051192, 2012.
- Forrest, D. R., Hetland, R. D., and DiMarco, S. F.: Multivariable statistical regression models of the areal extent of hypoxia over the Texas–LA continental shelf, *Environ. Res. Lett.*, 6, 045002, 2011.
- Green, R. E., Bianchi, T. S., Dagg, M. J., Walker, N. D., and Breed, G. A.: An organic carbon budget for the Mississippi River turbidity plume and plume contributions to air-sea CO₂

- fluxes and bottom water hypoxia, *Estuaries Coasts*, 29, 579-597, 10.1007/BF02784284, 2006.
- Green, R. E., Breed, G. A., Dagg, M. J., and Lohrenz, S. E.: Modeling the response of primary production and sedimentation to variable nitrate loading in the Mississippi River plume, *Cont. Shelf Res.*, 28, 1451-1465, 2008.
- Hetland, R. D., and DiMarco, S. F.: How does the character of oxygen demand control the structure of hypoxia on the Texas-LA continental shelf?, *J. Marine Syst.*, 70, 49-62, 2008.
- Ho, D. T., Law, C. S., Smith, M. J., Schlosser, P., Harvey, M., and Hill, P.: Measurements of air-sea gas exchange at high wind speeds in the Southern Ocean: Implications for global parameterizations, *Geophys. Res. Lett.*, 33, L16611, 10.1029/2006gl026817, 2006.
- Huang, W.-J., Wang, Y., and Cai, W.-J.: Assessment of sample storage techniques for total alkalinity and dissolved inorganic carbon in seawater, *Limnol. Oceanogr. Methods*, 10, 711-717, 10.4319/lom.2012.10.711, 2012.
- Jiang, L.-Q., Cai, W.-J., Wang, Y., Wanninkhof, R., and Lüger, H.: Air-sea CO₂ fluxes on the U.S. South Atlantic Bight: Spatial and seasonal variability, *J. Geophys. Res.*, 113, C07019, 10.1029/2007jc004366, 2008.
- John, D. E., Wang, Z. A., Liu, X., Byrne, R. H., Corredor, J. E., Lopez, J. M., Cabrera, A., Bronk, D. A., Tabita, F. R., and Paul, J. H.: Phytoplankton carbon fixation gene (RuBisCO) transcripts and air-sea CO₂ flux in the Mississippi River plume, *ISME J*, 1, 517-531, 2007.
- Lentz, S. J., and Fewings, M. R.: The wind- and wave-driven inner-Shelf circulation, *Annu. Rev. Mar. Sci.*, 4, 317-343, 10.1146/annurev-marine-120709-142745, 2012.
- Lohrenz, S. E., and Cai, W.-J.: Satellite ocean color assessment of air-sea fluxes of CO₂ in a river-dominated coastal margin, *Geophys. Res. Lett.*, 33, L01601, 2006.

- Lohrenz, S. E., Cai, W.-J., Chen, F., Chen, X., and Tuel, M.: Seasonal variability in air-sea fluxes of CO₂ in a river-influenced coastal margin, *J. Geophys. Res.*, 115, C10034, 10.1029/2009jc005608, 2010.
- Maske, H., Medrano, R. C., Castro, A. T., Mercado, A. J., Jauregui, C. O. A., Castro, G. G., and Ochoa, J.: Inorganic carbon and biological oceanography above a shallow oxygen minimum in the entrance to the Gulf of California in the Mexican Pacific, *Limnol. Oceanogr.*, 55, 481-491, doi: 10.4319/lo.2010.55.2.0481, 2010.
- Morey, S. L., Schroeder, W. W., O'Brien, J. J., and Zavala-Hidalgo, J.: The annual cycle of riverine influence in the eastern Gulf of Mexico basin, *Geophys. Res. Lett.*, 30, 1867, 2003.
- Ohlmann, J. C., and Niiler, P. P.: Circulation over the continental shelf in the northern Gulf of Mexico, *Prog. Oceanogr.*, 64, 45-81, 2005.
- Quiñones-Rivera, Z. J., Wissel, B., Justic, D., and Fry, B.: Partitioning oxygen sources and sinks in a stratified, eutrophic coastal ecosystem using stable oxygen isotopes, *Mar. Ecol.-Prog. Series*, 342, 69-83, 10.3354/meps342069, 2007.
- Quiñones-Rivera, Z. J., Wissel, B., Rabalais, N. N., and Justic, D.: Effects of biological and physical factors on seasonal oxygen dynamics in a stratified, eutrophic coastal ecosystem, *Limnol. Oceanogr.*, 55, 289-304, 10.4319/lo.2010.55.1.0289, 2010.
- Rabalais, N. N., Turner, R. E., Justic, D., Dortch, Q., Wiseman, W., and Sen Gupta, B.: Nutrient changes in the Mississippi River and system responses on the adjacent continental shelf, *Estuaries Coasts*, 19, 386-407, 1996.

- Rabalais, N. N., Diaz, R. J., Levin, L. A., Turner, R. E., Gilbert, D., and Zhang, J.: Dynamics and distribution of natural and human-caused hypoxia, *Biogeosciences*, 7, 585-619, 10.5194/bg-7-585-2010, 2010.
- Rabouille, C., Conley, D. J., Dai, M. H., Cai, W. J., Chen, C. T. A., Lansard, B., Green, R., Yin, K., Harrison, P. J., Dagg, M., and McKee, B.: Comparison of hypoxia among four river-dominated ocean margins: The Changjiang (Yangtze), Mississippi, Pearl, and Rhône rivers, *Cont. Shelf Res.*, 28, 1527-1537, 2008.
- Redfield, A. C.: The biological control of chemical factors in the environment, *Am. Sci.*, 46, 205-221, 1958.
- Rowe, G., Kaegi, M., Morse, J., Boland, G., and Escobar Briones, E.: Sediment community metabolism associated with continental shelf hypoxia, Northern Gulf of Mexico, *Estuaries Coasts*, 25, 1097-1106, 2002.
- Sarmiento, Jorge Louis, and Nicolas Gruber. *Ocean biogeochemical dynamics*. Vol. 503. Princeton, New Jersey, USA: Princeton University Press, 2006.
- Scavia, D., Rabalais, N. N., Turner, R. E., Justić, D., and William J. Wiseman, J.: Predicting the Response of Gulf of Mexico hypoxia to variations in Mississippi River nitrogen load, *Limnol. Oceanogr.*, 48(3), 951-956, 2003.
- Smith, S. R., and Jacobs, G. A.: Seasonal circulation fields in the northern Gulf of Mexico calculated by assimilating current meter, shipboard ADCP, and drifter data simultaneously with the shallow water equations, *Cont. Shelf Res.*, 25, 157-183, 2005.
- Strauss, J., Grossman, E. L., and DiMarco, S. F.: Stable isotope characterization of hypoxia-susceptible waters on the LA shelf: Tracing freshwater discharge and benthic respiration, *Cont. Shelf Res.*, 47, 7-15, doi: 10.1016/j.csr.2012.07.020, 2012.

- Taguchi, F., and Fujiwara, T.: Carbon dioxide stored and acidified low oxygen bottom waters in coastal seas, Japan, *Estuar. Coast. Shelf S.*, 86, 429-433, 10.1016/j.ecss.2009.07.037, 2010.
- Turner, R. E., Rabalais, N. N., and Justic, D.: Predicting summer hypoxia in the northern Gulf of Mexico: Riverine N, P, and Si loading, *Mar. Pollut. Bull.*, 52, 139-148, 10.1016/j.marpolbul.2005.08.012, 2006.
- Turner, R. E., Rabalais, N. N., and Justić, D.: Predicting summer hypoxia in the northern Gulf of Mexico: Redux, *Mar. Pollut. Bull.*, 64, 319-324, 10.1016/j.marpolbul.2011.11.008, 2012.
- Weiss, R. F.: Carbon dioxide in water and seawater: The solution of a non-ideal gas., *Mar. Chem.*, 2, 203-215, 1974.
- Williams, R. G., and Follows, M. J.: Physical transport of nutrients and the maintenance of biological production ocean biogeochemistry, in, edited by: Fasham, M. J. R., *Global Change — The IGBP Series (closed)*, Springer Berlin Heidelberg, 19-51, 2003.
- Wiseman, W. J., Rabalais, N. N., Turner, R. E., Dinnel, S. P., and MacNaughton, A.: Seasonal and interannual variability within the LA coastal current: stratification and hypoxia, *J. Marine Syst.*, 12, 237-248, 1997.
- Zavala-Hidalgo, J., Morey, S. L., and O'Brien, J. J.: Seasonal circulation on the western shelf of the Gulf of Mexico using a high-resolution numerical model, *J. Geophys. Res.*, 108, 3389, 10.1029/2003JC001879, 2003.
- Zhang, X., Hetland, R. D., Marta-Almeida, M., and DiMarco, S. F.: A numerical investigation of the Mississippi and Atchafalaya freshwater transport, filling and flushing times on the Texas-Louisiana Shelf, *J. Geophys. Res.*, 117, C11009, 10.1029/2012jc008108, 2012.

Table 3.1. Average $p\text{CO}_2$ (μatm) and air-sea CO_2 fluxes ($\text{mmol m}^{-2} \text{d}^{-1}$, positive values are CO_2 sources to the atmosphere) in the reference area and western and eastern areas.

	Reference area		Western area	Eastern area
	$p\text{CO}_2$	CO_2 flux	CO_2 flux	CO_2 flux
August 2007	347.8	-0.98	-0.1	-2.0
July 2009	403.7	3.31	5.4	0.8
ΔCO_2 flux		4.29	5.5	2.8

The reference area is the same as the survey area in August 2007. The western and eastern LA shelves were divided by longitude 91.5°W .

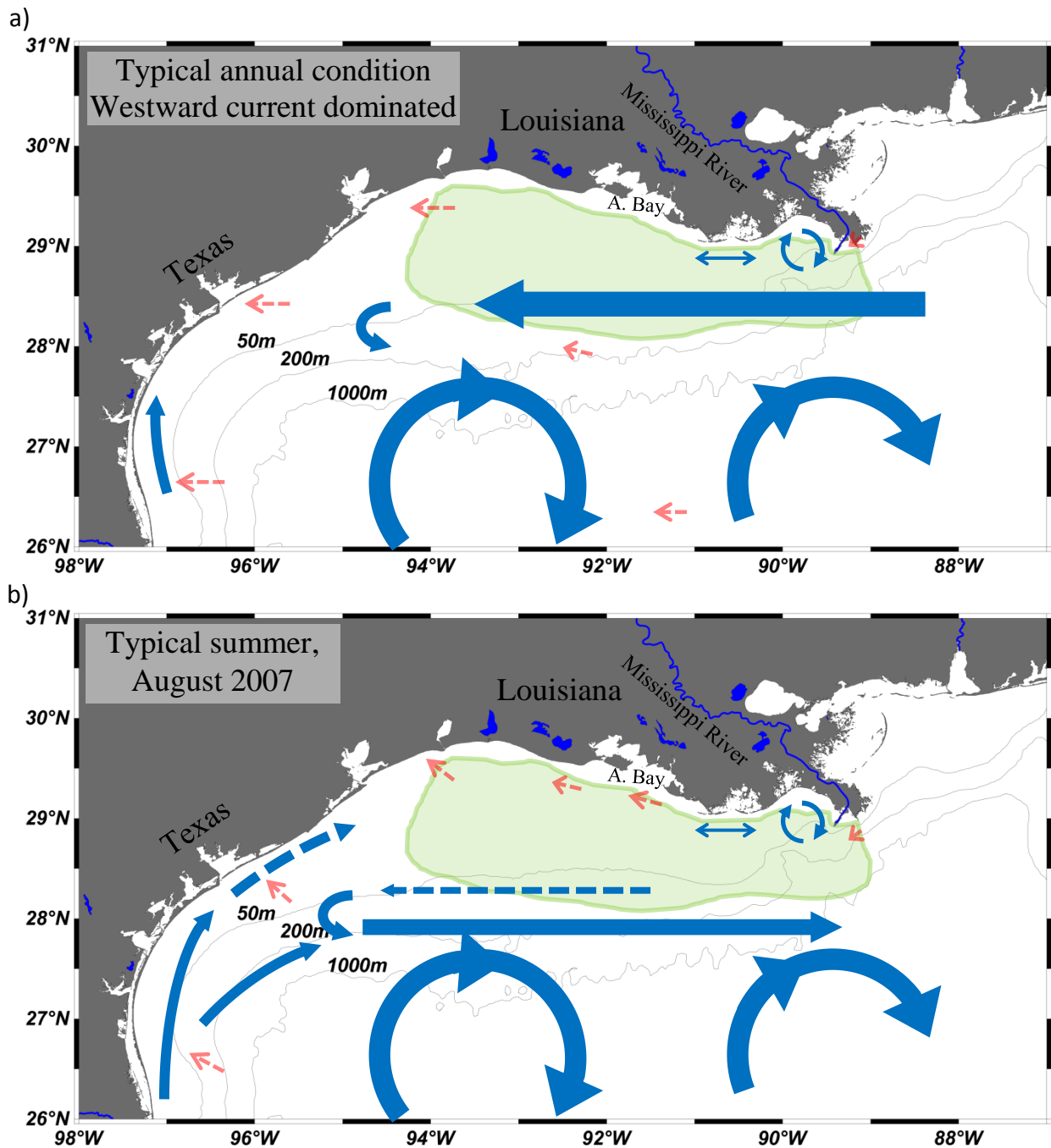


Figure 3.1. Conceptual shelf circulations (blue arrows), wind distributions (red dash arrows), and the distribution of MARS plume (the green area) on the Louisiana-Texas shelf. a) displayed the typical annual shelf circulation: a westward coastal current dominated the shelf circulation under easterly wind forcing and diminished along Texas or returned to join Loop Current eddies. The

near coast current between the Atchafalaya Bay and the Terrebone Bay may go back and forth. A weaker northward coast current along Texas coast diminished before reaching latitude 28°N. b) showed a typical summer shelf circulation in August 2007: this weak northward current along the Taxes coast would split to a weak current in the inner shelf and a stronger coastal current on the outer shelf, resulting in an eastward current confined the MARS plume on the Louisiana Shelf. Such inversed current (eastward) was mostly reported in summer and also during fall to winter (Chu et. al., 2005).

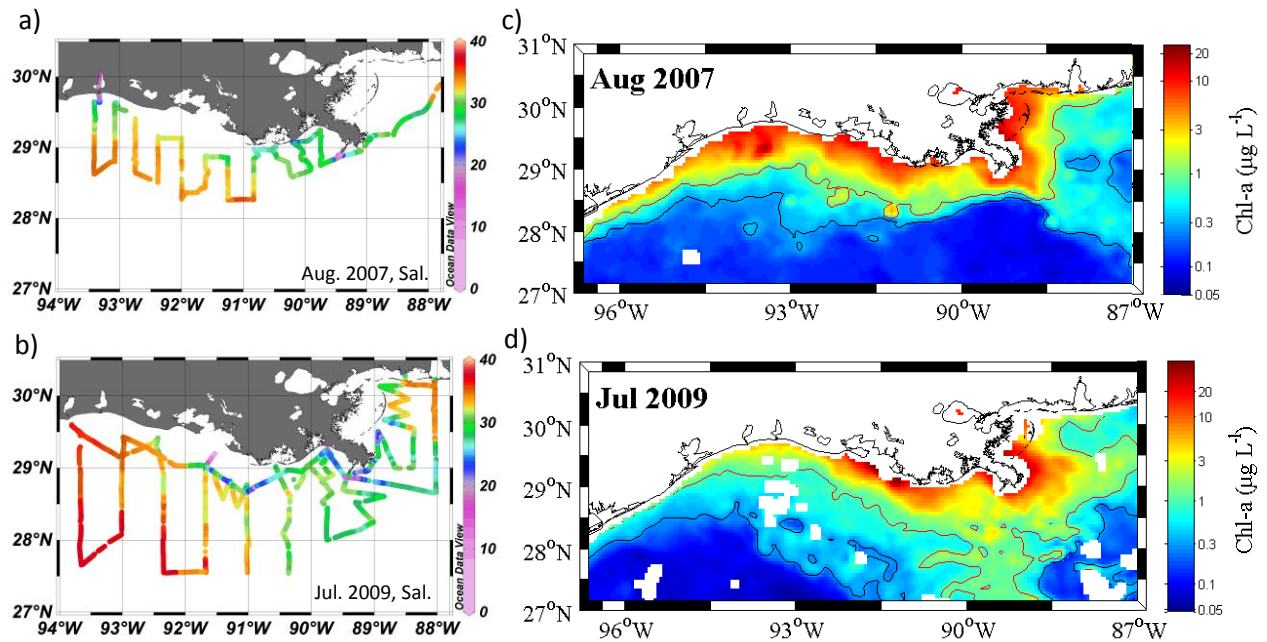


Figure 3.2. Distribution of surface seawater salinity and satellite monthly Chl-a. In August 2007 (a), low salinity waters were distributed on the inner shelf, and high salinity waters were distributed on the outer shelf. In July 2009 (b), low salinity waters were distributed mostly to the eastern shelf (both inner and outer); high salinity waters were observed on the western part of the inner shelf, except the Atchafalaya Bay and its adjacent areas. Satellite monthly Chl-a concentrations with contour lines of 0.3 (black) and 1 $\mu\text{g L}^{-1}$ (red) displayed an alongshore trajectory of MARS plume in August 2007 (c from SeaWiFS) and a cross-shelf plume on the LA shelf for July 2009 (d from MODIS). We used MODIS for July 2009, because the SeaWiFS Chl-a image was affected by cloud in the study area.

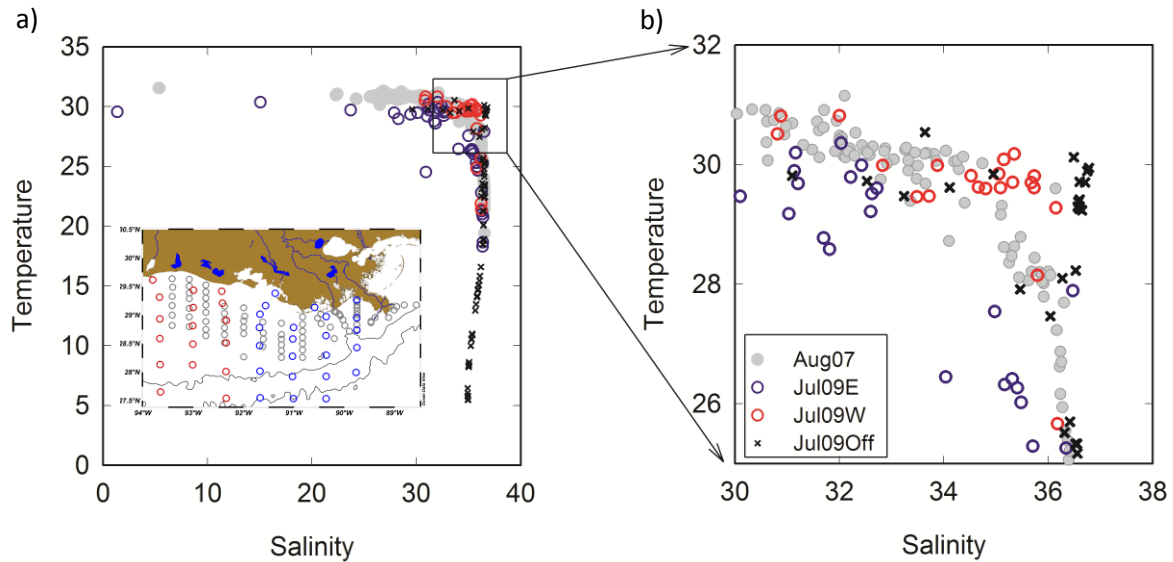


Figure 3.3. Temperature to salinity diagram during August 2007 (gray solid dots) and July 2009 (empty dots), displaying the mixing process between fresh water and deep seawaters (a) with its corresponding station map (the inserted figure in a). An enlarged diagram (b) focusing on the continental shelf, showing the variation of T-S relationship between August 2007 and July 2009. The temperature and salinity of the western shelf waters (red dots) were higher than waters in August 2007 and was close to those waters from outer shelf, suggesting the waters on the western shelf were affected by outer shelf waters. The temperature and salinity from the eastern shelf (blue dots) were generally lower than waters in August 2007, showing a “shortcut” mixing process between freshwater and deep seawaters.

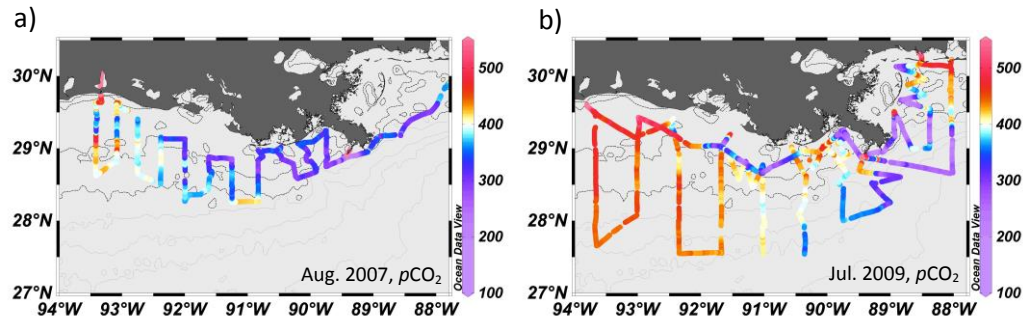


Figure 3.4. Distributions of sea surface $p\text{CO}_2$. Lower $p\text{CO}_2$ waters were also found in the inner shelf and higher $p\text{CO}_2$ were located in the outer shelf in August 2007 (a), except the waters in the Mississippi River channel and near the Lake showed high $p\text{CO}_2$. In contrast, low $p\text{CO}_2$ waters were observed in the eastern shelf (from inner to outer shelf) and high $p\text{CO}_2$ were observed in the western shelf. The distributions of sea surface $p\text{CO}_2$ showed the MARS plume was narrow and along shore in August 2007 but was promoted to the eastern shelf in July 2009.

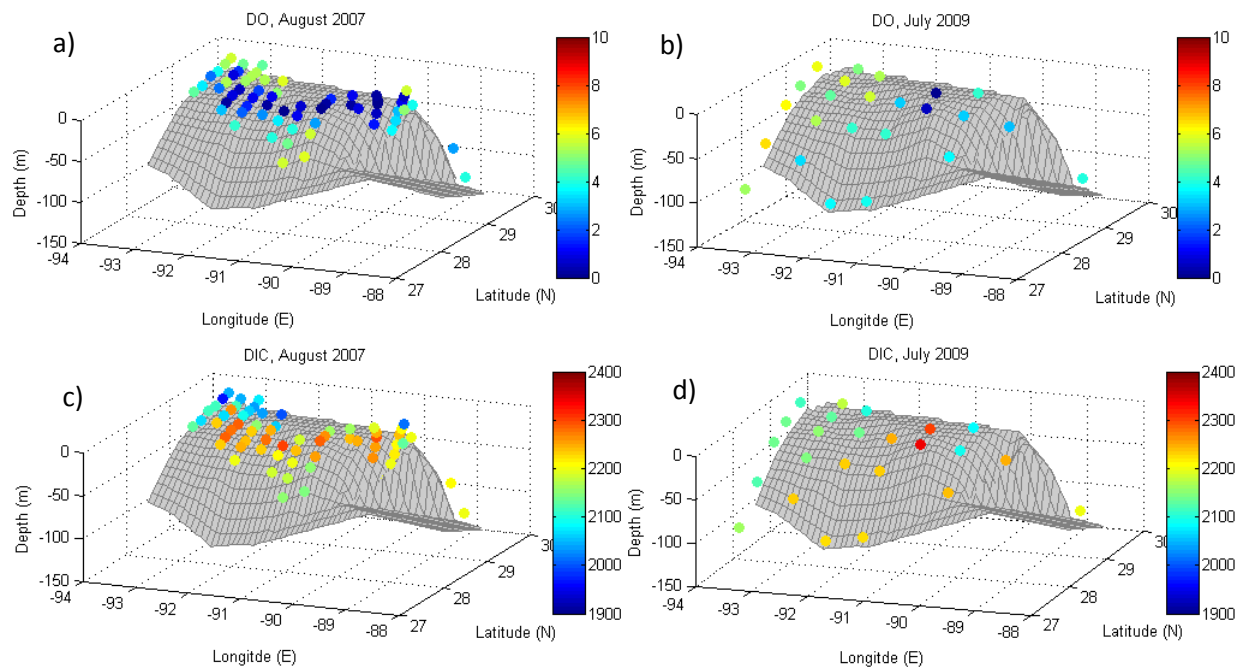


Figure 3.5. Spatial distributions of bottom-water DO (mg L^{-1}) and DIC (μM) concentrations on the Louisiana Shelf. Hypoxic water ($\text{DO} < 2 \text{ mg L}^{-1}$) (a) and high DIC concentrations (b) were observed along the coast in August 2007. In contrast, this situation was only found in the vicinity of the Atchafalaya Bay in July 2009 (c, d).

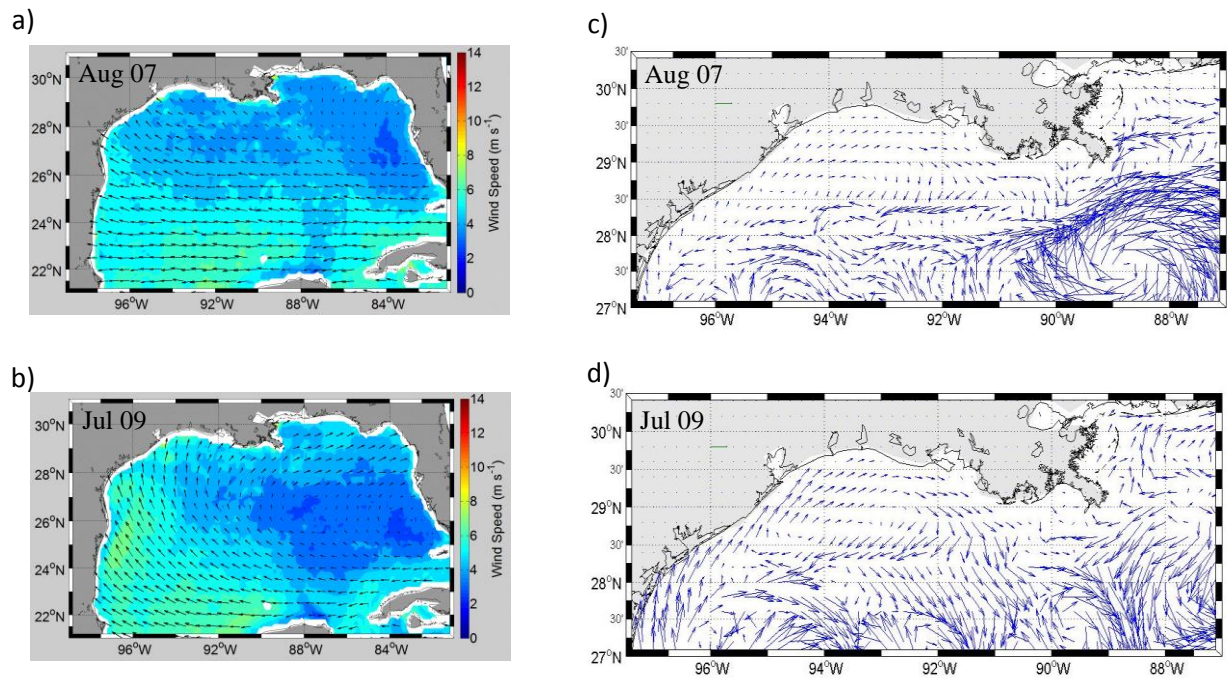


Figure 3.6. Distributions of HYCOM simulated surface currents and wind forcing. Easterly winds dominated the Gulf of Mexico in August 2007 (a) and a clockwise cyclonic wind forcing dominated in July 2009, resulting in southerly wind dominated the Louisiana-Texas shelf (b). The shelf circulation was dominated by eastward and westward current in August 2007 (c) and was dominated by more cross-shelf components in July 2009 (d).

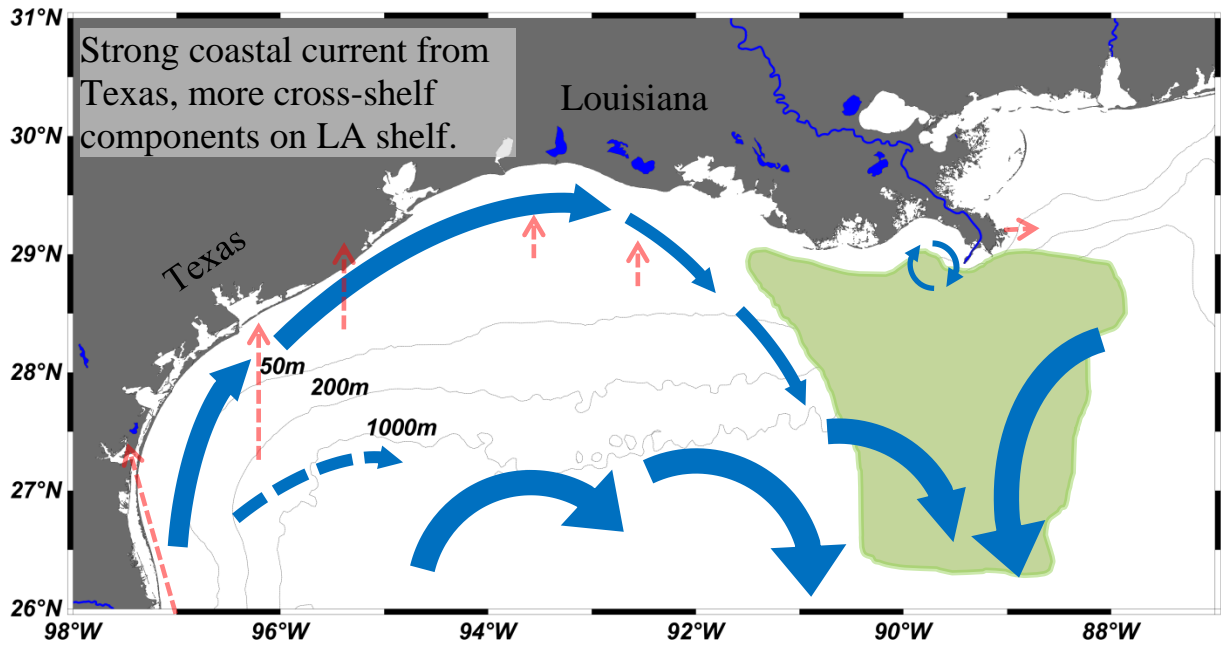


Figure 3.7. Conceptual shelf circulation in July 2009. This shelf circulation was characterized by the strong northward coastal current from the Texas coast to the western part of the inner LA shelf under their favorable wind forcing (southerly and southeasterly wind, red arrows). Thus, the MARS plume was promoted to the eastern and offshore Louisiana shelf.

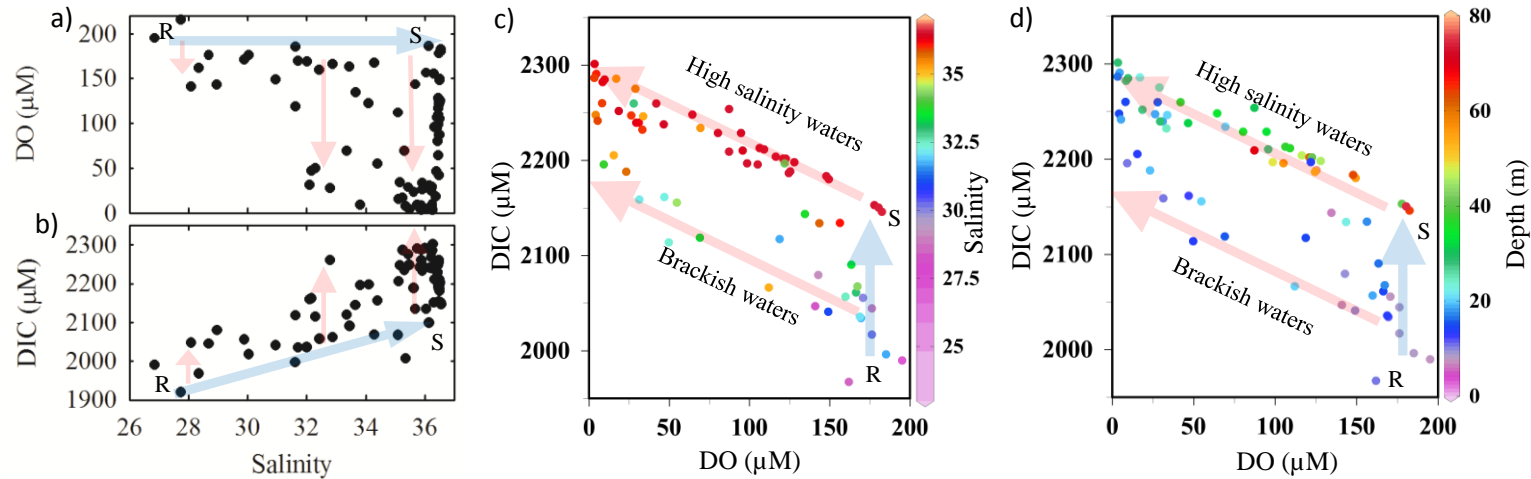


Figure 3.8. Mixing process (blue arrows) and respiration (red arrows) dominated the variations of DO and DIC concentrations in August 2007. The relationship of DO to salinity (a) was mirror to the relationship of DIC to salinity (b). River endmember (R) showed lower salinity and lower DIC concentration and seawater (S) showed higher salinity and higher DIC concentration. The relationship between DO and DIC in the bottom water can be observed in brackish waters and high salinity waters individually (c), which were separated by an alongshore isobaths zone between 10 and 20 m. The slope of DO-DIC relationship was close to a Redfield ratio of 138 to 106 respiration (the red arrows in c, d). Higher DO concentrations were corresponding to deeper bottom depth for high salinity waters (d), displaying cross-shelf gradient.

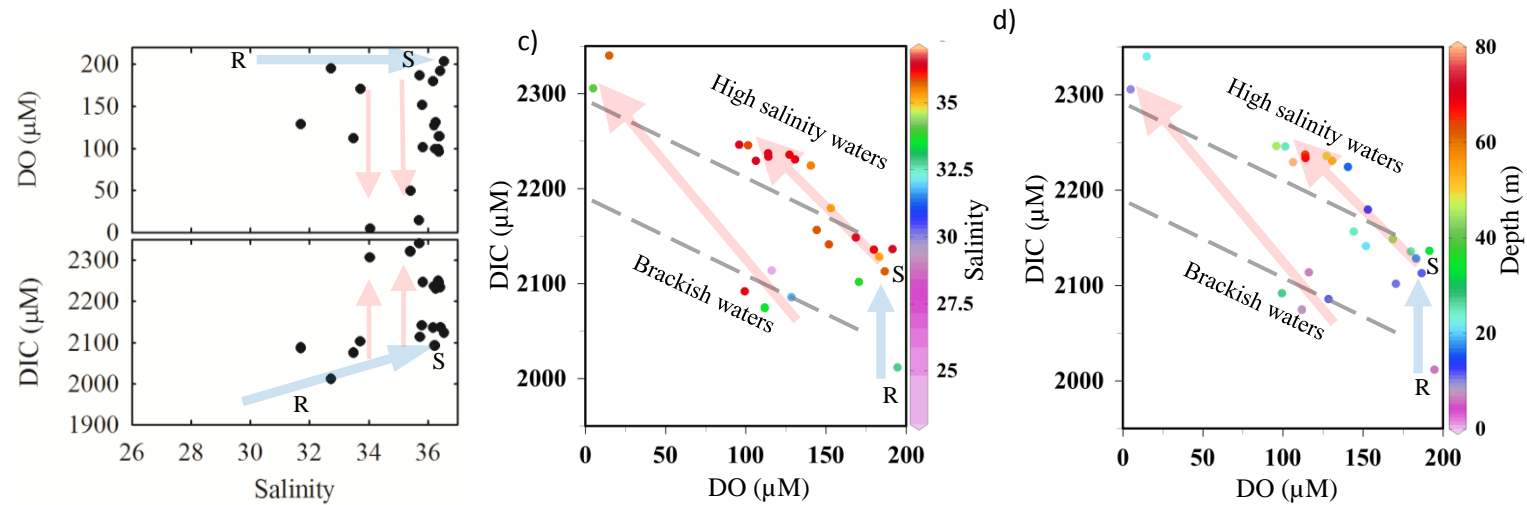


Figure 3.9. Mixing (blue arrows) and respiration (red arrows) contributed to variations of DO and DIC concentrations in bottom waters in July 2009. The relationship of DO to salinity (a) was also mirror to the relationship of DIC to salinity (b). The relationship between DO and DIC in the bottom water can also be observed in brackish waters and high salinity waters individually (c). But the slopes of DO-DIC relationship were higher than those in August 2007 (gray dash lines). The correspondence between DO and depth for sea waters was also disturbed in July 2009 (d) due to the changed shelf circulation.

CHAPTER 4

THE CARBON DIOXIDE (CO₂) SYSTEM IN THE MISSISSIPPI RIVER DOMINATED
CONTINENTAL SHELF, NORTHERN GULF OF MEXICO—I:
DISTRIBUTION AND AIR-SEA FLUX¹

¹ Wei-Jen Huang, Wei-Jun Cai, Yongchen Wang, Steven E. Lohrenz, and Michael C. Murrell. To be submit to *Journal of Geophysical Research*.

Abstract

River-dominated continental shelf environments are active sites of air-sea CO₂ exchange and represent an important component of global carbon budgets. We conducted 13 cruises on the Louisiana (LA) shelf, a region strongly influenced by fresh water and nutrients delivered from the Mississippi and Atchafalaya River system. Sea surface partial pressure of carbon dioxide ($p\text{CO}_2$) was measured, and air-sea CO₂ flux was calculated. The results showed a distinct seasonality indicating that the LA shelf was a net sink of atmospheric CO₂ during spring and early summer, and was neutral or a weak source to atmosphere during middle summer, fall, and winter with an annual net CO₂ uptake of $0.96 \text{ mol C m}^{-2} \text{ yr}^{-1}$. In addition, CO₂ exchange followed distinct patterns along the salinity gradient or across the shelf, being a source of CO₂ to the atmosphere in low salinity zones ($S < 17$) in near shore areas, a strong sink in the middle-high salinity zones ($S = 17-33$) in the inner shelf, near neutral CO₂ in the high salinity areas ($S > 33-35$) in the middle to outer shelf, and finally a weak source in open ocean GOM.

Furthermore, air-sea CO₂ fluxes on the LA Bight were highly correlated to nitrogen fluxes from the Mississippi River in one month earlier, implying a strong influence of riverine anthropogenic nitrogen export on air-sea CO₂ fluxes. However, the correlation was weakened when the river plume was redistributed by unusual regional wind forcing or currents. These results demonstrated that the river-to-sea interaction had significant impact on the air-sea CO₂ exchange and the regional carbon cycle, and the degree of impact was highly dependent on regional weather conditions.

1. Introduction

Although the continental shelf only covers about 7% of the seafloor in area, it accounts for about ~30% of oceanic net ecosystem production [Ducklow and McCallister, 2005] and 15-30% of the net annual carbon dioxide (CO₂) sink of global ocean and is an important component of global carbon budgets [Borges, 2011; Cai, 2011; Cai *et al.*, 2006; Chen and Borges, 2009]. However, the role that the continental shelf plays in the global ocean carbon cycle remains poorly constrained [Cai, 2011; Ducklow and McCallister, 2005]. This is because spatial and temporal heterogeneity of air-sea CO₂ fluxes on continental shelves is large yet data are sparse relative to open ocean environments [Takahashi *et al.*, 2009]. This is especially true for river-dominated continental shelves that receive large freshwater discharge and nutrient fluxes, and thus sharp variations in partial pressure of CO₂ ($p\text{CO}_2$) are expected in its plume and surrounding areas due to strong gradients in physical and biological processes [Cai, 2003; Cooley *et al.*, 2007; Kortzinger, 2003; Terner *et al.*, 2000; Tseng *et al.*, 2011; Tsunogai *et al.*, 1997; Zhai and Dai, 2009; Zhai *et al.*, 2007]. In particular, large river plumes with high anthropogenic nutrient fluxes could induce eutrophication, which has been suggested to strongly affect the CO₂ system [Borges and Gypens, 2010; Cai *et al.*, 2011; Chou *et al.*, 2011]. As such, a better understanding of CO₂ distributions and air-sea CO₂ fluxes in river-dominated continental shelves is needed.

The Louisiana (LA) shelf receives about 60% of the freshwater discharge from the Mississippi and Atchafalaya River system (MARS) [Walker *et al.*, 2005] and provides a good environment to study the CO₂ distribution over a large-river dominated shelf. Our previous high resolution but spatially limited in-situ measurements have shown that surface $p\text{CO}_2$ values were usually under-saturated (with respect to atmospheric CO₂) on the inner shelf and oversaturated on the outer shelf [Cai, 2003; Lohrenz and Cai, 2006]. Air-sea CO₂ fluxes near the Mississippi

River delta also appeared to change seasonally [Green *et al.*, 2006; Lohrenz *et al.*, 2010].

However, these studies had limited spatial and temporal coverage, thus more comprehensive seasonal and shelf coverage is needed to fully describe the $p\text{CO}_2$ distribution over the LA shelf.

The MARS delivers 1.5×10^{12} g (or Tg) of nitrogen, with 61% as nitrate N [Goolsby *et al.*, 2000] and 13-17 Tg bicarbonate annually to the northern Gulf of Mexico [Raymond *et al.*, 2008]. The riverine nitrogen flux has increased substantially between the 1950s and 1990s (United States Geological Survey, <http://toxics.usgs.gov/hypoxia/index.html>), which also is reflected by paleoindicators of eutrophication and oxygen condition from the sediments cores on the LA shelf [Osterman *et al.*, 2008; Rabalais *et al.*, 2007; Sen Gupta *et al.*, 1996]. While such riverine nitrogen flux induced air-sea CO_2 fluxes through enhanced biological activities has been known conceptually through previous studies [Cai, 2003; Dagg *et al.*, 2007; Green *et al.*, 2008; John *et al.*, 2007; Lohrenz *et al.*, 1990], however, there is still a pressing need, via fieldwork measurements, to examine, quantitatively, how terrestrial nitrogen export affects air-sea CO_2 exchanges on the shelf.

The purpose of this study is to determine surface $p\text{CO}_2$ spatial distribution, to identify surface $p\text{CO}_2$ along the salinity gradient, and to quantify the air-sea CO_2 fluxes over the LA shelf. We also discuss the relationship between this CO_2 fluxes and the riverine nitrogen fluxes. Finally, we provide a surface carbon budget in this river plume. While this study provides quantitative results, it is coherently followed by the other study, focusing on CO_2 dynamics, entitled: “The carbon dioxide system in the Mississippi River dominated continental shelf, the northern Gulf of Mexico Part II – the dynamics of surface CO_2 and oxygen”.

2. Method and Site Description

2.1. Site description

The Mississippi River is one of the world's largest rivers ranking 6th in freshwater discharge ($18,400 \text{ m}^3 \text{ s}^{-1}$) [Milliman and Meade, 1983]. 70% of the discharge is through the Mississippi River to the northern Gulf of Mexico, while the rest, ~30%, is via the Atchafalaya River to the LA shelf (Fig. 4.1) [Walker *et al.*, 2005]. But, each river contributes similar amount of freshwater discharge to the LA shelf because about half of the freshwater discharge from the Mississippi River advects westward to the LA shelf and the other half advects eastward to the Mississippi shelf, whereas almost all the freshwater discharge from the Atchafalaya River advects to the LA shelf [Dinnel and Wiseman, 1986; Etter *et al.*, 2004]. This MARS freshwater plume is usually confined to the north of 28°N on the LA shelf [Castillo *et al.*, 2001; Morey *et al.*, 2003a]. The plume area with high total suspended material ($> 5 \text{ mg L}^{-1}$) is highly related to freshwater discharge [Shi and Wang, 2009], which showed a distinct seasonal cycle, being high from March and May and low from August and October (Fig. 4.2). Furthermore, the flow-weighted nitrogen fluxes also demonstrated such seasonality (Fig. 4.2).

2.2. Field measurement

Thirteen cruises were conducted on the LA shelf and its surrounding area (Table 1). Four shelf-wide cruises covered the area that has high potential to develop the summer bottom-water hypoxia (the light gray area in Fig. 4.1) and was very close to the coverage of a long-term hypoxia (dissolved oxygen less than 2 mg L^{-1}) study conducted by N. N. Rabalais (<http://www.gulfhypoxia.net/>). Five cruises surveyed a wider area across the LA shelf (the gray dash circled area, Fig. 4.1), and another three cruises focused on the LA Bight, immediately west of the Mississippi River birdfoot delta, and one cruise surveyed the middle LA shelf. The

detailed tracks for each cruise are shown along with surface salinity distributions in Fig. 4.3. The October 2005 cruise was conducted about one month after Hurricane Katrina (23-30 August 2005) and two weeks after Hurricane Rita (18-26 September 2005).

During all cruises, surface water $p\text{CO}_2$ was measured by pumping water continuously through an underway $p\text{CO}_2$ analyzer installed in the shipboard laboratory. From 2003 to 2007, the system included a gas-water equilibrator and CO_2 detection via an infrared gas analyzer (LI-COR[®] 7000) as described in *Jiang et al.* [2008]. From 2008-2010, we used an upgraded system that included a Global Positioning System, a Seabird thermo-salinograph; and a water-gas equilibrator with an improved spray head, a temperature sensor, and a pressure sensor (manufacturer). This system also had improved the removal of water vapor via sequential Peltier cooling and gas permeable Nafion tubing. While the upgraded system yielded more reliable and consistent results, both systems had similar accuracy and precision (1 ppm). Periodically, the CO_2 analyzer was calibrated against CO_2 standards of 0, 197.5, 400.6, and 594.7, and 975.3 ppm. The atmospheric CO_2 values were measured every 6 or 12 hours from 2004 to 2007 and were measured every 3 to 4 hours during the cruises from 2008 to 2010 to determine the temporal and spatial variation of air $p\text{CO}_2$. Sea surface salinity (SSS) and temperature (SST) were measured by a Seabird SBE-45 flow through thermo-salinograph.

2.3. Air-Sea CO_2 flux calculation

As the instrument records the mole fraction of CO_2 in the dry air flow, $x\text{CO}_2$, it needs to be converted to the $p\text{CO}_2$ inside equilibrator at 100% water saturated condition via equation:

$$p\text{CO}_{2(\text{eq})} = x\text{CO}_{2(\text{eq})} \times (P_b - P_{\text{weq}}), \dots\dots\dots(1)$$

where $x\text{CO}_{2(\text{eq})}$ is the mole fraction concentration (ppm) of CO_2 in the dried sample gas; P_b is the barometric pressure (equal to the total pressure of equilibration) in atmospheres; and P_{weq} is the

equilibrium water vapor pressure at equilibrated temperature ($^{\circ}\text{C}$) and salinity. The $p\text{CO}_{2(\text{eq})}$ was converted to $p\text{CO}_{2(\text{water})}$ under in situ temperature [Takahashi *et al.*, 1993]:

$$p\text{CO}_{2(\text{water})} = p\text{CO}_{2(\text{eq})} \times \exp[0.0423 \times (T_{\text{in situ}} - T_{\text{eq}})] \dots\dots\dots(2)$$

For data before 2008, we estimated that the equilibrator temperature was 0.4°C lower than sea surface temperature by a comparison with water column salinity data from the rosette package, and thus correct the difference. The atmospheric $p\text{CO}_{2}$ ($p\text{CO}_{2(\text{air})}$) was corrected by the water vapor pressure as below:

$$p\text{CO}_{2(\text{air})} = x\text{CO}_{2(\text{air})} \times (P_{\text{b}} - P_{\text{w}}) \dots\dots\dots(3)$$

To calculate the air-sea CO_2 exchange flux, areal integrated of SSS, SST, $p\text{CO}_{2(\text{water})}$ and $p\text{CO}_{2(\text{air})}$ were calculated by gridded data with resolution of $0.1^{\circ}\text{W} \times 0.1^{\circ}\text{E}$. The $p\text{CO}_{2(\text{air})}$ value was set as a uniform value for each month over the LA shelf from 2004 to 2007 as we have less data. After 2008, we use intense $p\text{CO}_{2(\text{air})}$ data to interpolate a $p\text{CO}_{2(\text{air})}$ value for each $p\text{CO}_{2(\text{water})}$.

Air-sea CO_2 flux (F) was calculated as:

$$F = k \times K_0 \times [p\text{CO}_{2(\text{water})} - p\text{CO}_{2(\text{air})}] \dots\dots\dots(4)$$

where k is the gas transfer velocity of CO_2 ; K_0 is the CO_2 solubility coefficient at ambient temperature and salinity [Weiss, 1974]. To calculate k , we adopted the more recently recommended coefficient given by Ho *et al.* [2006]. It is very close to the commonly used coefficients given by Wanninkhof [1992] and Sweeney *et al.* [2007]. In dealing with the non-Gaussian distribution of the wind field between instant wind and averaged wind, we followed the approach given by Jiang *et al.* [2008] who suggested a combination of instant wind speed from coastal buoy stations and monthly wind from satellite products (QuikSCAT). Thus, the buoy stations provided high temporal resolution but of a limited area, while satellite products lower temporal resolution but high spatial resolution. Wind data were used from buoys stations: 42362,

42364, PSTL, LUML1, FGBL1, CAPL1, 42002, 42001, 42039, 42035 in the northern Gulf of Mexico to calculate monthly mean wind speed. Monthly QuikSCAT wind data were downloaded from a Live Access Server provided by Coast watch and SWFSC/Environmental Research Division (<http://las.pfeg.noaa.gov/>). The QuikSCAT wind data was interpolated to 0.1° by 0.1° to calculate the areal integrated air-sea CO₂ fluxes.

The monthly mean air-sea CO₂ flux was averaged from those areal integrated CO₂ fluxes in $0.1^\circ \times 0.1^\circ$ parcels over the LA shelf. To systematically compare this monthly mean CO₂ fluxes among each survey, we set a reference area based on the survey area between June 2006 and August 2007 (the light gray area in Fig. 4.1) as the survey areas during 2009-2010 were larger. For the three surveys focusing on the LA Bight from 2004 to April 2006, we should note that they do not represent a shelf-wide CO₂ flux but only for the LA Bight.

2.4. The uncertainties of air-sea CO₂ fluxes

The uncertainties of CO₂ fluxes were assessed by the methods described by *Jiang et al.* [2008], i.e., calculating the standard deviation of CO₂ fluxes using six available gas transfer velocities (including *Ho et al.* [2006], *Liss and Merlivat* [1986]; *Wanninkhof* [1992]; *Wanninkhof and McGillis* [1999]; *Nightingale et al.*, [2000a]; *Nightingale et al.*, [2000b]). By this approach, the uncertainty in monthly mean gas transfer velocity ranged from 11% to 15% with an average of 12% in this study. Such uncertainty constrained by the real distribution of wind field is much smaller than the differences between various coefficients under a fix wind speed, which are often as large as 2-fold [*Ho et al.*, 2006]. The average uncertainty of each month ranged from ± 0.05 to $\pm 2.98 \text{ mmol m}^{-2} \text{ d}^{-1}$ with an average of $\pm 1.15 \text{ mmol m}^{-2} \text{ d}^{-1}$, similar to the uncertainty estimated in the South Atlantic Bight [*Jiang et al.*, 2008].

Because the cruise tracks differed between 2006 to 2007 and 2009 to 2010, the averages of areal-integrated air-sea CO₂ fluxes calculated from the reference area and from the original survey area were compared, generally showing good agreement except in March 2010. This is because those areas out of the reference area usually displayed neutral CO₂ air-sea fluxes but they had lower values than usual in March 2010. Furthermore, the inner shelf region had larger special variation of SSS, SST, and *p*CO₂, thus also had highly variable CO₂ fluxes, than the outer shelf. To better account for this variability, an additional inshore alongshore track was added starting in January 2009.

3. Results

3.1. Distributions of sea surface salinity, temperature, and *p*CO₂

3.1.1. Sea surface salinity and temperature

Freshwater distributions were generally confined to the inner LA shelf toward the Texas coast. For example, the contour line of salinity 33 and 35 were distributed alongshore north of 28°N (Fig. 4.3d, e, f, g, i, j, l). For these alongshore plumes, most of their temperature distribution also showed alongshore distribution (Fig. 4.4d, g, i, l, m). In contrast, during March 2010, the freshwater plume was widely dispersed, extending southward of 28°N (Fig. 4.3m) and low temperature waters (less than 19°C) were also observed close to the 28°N (Fig. 4.4m). In July 2009, the freshwater plume was largely confined to the eastern LA shelf (Fig. 4.3k) and the temperature distribution showed a similar pattern (Fig. 4.4k).

3.1.2. *p*CO₂ in lower rivers, bays, and their adjacent nearshore areas

The Mississippi River and the Atchafalaya River waters had characteristically high *p*CO₂ values ranging from 900 and 2300 μatm (Table 2) with noticeable seasonal variation, being low

in the winter and high in the summer. In addition, the Mississippi river end-members were lower than those from the Atchafalaya River by 10% to 40% in winter, but were higher by 10% to 20% from spring to fall. Furthermore, in the Mississippi River plume, the surface water's $p\text{CO}_2$ decreased rapidly to near atmospheric values as it flowed onto the shelf (Fig. 4.5). In contrast, $p\text{CO}_2$ values remained oversaturated ($> 700 \mu\text{atm}$) in the Atchafalaya River plume well into Atchafalaya Bay (Fig. 4.5).

Water $p\text{CO}_2$ values in inland bays (i.e., Terrebonne Bay and Calcasieu Lake) without major freshwater inputs were much lower than those in the two major river systems (Table 2, Fig. 4.5). For example, in the Terrebonne Bay, $p\text{CO}_2$ was only slightly oversaturated in January 2009 and July 2009, and under-saturated in April 2009, November 2009, and March 2010.

3.1.3. $p\text{CO}_2$ on the inner, middle, and outer shelves

The distribution of the under-saturated $p\text{CO}_2$ waters consistently mirrored the freshwater distribution, being alongshore for most of the time (Fig. 4.5d,e,f,g,i,j), being confined to the east in July 2009 (Fig. 4.5k), or extending across 28°N as in March 2010 (Fig. 4.5m). During times when the MARS plume trajectory extended alongshore (Fig. 4.5d,e,h,g), there was a consistent gradient in $p\text{CO}_2$ values being under-saturated in the east and becoming progressively more oversaturated to the west. An exception to this pattern occurred in November (Fig. 4.5l), when $p\text{CO}_2$ values were rarely below $300 \mu\text{atm}$ and showed a small variation over the middle and outer shelf; but still displayed east-to-west gradient.

To show the detailed $p\text{CO}_2$ variations from inner to outer shelves in each cruise, two cross-shelf transects were chosen as examples (Fig. 4.6). The first one was Transect B, starting from the north of LA Bight along the longitude 89.76°W ; and the second one was Transect E, from the Atchafalaya Bay along the longitude 91.68°W . The lowest $p\text{CO}_2$ value for each cruise

was under-saturated and was usually observed on the inner shelf. The low $p\text{CO}_2$ values increased either toward to the land to oversaturated or toward to sea to near atmospheric values. Surface water $p\text{CO}_2$ values were more variable on the inner shelf (± 200 ppm) than the outer shelf (± 100 ppm) for each cruise (Fig. 4.6).

3.2. $p\text{CO}_2$ and property relationships

The $p\text{CO}_2$ and salinity relationship was a parabolic curve and varied seasonally. We show the areal-integrated $p\text{CO}_2$ values in relation to areal-integrated salinity bin as seasonal and annual averages (Fig. 4.7). In general, $p\text{CO}_2$ values were highest in the freshwater end-member and oversaturated with respect to the atmosphere (Fig. 4.7a). In the annual average, $p\text{CO}_2$ values were under-saturated between 17 to 33 salinity, and were significantly low ($<300 \mu\text{atm}$) for waters with salinities between 23 to 26. Seasonally, the lowest $p\text{CO}_2$ was observed in spring (Fig 4.7b) and this low- $p\text{CO}_2$ salinity range became wider in summer (Fig 4.7c). The under-saturated $p\text{CO}_2$ values fell within a smaller salinity range in fall than in spring or summer (Fig 4.7d). The $p\text{CO}_2$ values were mostly equal to the atmospheric values from salinity 20 to 36 in winter (Fig. 4.7e). This river-to-sea bimodal distribution was also showed in the $p\text{CO}_2$ and temperature relationship (Fig. 4.8). Both freshwater and seawater end-members showed seasonal variation in this bimodal relationship: i.e., below 25°C in January and increased to near 30°C during July and August for seawater end-member; and below 15°C in January and increased to over 30°C in July and September for the freshwater one.

3.3. Air-sea CO_2 flux

3.3.1. Seasonal variation and annual flux

To examine seasonal patterns of air-sea CO_2 flux, we present average values of wind speed, $p\text{CO}_2$ and air-sea CO_2 flux for the reference area (Fig 9). First, monthly average wind

speed was strong in spring (6 to 8 m s⁻¹), fall, and winter (~7-8m s⁻¹) and low in summer (~5m s⁻¹) (Fig. 4.9a). Areal-integrated *p*CO₂ was generally <300 μatm during spring and summer, and increased to above saturation during fall (Fig. 4.9b). Areal-integrated air-sea CO₂ fluxes showed that the LA shelf acted as a strong sink for atmospheric CO₂ in spring, a weak sink in summer, a source in fall, and nearly neutral in winter (Fig. 4.9c). In particular, the shelf was a strong CO₂ source in October 2005 and a strong sink in March 2010, reflecting unusual or extreme weather events.

The eastern LA shelf was a stronger CO₂ sink of atmosphere (-3.22 mmol m⁻² d⁻¹) than the western LA shelf (-2.05 mmol m⁻² d⁻¹). The seasonal variation between them also differed, i.e. the eastern region was a weaker CO₂ sink than the western region from January to April; but was a stronger sink from May to November. To sum up, the LA shelf acted as a sink of atmospheric CO₂ by (-2.64±0.41 mmol m⁻² d⁻¹) and, within it, the LA Bight acted as a particularly strong sink by (-4.89 mmol m⁻² d⁻¹).

3.3.2. Categorized by water depth and salinity sub-division

To be comparable to other studies, we organized the CO₂ fluxes by the water depth. For the inner shelf (bottom depth less than 20 m), the middle shelf (20 to 45 m), the outer shelf (45 to 200 m) and pelagic ocean (depth deeper than 200m), their corresponding annual CO₂ flux were -3.35 mmol m⁻² d⁻¹, -2.14 mmol m⁻² d⁻¹, 0.08 mmol m⁻² d⁻¹, and 1.46 mmol m⁻² d⁻¹, respectively. The strong sink from spring to June was mostly contributed by the inner and middle shelves. More detailed CO₂ fluxes for various subdivisions are given in Table 3.

We summarized annual CO₂ fluxes by salinity zones: 0 to 17, 17 to 25, 25 to 33, and 33 to 35 based on the result on Fig. 4.7a, indicated that 0-17 salinity zone was a source of atmospheric CO₂ (6.8 mmol m⁻² d⁻¹), and the 17-25 salinity zone was a strong sink of

atmospheric CO₂ (-4.8 mmol m⁻² d⁻¹). The annual average of areal-integrated pCO₂ shifted from oversaturation to under-saturation and reached the lowest value in this region. The 25-33 salinity zone was also a strong sink (-4.5 mmol m⁻² d⁻¹) and the annual average of areal-integrated pCO₂ increased with increasing salinity in this salinity range. Finally, the 33-35 salinity zone was a weak sink of atmospheric CO₂ (-0.5 mmol m⁻² d⁻¹). The low salinity region was a strong CO₂ source but it only covered a small proportion for the surface area of the LA shelf while the other salinity sub-regions covered the majority of this shelf. Thus, the MARS plume as a whole was still a CO₂ sink.

4. Discussion

4.1. Variations along the salinity gradient

Variation of pCO₂ along the salinity gradient indicated a combination of physical mixing and biological processes. Previous studies have shown that river-to-ocean abiotic mixing would lead to lower pCO₂ in its variation along the salinity gradient [*Salisbury et al.*, 2009]. In this study, we simulate this abiotic mixing with conservative mixings of total alkalinity (TA) and dissolved inorganic carbon (DIC) between the Mississippi River and seawater. We use the method given by *Huang et al.* [2012] (end-members in Table 4.5) and convert these average TA and DIC data (Cai, unpublished data) to pCO₂ through CO2SYS (Matlab version). The result showed that observed areal-integrated pCO₂ values were lower than these conservative mixing values (blue lines in Fig. 4.7). For example, these conservative mixing model predicted pCO₂ values of 489.4 and 438.2 at salinity 25 and 30, respectively, for the annual result, and the observations were all lower than these two predicted numbers. In other plume and coast systems, the difference between the observation and conservative mixing model predictions can be caused

by biological processes [Cooley and Yager, 2006; Salisbury et al., 2008], as shown in previous Mississippi River plume studies (Guo et al. [2012] and Huang et al. [2012]) that have shown that nutrient removal coincided with inorganic carbon uptake in the mid-salinity zones. Lohrenz et al. [2010] also concluded that Chl-a was the dominant factor for $p\text{CO}_2$ variation in waters of salinity 20 to 28 in this area.

Therefore, we simulated the effects of biological activities on $p\text{CO}_2$ variation along the salinity gradient by converting the effect of net biological NO_3 removal to DIC uptake and TA variation by applying Redfield stoichiometry [Huang et al., 2012]. The net NO_3 removal was estimated by deviation from conservative mixing curves to the fitting curves of measured NO_3 data from our available cruises (Lohrenz, unpublished data). Our under-saturated $p\text{CO}_2$ observations were close to net NO_3 -removal predicted values (red lines in Fig. 4.7), demonstrating the importance of biological activities in addition to conservative mixing on $p\text{CO}_2$ variations, such as in annual, spring, and winter results. The observed data in fall were slightly higher than the NO_3 -removal predicted values and close to the atmospheric values (Fig. 4.7d), suggesting additional factors may be involved. Therefore, we provided a coupled oxygen and $p\text{CO}_2$ model with impacts of gas exchanges and transition of net ecosystem production to explain CO_2 dynamics over the LA shelf in our coherent Study Part II.

4.2. Variations dependence on MARS plume distributions

The $p\text{CO}_2$ spatial variations also varied correspondingly to the freshwater distribution on the LA shelf in a meso-scale. Previous studies have observed that the MARS plume is frequently distributed along the inshore areas near the Louisiana coast extending toward Texas (Fig. 4.1) [Dinnel and Wiseman, 1986; Morey et al., 2003b; Zhang et al., 2012]. For these periods, there was a strong cross-shelf $p\text{CO}_2$ gradient except in November (Fig. 4.3, 5). This finding was

consistent with limited previous studies [Lohrenz and Cai, 2006; Lohrenz et al., 2010]. As the shelf circulation have been found to affect the distribution of surface PP [Chen et al., 2000], we further show it also affect surface $p\text{CO}_2$ distribution [Chapter 2, 3].

Furthermore, as the plume trajectory is subjected to wind forcing [Cochrane and Kelly, 1986; Schiller et al., 2011; Walker et al., 2005; Zhang et al., 2012], wind forcing therefore affects the distribution of $p\text{CO}_2$ through shelf circulation. When northerly winds dominated in March 2010, the trajectory of the alongshore plume thus became wider and covered the area between 28°N and 25°N (Fig. 4.3m, 10a); and low $p\text{CO}_2$ values also extended to the middle and outer shelves (Fig. 4.5m, 6) [Chapter 2]. Moreover, the unusual shelf circulation in July 2009 (high surface salinity was observed on the western inner shelf while freshwater plume was confined to the eastern side, Fig. 4.3k, 10b) was largely affected by consistent southerly winds along the Texas coast [Zhang et al., 2012; Chapter 3]. Under this unusual shelf circulation, $p\text{CO}_2$ was oversaturated west of longitude 90°W , especially on the inner shelf; areas in the east of 90°W were under-saturated, especially on the outer shelf (Fig. 4.5k). This pattern can also be seen on the transect view in Fig 6: $p\text{CO}_2$ values were under-saturated in July 2009 on the outer shelf in Transect B, and were oversaturated in the middle and outer shelves in Transect E.

4.3. Major disturbance by hurricanes

The anomalous surface water $p\text{CO}_2$ values observed in October 2005 were likely affected by the Hurricanes Katrina (23-30 August 2005) and Rita (18-29 September 2005), showing higher $p\text{CO}_2$ values than the mean values from September and November, i.e. the average of fall in this study (Fig. 4.7d). As in-situ $p\text{CO}_2$ measurements was limited on the inner shelf, Lohrenz et al. [2010] extrapolated them to the LA Bight by using remote sensing techniques and estimated the air-sea CO_2 flux of $5.4 \text{ mmol m}^{-2} \text{ d}^{-1}$. Compared to the CO_2 fluxes from non-storm

months in September 2006 and November 2009 (average of $1.79 \text{ mmol m}^{-2} \text{ d}^{-1}$), the additional CO_2 fluxes ($3.61 \text{ mmol m}^{-2} \text{ d}^{-1}$) represents the contribution induced by hurricanes. These sources of high CO_2 values might be from terrestrial input and/or bottom sediment stirred up by hurricanes [Lohrenz *et al.*, 2010]. In addition, the uncertainty of gas transfer velocity was large under high wind speeds [Wanninkhof *et al.*, 2009], resulting in larger uncertainty to air-sea CO_2 fluxes. Nonetheless, it is clear, and perhaps not a surprising conclusion, that hurricanes can exert dramatic changes to normal sea surface $p\text{CO}_2$ distribution and thus the flux of air-sea CO_2 exchange.

4.4. Relationship between riverine nitrogen fluxes and shelf air-sea CO_2 fluxes

To quantify the relationship between the air-sea CO_2 flux and riverine nitrate plus nitrite flux (NN flux), two correlations were determined: 1) the relationship between air-sea CO_2 fluxes on the LA Bight and the NN fluxes (USGS data) (both monthly) from the Mississippi River; 2) the relationship between the coverage of enhanced PP areas ($p\text{CO}_2 < 300 \mu\text{atm}$) on the LA shelf (monthly) and the NN fluxes (two-month average) from the MARS.

4.4.1. On the Louisiana Bight

We compared the Mississippi NN fluxes to CO_2 fluxes over the LA Bight finding that they were highly correlated (Fig. 4.11). The relationship was particularly strong during times when the plume was distributed alongshore with the coefficient of determination (R^2) of 0.85. The data for March 2010 appeared different suggesting a poor relationship between NN and CO_2 fluxes, likely due to other unusual physical conditions, such as varied dilution and water depth [Green *et al.*, 2008; Lohrenz *et al.*, 1997]. By considering the gross primary production and respiration, [Green *et al.*, 2006] estimated air-sea CO_2 fluxes for this turbidity plume and estimated that this area was autotrophic and was a strong sink of the atmospheric CO_2 . These previous studies

together have also implied that the CO₂ fluxes should be correlated to the riverine nitrogen flux when the physical conditions among them were also proportional to each other. Based on the slope between riverine nitrogen fluxes and our air-sea CO₂ fluxes on the LA Bight, we provide an empirical interactive coefficient for the riverine nutrient in promoting atmospheric CO₂ uptake in the river plume on the LA Bight by excluding the MARS plume under unusual weather. That is every 1×10^9 g N from the Mississippi River can induce a CO₂ uptake of $0.109 \text{ mmol m}^{-2} \text{ d}^{-1}$ (Fig. 4.11).

4.4.2. When scaled on the wider Louisiana shelf

Over the LA shelf, the relationship between riverine NN fluxes and air-sea CO₂ fluxes was not observed. However, there was a positive relationship between MARS NN fluxes and the area of enhanced PP (defined as interpolated area $< 300 \mu\text{atm } p\text{CO}_2$) (Fig. 4.12). This finding is similar to the East China Sea, where surface $p\text{CO}_2$ values were found to be related to freshwater discharge from the Changjiang River [Chou *et al.*, 2011; Tseng *et al.*, 2011]. Moreover, relationships between surface Chl-a concentration and riverine nitrogen flux were also observed on the LA shelf [Lehrter *et al.*, 2009]. This result also supports and explained the nitrate removal predicted $p\text{CO}_2$ values in Section 4.1, showing that riverine nitrogen fluxes were largely responsible for the CO₂ drawdown in its dominated region. The relationship between $p\text{CO}_2$ and NN flux was significant when the MARS plume trajectory was alongshore and was disturbed under extreme/unusual weather patterns, such as in March 2010, July 2009, and October 2005. Therefore, we suggest that plume trajectory was also important to the relationships between riverine NN fluxes to the enhanced PP coverage on the LA shelf.

Compared these two relationships, we notice the response of sea surface $p\text{CO}_2$ to riverine nitrogen flux was inconsistent between on the LA bight and on the shelf. Hydrologically,

freshwater distribution on this region is primarily controlled by the discharge from the Mississippi River [Schiller *et al.*, 2011], and the western region is primarily influenced by both the discharge from the Atchafalaya River and the shelf-wide wind driven currents [Hetland and DiMarco, 2008]. Furthermore, previous study have found autotrophy from Spring to fall in the LA Bight [Green *et al.*, 2006]; and more heterotrophy was observed on the western shelf [Murrell *et al.*, 2013].

4.4.3. The delayed response time of plume CO₂ to riverine nitrogen fluxes

There was a one-month time delay between CO₂ fluxes on the LA Bight to Mississippi riverine NN fluxes, and 1- to 1.5-months delay for enhanced PP area on the LA shelf to MARS NN fluxes (Fig. 4.13). Each relationship was determined by changing the month of the NN fluxes in advance to the CO₂ fluxes from zero to three months with half month ascending. Thus, seven R² were calculated and compared for each relationship. For the relationship in Section 4.4.1, Fig. 4.13 displayed that the highest R² was observed when the riverine NN fluxes was one month in advance to the CO₂ flux on the LA Bight (blue solid lines). When data from March 2010 was neglected, the highest R² was still observed in one month in advance but was higher (blue dash line) than being included. This relationship in the highest R² in one month in advance was displayed on Fig. 4.11. For the relationship in Section 4.4.2, the highest R² was observed when the average riverine NN flux was 1.5 month in advance (red line in Fig. 4.13). Because the R² in one month in advance was slightly lower than in 1.5 month, we suggest that 1 to 1.5 months are reasonable for the second relationship. This relationship with the highest R² in 1.5 month in advance was presented on Fig. 4.12.

Previous studies have demonstrated various time scales to describe the physical or biological correlations to the Mississippi River discharge or nitrogen fluxes. The response times

for air-sea CO₂ fluxes on the LA Bight and enhanced PP area on the LA shelf in this study corresponded to them well. First, the water transit time in the Mississippi River turbidity plume area is about two weeks depending on the water salinity [Green *et al.*, 2006]. As that residence time for the plume area was limited on small areas based on sediment distributions, the one month lag between the surface water pCO₂ and the nitrogen induced primary production on the LA Bight is reasonable because the LA Bight is larger. Third, for the enhanced PP area on LA shelf, as this area is even larger than the LA Bight, it is reasonable that we found the response time of 1 to 1.5 month. Fourth, the response time of the summer bottom-water hypoxic area to riverine nitrogen fluxes is two month [Justic *et al.*, 1993]. The one half to one month time-lag between the response time of surface enhanced PP area and the bottom water hypoxia was sufficient for respiration rate to reduce dissolved oxygen concentration to hypoxia level [Turner *et al.*, 1998]. Finally, the water residence time is usually longer than 3 months (as long as one year) for the entire LA shelf [Zhang *et al.*, 2012], showing enough time scale to support these biogeochemical processes.

4.5. Conceptual model and carbon budget of the MARS plume

We conclude the surface inorganic carbon budget of the MARS plume on the LA shelf and explain the variation in this budget (Fig. 4.14). Annually, the MARS exported 15.2×10^{12} gC yr⁻¹ of DIC to the coastal ocean [Cai *et al.*, 2008] while it also transported 1.57×10^{12} gN yr⁻¹ of inorganic nitrogen [Goolsby *et al.*, 2000]. In the sub-region of salinity 0-17 in the river plume, water-transit time was only two days [Green *et al.*, 2006] and turbidity was high and inhibited light attenuation for phytoplankton [Dagg *et al.*, 2007; Lohrenz *et al.*, 1990], resulting this sub-region was a source of atmospheric CO₂ (47 Tg C yr⁻¹). In the sub-regions of salinity 17-24, its coverage area was relatively large and turbidity was reduced and is favorable for light

penetration, resulting in high PP in this region as well as large deficit nutrient was usually observed in this region [Dagg *et al.*, 2007; Lohrenz *et al.*, 1990]. Thus, these two sub-regions acted as a strong sink of atmospheric CO₂ (150 Tg C yr⁻¹) for salinity waters 17-24 and 457 Tg C yr⁻¹ for 25-33). As the river plume more inorganic nutrient and carbon were converted to organic material, the respiration and heterotrophic biological activities increased with increasing salinity [Dagg and Breed, 2003; Dagg *et al.*, 2004]. In the rest salinity regions (salinity 33-35), these areas gradually shifted from a sink to near neutral or a weak source towards high salinity area, where was a weak sink of 9 Tg C yr⁻¹.

5. Summary

The surface water *p*CO₂ distribution showed both seasonal and spatial variations on the LA shelf. The average of the areal-integrated *p*CO₂ values was under-saturated in spring, close to atmospheric CO₂ values in summer, oversaturated in fall, and close to the atmosphere again in winter. These *p*CO₂ values showed large spatial variations in low salinity areas than in high salinity areas. Generally, the inner to middle shelf acted as a sink of atmospheric CO₂ and the outer shelf acted as a weak source. The eastern LA shelf, especially in the LA Bight, acted as a stronger sink than the western LA shelf. In terms of salinity sub-division, low salinity regions (0 to 17) were a CO₂ source, middle to high salinity areas (17 to 33) were a strong CO₂ sink, and near high salinity (33-35) areas acted as near neutral to a weak CO₂ source. To sum up, the LA shelf acted as a sink of atmospheric CO₂ annually (-0.963 mol C m⁻² yr⁻¹).

The observed nitrate removal was stoichiometrically coupled to the *p*CO₂ variation in addition to the conservative mixing along the salinity gradient on the LA shelf. Furthermore, the relationship between the Mississippi riverine NN fluxes and the air-sea CO₂ fluxes on the LA

Bight were quantified to be with one month lag. The MARS NN fluxes were also correlated to the enhanced PP coverage on the LA shelf with 1- to 1.5-month lag. These two relationships were observed when the MARS plumes were distributed alongshore to the north of 28°N. When the MARS plume was relocated to other type of distribution, they behaved differently from those alongshore plume in responding to riverine nitrogen fluxes, such as in March 2010, July 2009, and October 2005. Based on the importance of freshwater distribution and riverine nitrogen fluxes in CO₂ variations over the LA shelf, we suggested that air-sea CO₂ fluxes on large-river dominated selves were largely related to anthropogenic nitrogen exports and regional weather events.

References

- Borges, A. V. (2011), Present Day Carbon Dioxide Fluxes in the Coastal Ocean and Possible Feedbacks Under Global Change Oceans and the Atmospheric Carbon Content, edited by P. Duarte and J. M. Santana-Casiano, pp. 47-77, Springer Netherlands.
- Borges, A. V., and N. Gypens (2010), Carbonate chemistry in the coastal zone responds more strongly to eutrophication than to ocean acidification, *Limnology and Oceanography*, 55(1), 346-353.
- Cai, W.-J. (2003), Riverine inorganic carbon flux and rate of biological uptake in the Mississippi River plume, *Geophysical Research Letters*, 30(2), 1032.
- Cai, W.-J. (2011), Estuarine and Coastal Ocean Carbon Paradox: CO₂ Sinks or Sites of Terrestrial Carbon Incineration?, *Annual Review of Marine Science*, 3(1), 123-145.
- Cai, W.-J., M. Dai, and Y. C. Wang (2006), Air-sea exchange of carbon dioxide in ocean margins: A province-based synthesis, *Geophysical Research Letters*, 33(12), L12603.
- Cai, W.-J., X. Guo, C.-T. A. Chen, M. Dai, L. Zhang, W. Zhai, S. E. Lohrenz, K. Yin, P. J. Harrison, and Y. Wang (2008), A comparative overview of weathering intensity and HCO₃⁻ flux in the world's major rivers with emphasis on the Changjiang, Huanghe, Zhujiang (Pearl) and Mississippi Rivers, *Continental Shelf Research*, 28(12), 1538-1549.
- Cai, W.-J., et al. (2011), Acidification of subsurface coastal waters enhanced by eutrophication, *Nature Geosci*, 4(11), 766-770.
- Castillo, D., E. Carlos, P. G. Coble, R. N. Conmy, F. E. Müller-Karger, L. Vanderbloemen, and G. A. Vargo (2001), Multispectral in situ Measurements of Organic Matter and Chlorophyll Fluorescence in Seawater: Documenting the Intrusion of the Mississippi River Plume in the West Florida Shelf, *Limnology and Oceanography*, 46(7), 1836-1843.

- Chen, C.-T. A., and A. V. Borges (2009), Reconciling opposing views on carbon cycling in the coastal ocean: Continental shelves as sinks and near-shore ecosystems as sources of atmospheric CO₂, *Deep Sea Research Part II: Topical Studies in Oceanography*, 56(8-10), 578-590.
- Chen, X., S. E. Lohrenz, and D. A. Wiesenburg (2000), Distribution and controlling mechanisms of primary production on the Louisiana-Texas continental shelf, *Journal of Marine Systems*, 25(2), 179-207.
- Chou, W.-C., G.-C. Gong, C.-M. Tseng, D. D. Sheu, C.-C. Hung, L.-P. Chang, and L.-W. Wang (2011), The carbonate system in the East China Sea in winter, *Marine Chemistry*, 123(1-4), 44-55.
- Cochrane, J. D., and F. J. Kelly (1986), Low-frequency circulation on the Texas-Louisiana continental shelf, *Journal of geophysical research. Part C, Oceans and atmospheres*, 91(9), 10645-10659.
- Cooley, S. R., and P. L. Yager (2006), Physical and biological contributions to the western tropical North Atlantic Ocean carbon sink formed by the Amazon River plume, *Journal of Geophysical Research*, 111(C8), C08018.
- Cooley, S. R., V. J. Coles, A. Subramaniam, and P. L. Yager (2007), Seasonal variations in the Amazon plume-related atmospheric carbon sink, *Global Biogeochem. Cycles*, 21(3), GB3014.
- Dagg, M. J., and G. A. Breed (2003), Biological effects of Mississippi River nitrogen on the northern Gulf of Mexico—a review and synthesis, *Journal of Marine Systems*, 43(3/4), 133.

- Dagg, M. J., J. Ammerman, R. Amon, W. Gardner, R. Green, and S. Lohrenz (2007), A review of water column processes influencing hypoxia in the northern Gulf of Mexico, *Estuaries and Coasts*, 30(5), 735-752.
- Dagg, M. J., R. Benner, S. Lohrenz, and D. Lawrence (2004), Transformation of dissolved and particulate materials on continental shelves influenced by large rivers: plume processes, *Continental Shelf Research*, 24(7-8), 833-858.
- Dinnel, S. P., and J. W. J. Wiseman (1986), Fresh water on the Louisiana and Texas shelf, *Continental Shelf Research*, 6(6), 765-784.
- Ducklow, H. W., and S. L. McCallister (2005), The biogeochemistry of carbon dioxide in the coastal oceans, in *The global coastal ocean. Multiscale interdisciplinary processes. The sea: ideas and observations on progress in the study of the seas.*, edited by A. R. Robinson and K. H. Brink, pp. 269-315, Harvard University Press, Cambridge, MA
- Etter, P. C., M. K. Howard, and J. D. Cochran (2004), Heat and freshwater budgets of the Texas-Louisiana shelf, *J. Geophys. Res.*, 109, C02024.
- Goolsby, D. A., W. A. Battaglin, B. T. Aulenbach, and R. P. Hooper (2000), Nitrogen flux and sources in the Mississippi River Basin, *The Science of The Total Environment*, 248(2-3), 75-86.
- Green, R. E., G. A. Breed, M. J. Dagg, and S. E. Lohrenz (2008), Modeling the response of primary production and sedimentation to variable nitrate loading in the Mississippi River plume, *Continental Shelf Research*, 28(12), 1451-1465.
- Green, R. E., T. S. Bianchi, M. J. Dagg, N. D. Walker, and G. A. Breed (2006), An organic carbon budget for the Mississippi River turbidity plume and plume contributions to air-sea CO₂ fluxes and bottom water hypoxia, *Estuaries and Coasts*, 29(4), 579-597.

- Guo, X., et al. (2012), Carbon dynamics and community production in the Mississippi River plume, *Limnology and Oceanography*, 57(1), 1-17.
- Hetland, R. D., and S. F. DiMarco (2008), How does the character of oxygen demand control the structure of hypoxia on the Texas-Louisiana continental shelf?, *Journal of Marine Systems*, 70(1-2), 49-62.
- Ho, D. T., C. S. Law, M. J. Smith, P. Schlosser, M. Harvey, and P. Hill (2006), Measurements of air-sea gas exchange at high wind speeds in the Southern Ocean: Implications for global parameterizations, *Geophys. Res. Lett.*, 33(16), L16611.
- Huang, W.-J., W.-J. Cai, R. T. Powell, S. E. Lohrenz, Y. Wang, L. Q. Jiang, and C. S. Hopkinson (2012), The stoichiometry of inorganic carbon and nutrient removal in the Mississippi River plume and adjacent continental shelf, *Biogeosciences*, 9(7), 2781-2792.
- Jiang, L.-Q., W.-J. Cai, Y. Wang, R. Wanninkhof, and H. Lüger (2008), Air-sea CO₂ fluxes on the U.S. South Atlantic Bight: Spatial and seasonal variability, *J. Geophys. Res.*, 113, C07019.
- John, D. E., Z. A. Wang, X. Liu, R. H. Byrne, J. E. Corredor, J. M. Lopez, A. Cabrera, D. A. Bronk, F. R. Tabita, and J. H. Paul (2007), Phytoplankton carbon fixation gene (RuBisCO) transcripts and air-sea CO₂ flux in the Mississippi River plume, *ISME J*, 1(6), 517-531.
- Justic, D., N. N. Rabalais, R. E. Turner, and W. J. Wiseman Jr (1993), Seasonal coupling between riverborne nutrients, net productivity and hypoxia, *Marine Pollution Bulletin*, 26(4), 184-189.
- Kortzinger, A. (2003), A significant CO₂ sink in the tropical Atlantic Ocean associated with the Amazon River plume, *Geophysical Research Letters*, 30(24), 4.

- Lehrter, J. C., M. C. Murrell, and J. C. Kurtz (2009), Interactions between freshwater input, light, and phytoplankton dynamics on the Louisiana continental shelf, *Continental Shelf Research*, 29(15), 1861-1872.
- Liss, P., and L. Merlivat (1986), Air-sea gas exchange rates: introduction and synthesis, in *The Role of Air-Sea Exchange in Geochemical Cycling*, edited by P. Buat-Menard, pp. 113-129, Boston, MA.
- Lohrenz, S. E., and W.-J. Cai (2006), Satellite ocean color assessment of air-sea fluxes of CO₂ in a river-dominated coastal margin, *Geophysical Research Letters*, 33(1), L01601.
- Lohrenz, S. E., M. J. Dagg, and T. E. Whitledge (1990), Enhanced primary production at the plume/oceanic interface of the Mississippi River, *Continental Shelf Research*, 10(7), 639-664.
- Lohrenz, S. E., W.-J. Cai, F. Chen, X. Chen, and M. Tuel (2010), Seasonal variability in air-sea fluxes of CO₂ in a river-influenced coastal margin, *J. Geophys. Res.*, 115(C10), C10034.
- Lohrenz, S. E., G. L. Fahnenstiel, D. G. Redalje, G. A. Lang, X. Chen, and M. J. Dagg (1997), Variations in primary production of northern Gulf of Mexico continental shelf waters linked to nutrient inputs from the Mississippi River, *Marine Ecology Progress Series*, 155, 45-54.
- Milliman, J. D., and R. H. Meade (1983), World-Wide Delivery of River Sediment to the Oceans, *The Journal of Geology*, 91(1), 1-21.
- Morey, S. L., W. W. Schroeder, J. J. O'Brien, and J. Zavala-Hidalgo (2003a), The annual cycle of riverine influence in the eastern Gulf of Mexico basin, *Geophys. Res. Lett.*, 30(16), 1867.

- Morey, S. L., P. J. Martin, J. J. O'Brien, A. A. Wallcraft, and J. Zavala-Hidalgo (2003b), Export pathways for river discharged fresh water in the northern Gulf of Mexico, *Journal of Geophysical Research*, 108(C10), 3303.
- Murrell, M. C., R. S. Stanley, J. C. Lehrter, and J. D. Hagy Iii (2013), Plankton community respiration, net ecosystem metabolism, and oxygen dynamics on the Louisiana continental shelf: Implications for hypoxia, *Continental Shelf Research*, 52(0), 27-38.
- Nightingale, P. D., P. S. Liss, and P. Schlosser (2000a), Measurements of air-sea gas transfer during an open ocean algal bloom, *Geophys. Res. Lett.*, 27(14), 2117-2120.
- Nightingale, P. D., G. Malin, C. S. Law, A. J. Watson, P. S. Liss, M. I. Liddicoat, J. Boutin, and R. C. Upstill-Goddard (2000b), In situ evaluation of air-sea gas exchange parameterizations using novel conservative and volatile tracers, *Global Biogeochem. Cycles*, 14(1), 373-387.
- Osterman, L. E., R. Z. Poore, and P. W. Swarzenski (2008), The last 1000 years of natural and anthropogenic low-oxygen bottom-water on the Louisiana shelf, Gulf of Mexico, *Marine Micropaleontology*, 66(3-4), 291-303.
- Rabalais, N. N., R. E. Turner, B. K. S. Gupta, E. Platon, and M. L. Parsons (2007), Sediments tell the history of eutrophication and hypoxia in the northern Gulf of Mexico, *Ecological Applications*, 17(sp5), S129-S143.
- Raymond, P. A., N.-H. Oh, R. E. Turner, and W. Broussard (2008), Anthropogenically enhanced fluxes of water and carbon from the Mississippi River, *Nature*, 451(7177), 449-452.
- Salisbury, J., D. Vandemark, C. Hunt, J. Campbell, B. Jonsson, A. Mahadevan, W. McGillis, and H. Xue (2009), Episodic riverine influence on surface DIC in the coastal Gulf of Maine, *Estuarine, Coastal and Shelf Science*, 82(1), 108-118.

- Salisbury, J. E., D. Vandemark, C. W. Hunt, J. W. Campbell, W. R. McGillis, and W. H. McDowell (2008), Seasonal observations of surface waters in two Gulf of Maine estuary-plume systems: Relationships between watershed attributes, optical measurements and surface pCO₂, *Estuarine, Coastal and Shelf Science*, 77(2), 245-252.
- Schiller, R. V., V. H. Kourafalou, P. Hogan, and N. D. Walker (2011), The dynamics of the Mississippi River plume: Impact of topography, wind and offshore forcing on the fate of plume waters, *J. Geophys. Res.*, 116(C6), C06029.
- Sen Gupta, B. K., R. Eugene Turner, and N. N. Rabalais (1996), Seasonal oxygen depletion in continental-shelf waters of Louisiana: Historical record of benthic foraminifers, *Geology*, 24(3), 227-230.
- Shi, W., and M. Wang (2009), Satellite observations of flood-driven Mississippi River plume in the spring of 2008, *Geophys. Res. Lett.*, 36(7), L07607.
- Sweeney, C., E. Gloor, A. R. Jacobson, R. M. Key, G. McKinley, J. L. Sarmiento, and R. Wanninkhof (2007), Constraining global air-sea gas exchange for CO₂ with recent bomb 14C measurements, *Global Biogeochem. Cycles*, 21(2), GB2015.
- Takahashi, T., J. Olafsson, J. G. Goddard, D. W. Chipman, and S. C. Sutherland (1993), Seasonal Variation of CO₂ and Nutrients in the High-Latitude Surface Oceans: a Comparative Study, *Global Biogeochem. Cycles*, 7(4), 843-878.
- Takahashi, T., et al. (2009), Climatological mean and decadal change in surface ocean pCO₂, and net sea-air CO₂ flux over the global oceans, *Deep Sea Research Part II: Topical Studies in Oceanography*, 56(8-10), 554-577.

- Ternon, J. F., C. Oudot, A. Dessier, and D. Diverres (2000), A seasonal tropical sink for atmospheric CO₂ in the Atlantic ocean: the role of the Amazon River discharge, *Marine Chemistry*, 68(3), 183-201.
- Tseng, C.-M., K. K. Liu, G. C. Gong, P. Y. Shen, and W. J. Cai (2011), CO₂ uptake in the East China Sea relying on Changjiang runoff is prone to change, *Geophys. Res. Lett.*, 38(24), L24609.
- Tsunogai, S., S. Watanabe, J. Nakamura, T. Ono, and T. Sato (1997), A preliminary study of carbon system in the East China Sea, *Journal of Oceanography*, 53(1), 9-17.
- Turner, R. E., N. Qureshi, N. N. Rabalais, Q. Dortch, D. Justic, R. F. Shaw, and J. Cope (1998), Fluctuating silicate:nitrate ratios and coastal Plankton food webs, *Proceedings of the National Academy of Sciences of the United States of America*, 95(22), 13048-13051.
- Walker, N. D., W. J. Wiseman, L. J. Rouse, and A. Babin (2005), Effects of river discharge, wind stress, and slope eddies on circulation and the satellite-observed structure of the Mississippi River plume, *Journal of Coastal Research*, 21(6), 1228-1244.
- Wanninkhof, R. (1992), Relationship Between Wind Speed and Gas Exchange Over the Ocean, *Journal of Geophysical Research*, 97(C5), 7373-7382.
- Wanninkhof, R., and W. R. McGillis (1999), A cubic relationship between air-sea CO₂ exchange and wind speed, *Geophys. Res. Lett.*, 26(13), 1889-1892.
- Wanninkhof, R., W. E. Asher, D. T. Ho, C. Sweeney, and W. R. McGillis (2009), Advances in Quantifying Air-Sea Gas Exchange and Environmental Forcing*, *Annual Review of Marine Science*, 1(1), 213-244.
- Weiss, R. F. (1974), Carbon dioxide in water and seawater: the solubility of a non-ideal gas, *Marine Chemistry*, 2(3), 203-215.

- Zhai, W., and M. Dai (2009), On the seasonal variation of air - sea CO₂ fluxes in the outer Changjiang (Yangtze River) Estuary, East China Sea, *Marine Chemistry*, *117*(1-4), 2-10.
- Zhai, W., M. Dai, and X. Guo (2007), Carbonate system and CO₂ degassing fluxes in the inner estuary of Changjiang (Yangtze) River, China, *Marine Chemistry*, *107*(3), 342-356.
- Zhang, X., R. D. Hetland, M. Marta-Almeida, and S. F. DiMarco (2012), A numerical investigation of the Mississippi and Atchafalaya freshwater transport, filling and flushing times on the Texas-Louisiana Shelf, *J. Geophys. Res.*, *117*(C11), C11009.

Table 4.1. Summary of survey cruises.

	Season	Date, Year	Boat	Survey Region	Coverage	MARS	NO ₃ +NO ₂	note	
					area	discharge	flux		
					km ²	m ³ s ⁻¹	10 ⁹ gC		
1	Spring	4/27-5/1, 2006	R/V Pelican	LA Bight	7200	17900	83900		
2	Spring	5/2- 7, 2007	OSV Bold	LA shelf	39100	25700	151000		
3	Spring	4/20-5/1, 2009	Cape Hetterass	LA shelf	41400	23300	124000		
4	Spring	3/9-21, 2010	Cape Hetterass	LA shelf	40900	38400	103000	Weather event	
5	Summer	8/9-12, 2004	R/V Pelican	LA Bight	9200	25700	105000		
6	Summer	6/6-11, 2006	OSV Bold	LA shelf	34100	19500	115000		
7	Summer	8/18-24, 2007	OSV Bold	LA shelf	41400	19500	62000		
8	Summer	7/17-20, 2008	R/V Pelican	Center LA s.	14900	32600	151000		
9	Summer	7/19-29, 2009	Cape Hetterass	LA shelf	41400	36500	126000	Weather event	
10	Fall	10/4-7, 2005	R/V Pelican	LA Bight	4400	9640	23400	Post hurricane	
11	Fall	9/6-11, 2006	OSV Bold	LA shelf	34700	7170	20100		
12	Fall	10/28-11/7, 2009	Sharp	LA shelf	41400	25600	52400		
13	Winter	1/9-20, 2009	Cape Hetterass	LA shelf	41400	13400	39600		

Table 4.2. Surface water $p\text{CO}_2$ values from bays along the coast of the LA shelf and from the lower Mississippi River.

Cruise Month	Salinity		$p\text{CO}_2$ (ppm)		
	mean	s.d.	mean	s.d.	n
<i>lower Mississippi</i>					
Aug-	2.0	0.2	1628.3	18.0	32
Oct-2005	5.9	0.4	1348.8	32.3	62
Jun-2006	1.9	0.7	1708.6	281.4	153
Sep-2006	6.2	0.8	1209.8	52.9	72
May-	1.2	1.0	1732.9	39.2	74
Aug-	5.0	0.7	1362.7	103.6	143
Jan-2009	0.1	0.0	977.4	77.7	46
Apr-2009	0.1	0.1	1663.2	53.2	86
Jul-2009	1.4	0.4	2222.4	57.2	91
Nov-	0.2	0.1	1611.9	78.5	63
Mar-2010	0.2	0.1	1407.5	164.6	76
<i>Atchafalaya</i>					
Jan-2009	0.1	0.1	1361.6	142.6	55
Apr-2009	1.2	1.7	1310.3	553.8	42
Jul-2009	0.5	0.7	2072.8	402.4	84
Nov-	0.6	0.8	1813.7	208.2	23
Mar-2010	0.1	0.0	1682.4	111.9	45
<i>Terrebonne</i>					
Jan-2009	30.7	1.0	532.4	95.3	55
Apr-2009	26.1	0.6	257.3	15.0	46
Jul-2009	28.6	0.3	486.4	52.5	66
Nov-	27.0	1.0	314.4	29.7	44
Mar-2010	23.1	0.7	293.6	23.7	56
<i>Calcasieu Lake</i>					
May-	22.8	0.1	171.5	5.0	20
Aug-	17.9	0.9	768.8	264.7	228

Table 4.3. Monthly air-sea CO₂ fluxes in the northern Gulf of Mexico (unit: mmol m⁻² d⁻¹). CO₂ fluxes were calculated for various regions: for the cruise survey area, the reference area (the gray area in Fig. 4.1), the inner shelf (bottom depth less than 20 m), the middle shelf (20 to 45 m), the outer shelf (45 to 200 m) and pelagic ocean (depth deeper than 200m), and LA Bight.

Year	Month	Survey area	Reference area	Inner	middle	outer	pelagic	LA Bight
2004	Aug	-5.26	-5.58	-5.29	-5.81	-	-	-4.9
2005	Oct	15.54	15.44	15.44	-	-	-	-5.4
2006	Apr	-3.36	-5.19	-7.44	-2.41	-	-	-5.4
2006	Jun	-2.64	-2.78	-5.76	-0.69	2.78	-	-7.2
2006	Sep	0.40	0.31	-0.20	0.58	2.62	-	-0.8
2007	May	-6.73	-6.99	-11.37	-2.70	-1.04	-	-12.9
2007	Aug	-0.98	-0.98	-0.64	-1.40	0.32	-	-2.7
2008	Jul	-1.00	-1.00	1.26	-4.32	-	-	-
2009	Jan	-1.00	-1.19	-1.14	-1.31	-0.02	1.39	-1.3
2009	Apr	-0.70	-1.33	-1.00	-1.97	3.43	2.13	-5.5
2009	Jul	2.08	3.31	3.62	3.04	2.66	1.98	1.1
2009	Nov	3.64	3.27	3.81	2.77	2.54	3.20	-1.6
2010	Mar	-10.26	-17.40	-17.49	-17.61	-12.57	-1.42	-12.4

Table 4.4. Average CO₂ flux, temperature, pCO₂, and area in the LA shelf of each cruise. (unit: mmol m⁻² d⁻¹)

Salinity	Aug-04	Oct-05	Apr-06	Jun-06	Sep-06	May-07	Aug-07	Jul-08	Jan-09	Apr-09	Jul-09	Nov-09	Mar-10
<i>Average of areal-integrated CO₂ flux</i>													
0 to 17	0.00	27.39	0.00	-5.03	-7.85	-6.21	31.53	-4.70	13.07	17.15	2.94	10.17	5.17
17 to 25	-7.75	25.62	-7.61	-9.83	-3.91	-19.45	2.18	-0.78	1.82	-5.24	-1.48	3.63	-19.65
25 to 33	-4.63	12.39	-7.46	-4.45	0.01	-11.79	-2.14	2.59	-2.63	-11.04	2.37	0.47	-18.07
33 to 35	-	16.56	-2.93	0.54	2.14	-2.81	0.65	-	-1.99	-2.37	5.27	2.31	-
<i>Average of areal-integrated temperature</i>													
0 to 17	-	28.2	-	27.5	31.0	23.0	31.4	31.6	12.6	21.5	29.5	20.0	16.1
17 to 25	-	28.4	-	29.6	31.2	25.5	31.1	31.2	15.7	23.8	29.3	21.9	17.3
25 to 33	30.6	28.3	25.2	29.4	29.8	25.1	30.8	30.9	18.1	23.2	29.8	23.9	18.3
33 to 35	-	28.3	24.9	28.5	29.5	24.2	30.3	-	19.7	23.1	30.0	25.4	-
<i>Average of areal-integrated pCO₂</i>													
0 to 17	-	506.9	-	305.3	297.2	316.2	616.0	286.1	549.1	483.0	419.5	445.1	426.8
17 to 25	-	539.2	-	199.0	323.8	195.3	390.9	350.7	399.6	340.7	336.0	403.6	259.2
25 to 33	300.2	442.9	279.3	296.2	364.5	252.7	328.1	410.1	356.2	302.7	389.4	385.0	255.7
33 to 35	-	457.4	329.0	380.4	394.4	336.6	380.8	-	359.7	362.2	444.0	395.5	-
<i>Area (km²)</i>													
0 to 17	-	433	-	866	541	1407	325	4109	1842	1841	2167	3360	3789
17 to 25	2812	433	975	3463	541	4225	1843	7039	2815	5742	4222	7479	10504
25 to 33	6367	3681	3568	18289	27574	14623	29096	7897	16899	18401	23332	18280	30352
33 to 35	2812	757	2162	9178	3235	11469	12304	7039	9515	11899	14487	15257	10504

Table 4.5. Averages carbonate, nutrient, and salinity data used as end-members for the mixing model. (Data from Cai and Lohrenz, unpublished data.)

		Winter	Spring	Summer	Fall	Annual
<i>Mississippi River end-member</i>						
TA	μM	2067.7	2277.3	2617.9	1787.4	2187.6
DIC	μM	2108.5	2302.7	2634.3	1826.7	2218.1
NO ₃	μM	50.1	96.5	86.3	54.7	71.9
Salinity		1.50	0.60	1.21	0.15	0.86
Temperature	°C	7.95	16.39	27.57	16.69	17.15
<i>Seawater end-member</i>						
TA	μM	2470.0	2469.9	2453.0	2467.0	2453.1
DIC	μM	2137.0	2133.0	2130.0	2123.0	2107.1
NO ₃	μM	0.0	0.2	0.8	0.1	0.7
Salinity		36.45	36.53	35.60	36.52	36.57
Temperature	°C	23.23	23.36	29.00	26.11	26.00

The temperatures were used to convert the unit from μM to μmol kg⁻¹ and were not involved in the conservative mixing model.

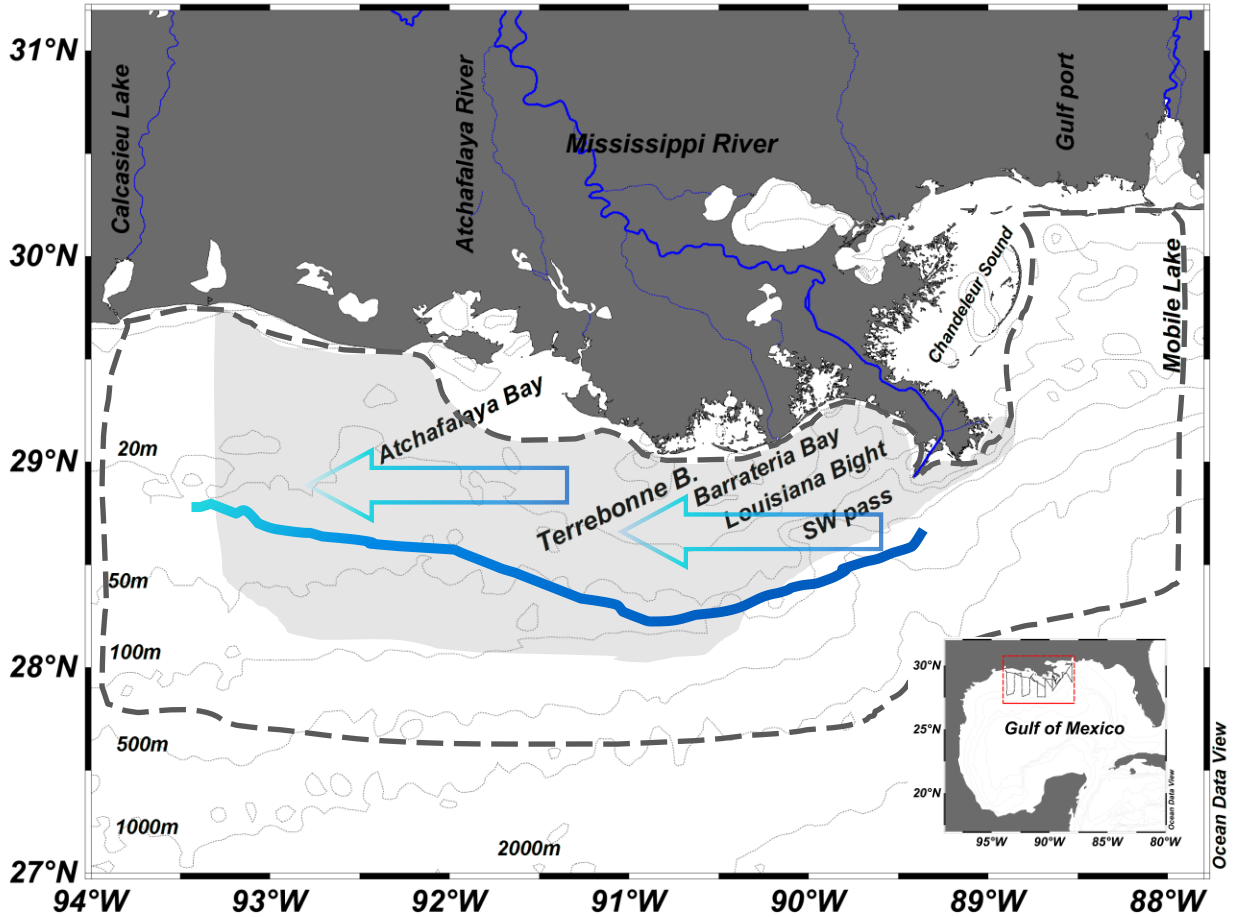


Figure 4.1. The survey area. The shelf-wide area was surveyed during June 2006 to 2007 (the light gray area); cross-shelf area was surveyed during 2009 to 2010 (the gray dash line circled area); and areas on/near LA Bight were surveyed from 2004 to June 2006. The blue arrows and lines conceptually shows the direction and boundary of the MARS plume, respectively, which was usually confined to the north of 28°N on the LA shelf (the blue line is an arbitrary boundary). The light gray area was used as a reference area to unify the shelf-wide and cross-shelf survey areas when discussing air-sea CO₂ fluxes.

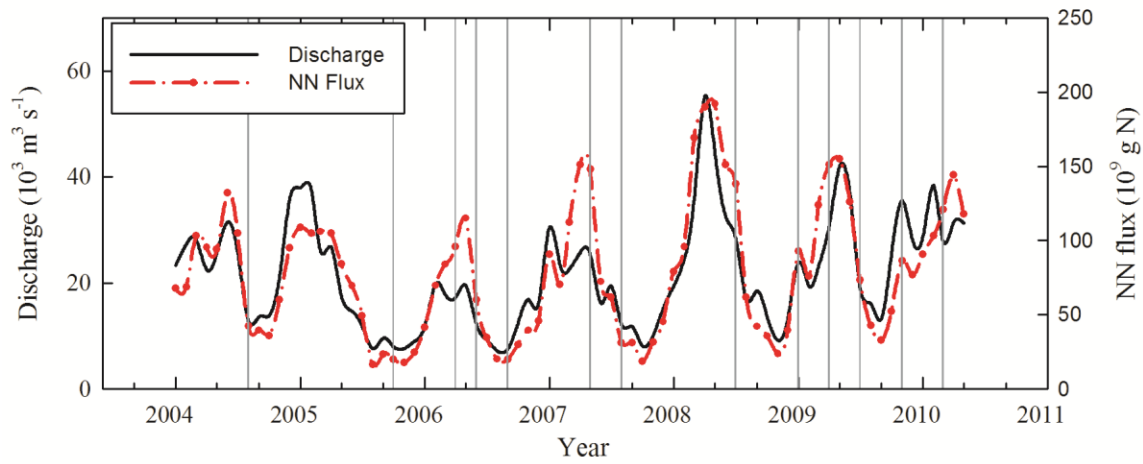


Figure 4.2. The variations of monthly freshwater discharge (black line), and nitrate plus nitrite (NN) fluxes (red line) from the MARS from 2004 to May 2010. Both data were from U.S. Geological Survey (USGS, “Hypoxia in the Gulf of Mexico studies”, <http://toxics.usgs.gov/hypoxia/index.html>). The vertical gray line indicates the first day of each survey cruise.

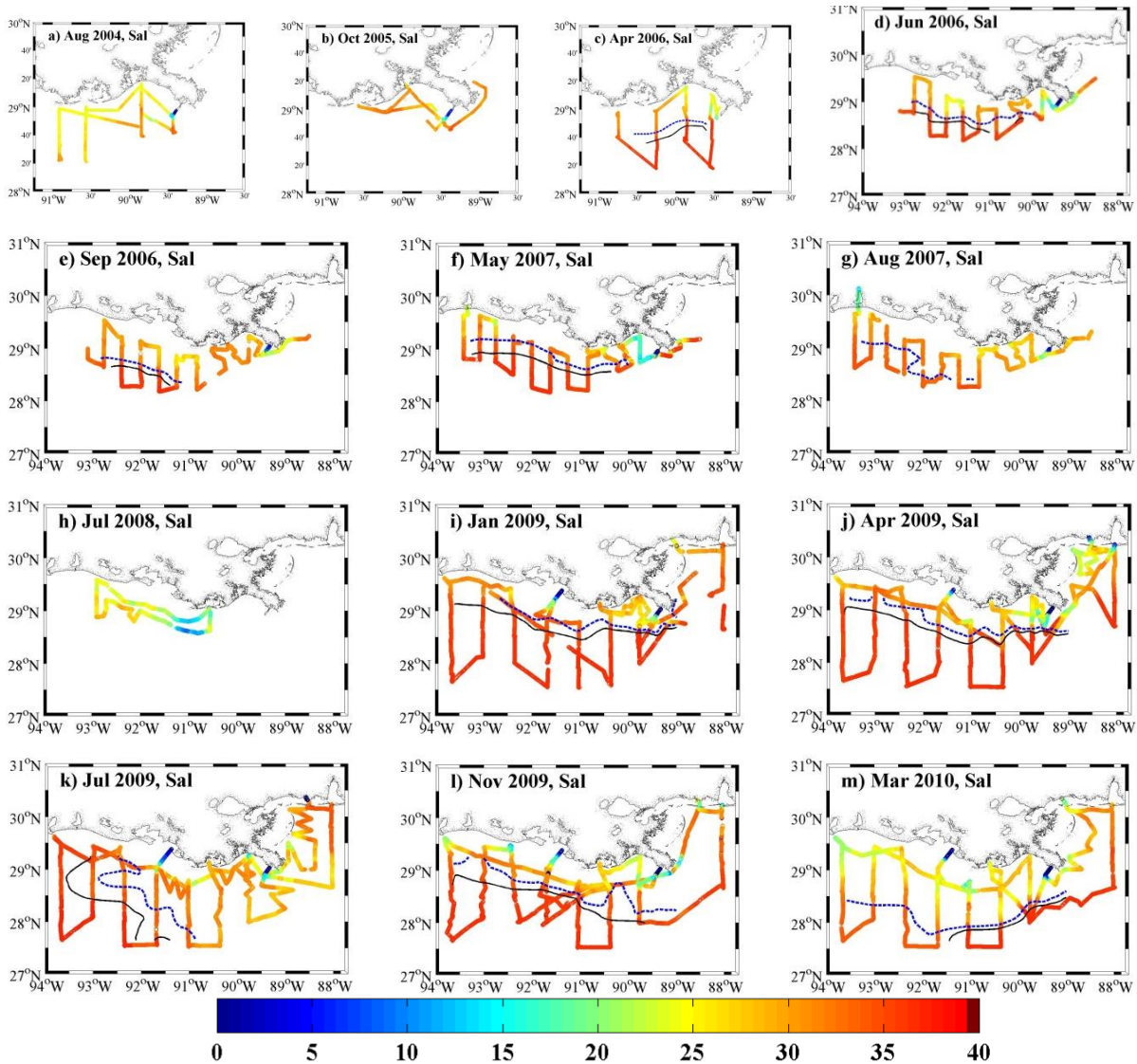


Figure 4.3. Distributions of sea surface salinity along cruise tracks in each cruise. a) August 2004, b) October 2005, c) April 2006, d) June 2006, e) September 2006, f) May 2007, g) August 2007, h) July 2008, i) January 2009, j) April 2009, k) July 2009, l) November 2009, and m) March 2010. Not that the freshwater plume was usually distributed alongshore to the north of 28°N, such but was confined to the eastern shelf in July 2009, and extended over 28°N to pelagic Gulf of Mexico in March 2010. Blue dash and black lines represented salinity contour line of 33 and 35, respectively, and were not shown when such high salinity waters were merely observed.

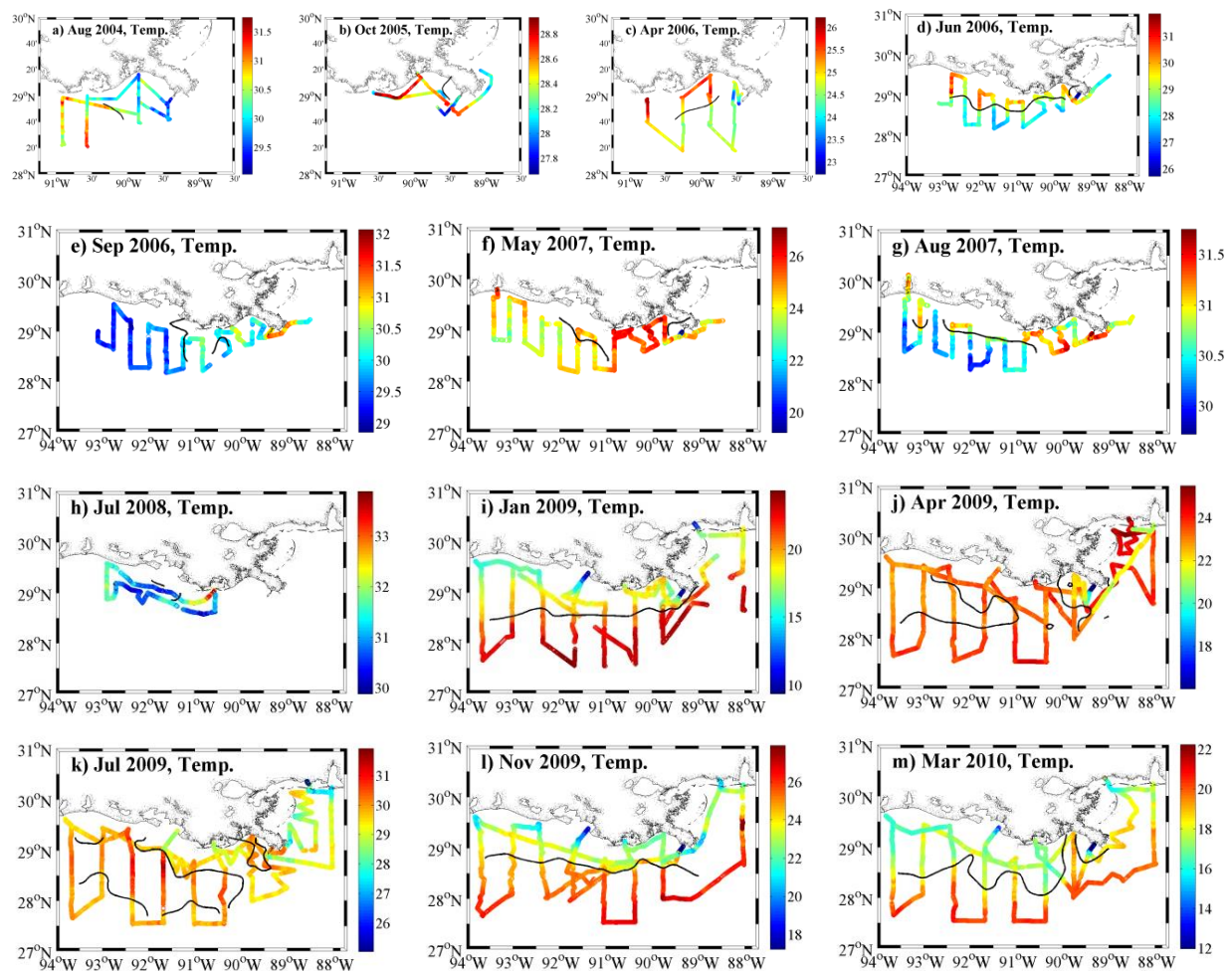


Figure 4.4. Distributions of sea surface temperature in each cruise. The black lines displayed the contour line of mean temperature for each cruise. Each panel displayed the same cruise as in Figure 4.3.

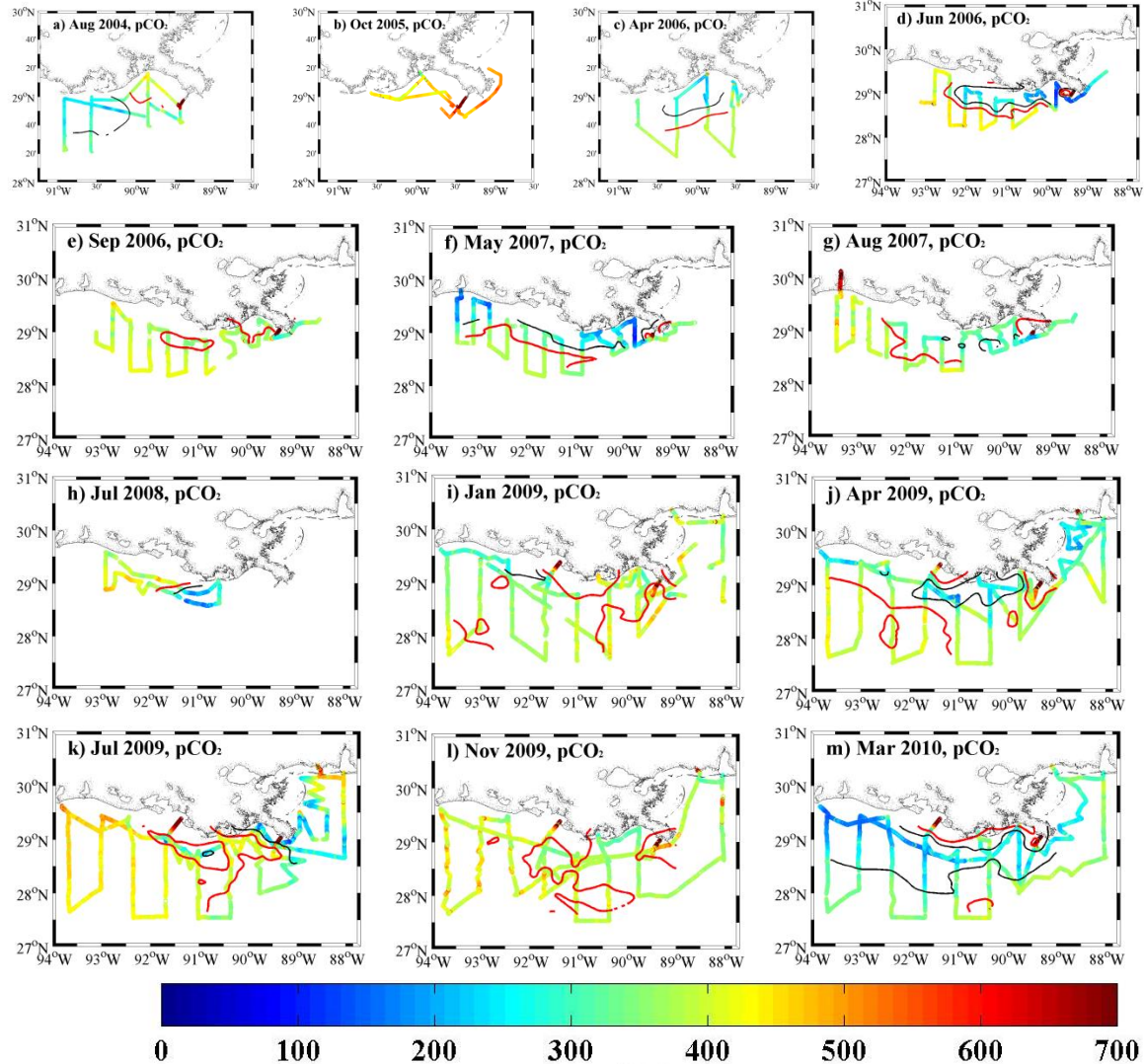


Figure 4.5. Distributions of sea surface $p\text{CO}_2$. The black and red lines represented contour line of 300 and 390 μatm , respectively. Each panel displayed the same cruise as in Figure 4.3. The distribution of under-saturated $p\text{CO}_2$ was corresponded to the freshwater distribution in a meso-scale, when the MARS plumes were distributed alongshore (c,d,e,f,g,j), confined to the eastern shelf in July 2009, or extended crossed 28°N in March 2010, except in November and in the offshore in January.

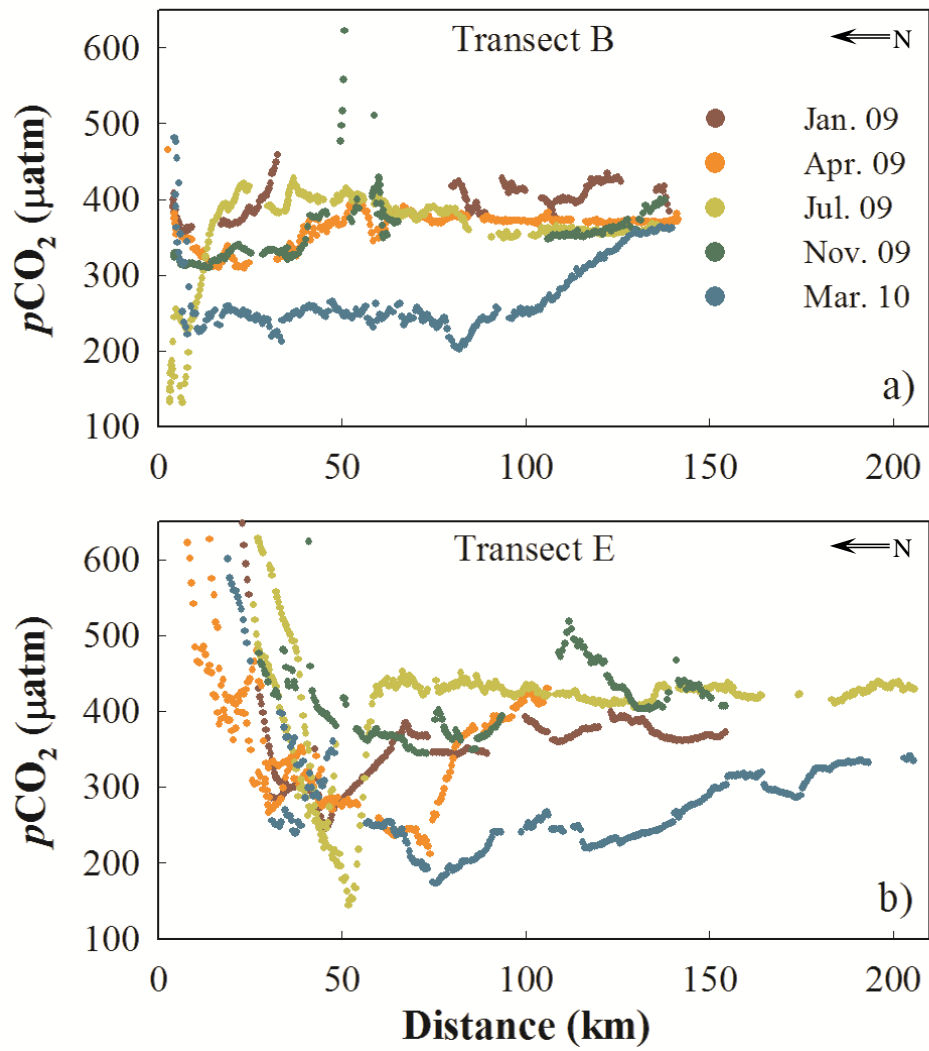


Figure 4.6. Variations of sea surface $p\text{CO}_2$ values across the LA shelf. Data were from five cruises between 2009 to 2010 and display for a) transect B on longitude 89.76°W , and for b) transect E on longitude 91.68°W .

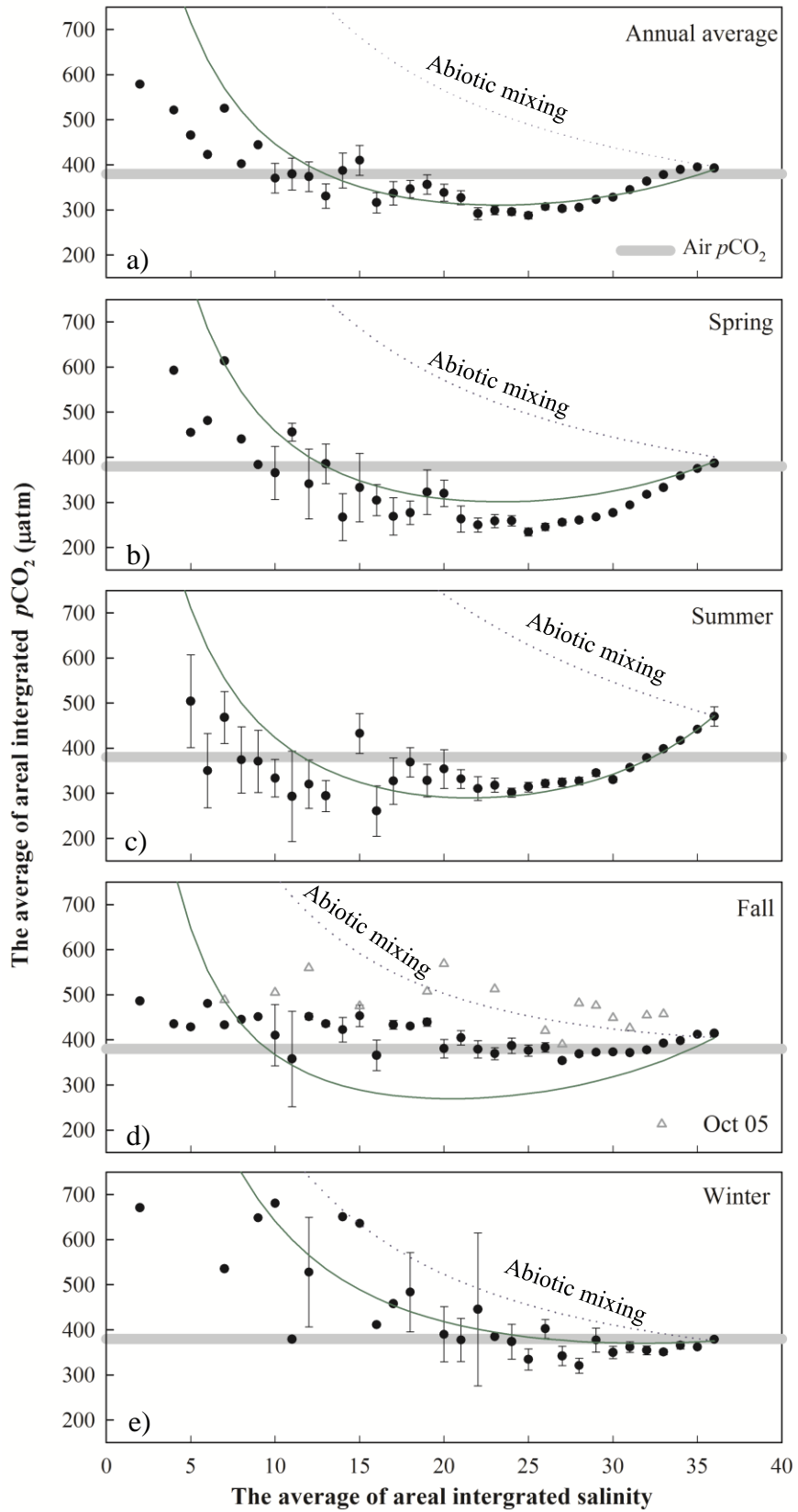


Figure 4.7. Relationship between $p\text{CO}_2$ values and salinity. Both $p\text{CO}_2$ and salinity were averaged from the mean in $0.1^\circ \times 0.1^\circ$ area. This relationship was demonstrated in a) annual average, b) spring, c) summer, d) fall, and e) winter. ± 1 standard error was shown for the average of areal-integrated $p\text{CO}_2$ value. Dotted lines and solid lines represent abiotic mixing and NO_3^- removal predicted $p\text{CO}_2$ values, respectively. The end-members for these predictions are in Table 4. Triangle markers in d) were the areal integrated values in October 2005, which was affected by remaining effects of Hurricanes.

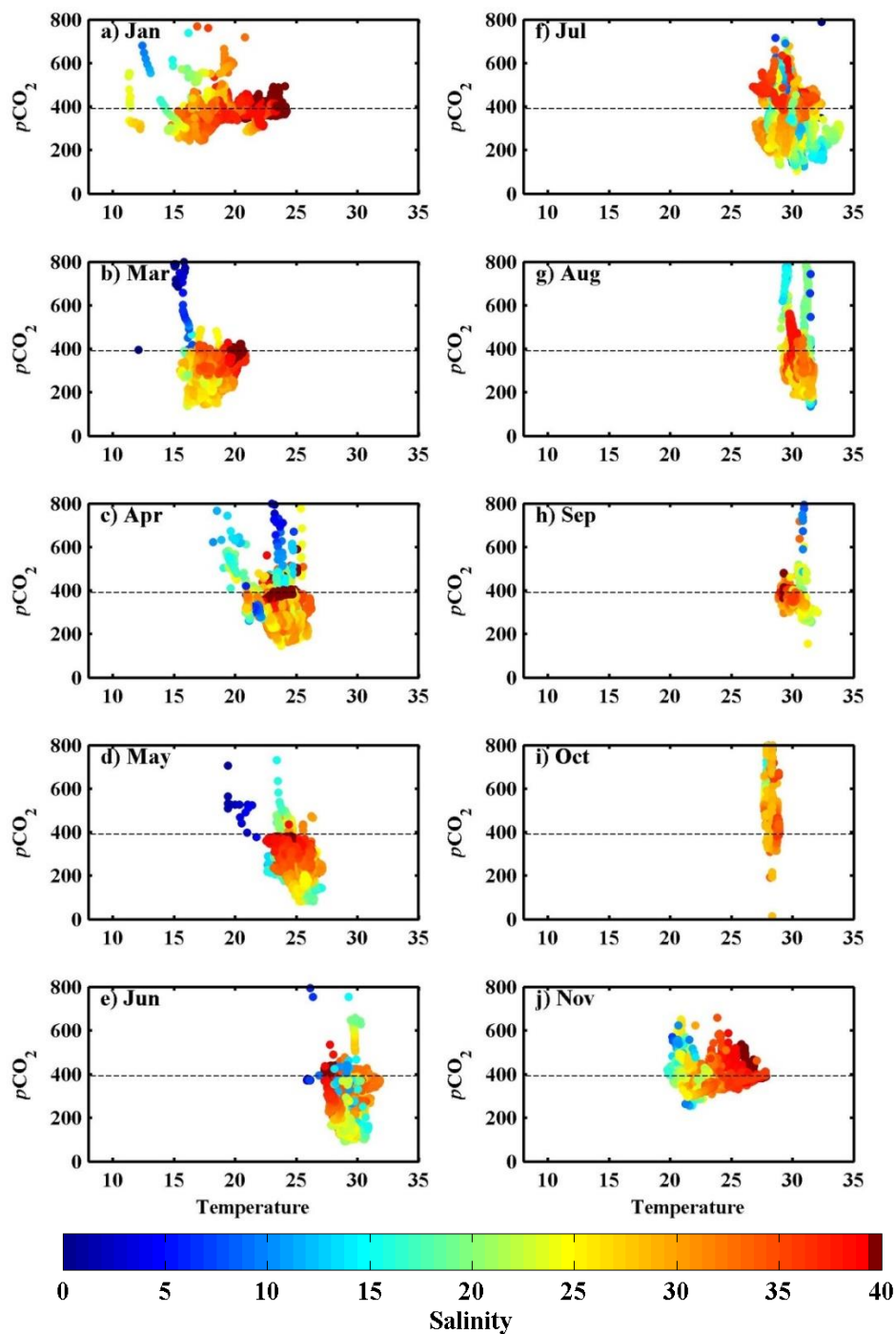


Figure 4.8. Relationships between sea surface $p\text{CO}_2$ and its temperature. Data from thirteen cruises are categorized in ten months: a) January, b) March, c) April, d) May, e) June, f) July, g) August, h) September, i) October, and j) November. The color of each marker represented its salinity.

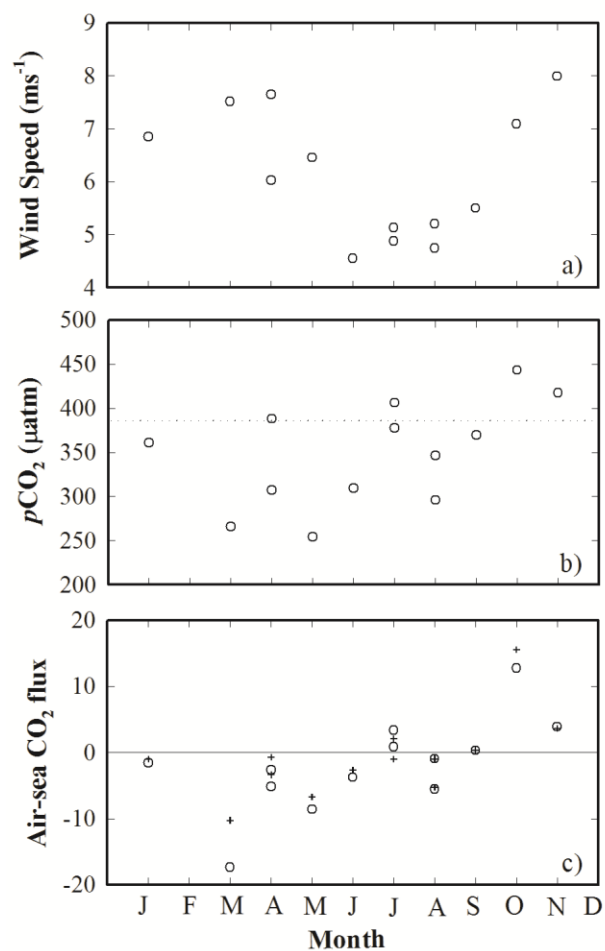


Figure 4.9. Seasonal variations of the average of areal-averaged values in the reference area. a) QuikSCAT satellite wind, b) sea surface $p\text{CO}_2$, and c) air-sea CO_2 flux in the reference area (circles) and over the cruise surveyed area (cross markers). The dash line in b) represents the atmospheric CO_2 value.

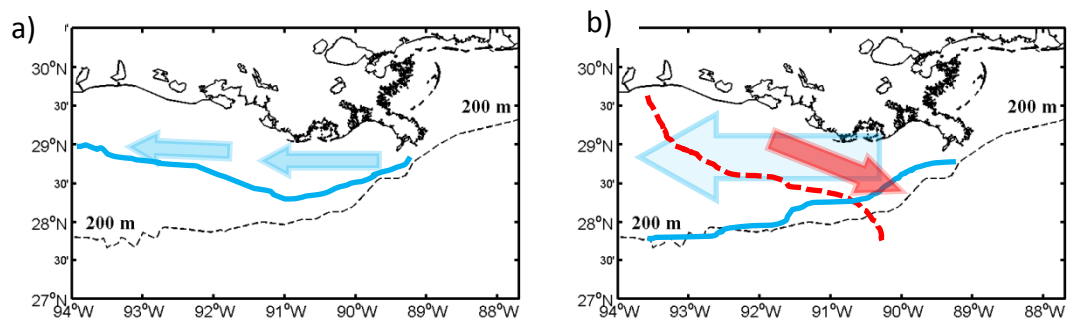


Figure 4.10. Conceptual diagrams for two unusual MARS plumes. a) Due to northerly wind and high freshwater discharge, the plume extended over 28°N, such as in March 2010 (modified from Huang et. al., under review); b) due to an unusual shelf circulation, the plume was confined to the eastern shelf and more cross-shelf component was observed on the LA shelf, such as in July 2009 (modified from Huang et al., in preparation).

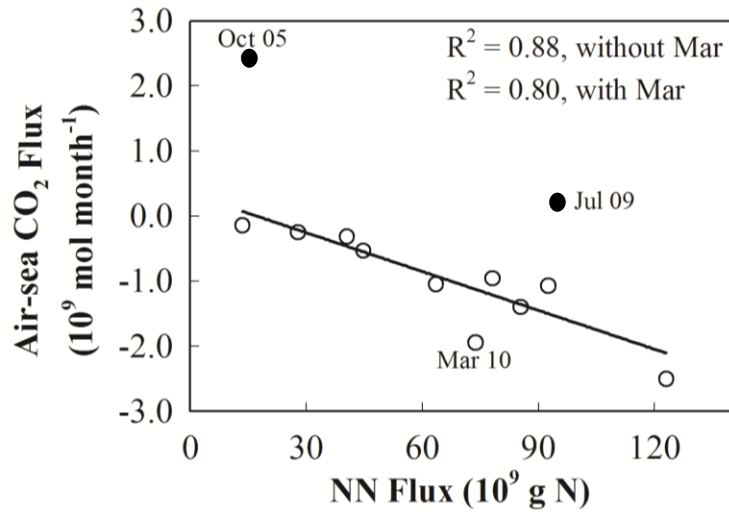


Figure 4.11. The correlation between air-sea CO₂ fluxes and riverine NN fluxes on the LA Bight. The air-sea CO₂ fluxes were monthly averages of areal-integrated values, and NN fluxes (USGS data) were from the Mississippi River in one month in advance to the month of air-sea CO₂ flux. Data from unusual plumes, such as July 2009 or affected by Hurricanes in October 2005 were exceptions and were not included in the linear regression.

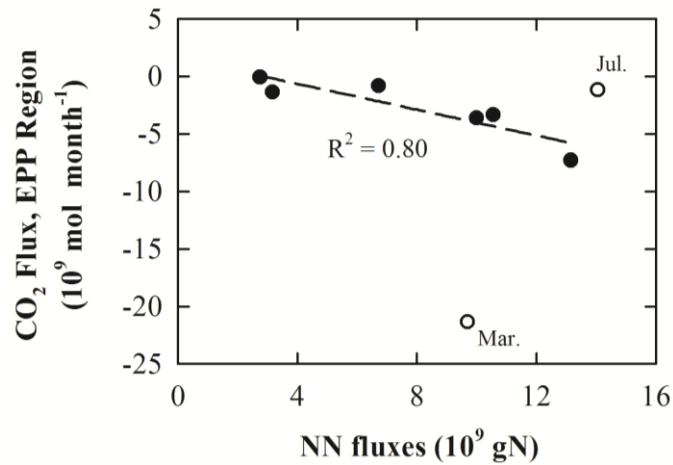


Figure 4.12. The correlation between air-sea CO_2 flux in the enhanced PP region and riverine NN fluxes on the entire LA shelf. The enhanced PP was defined by waters with areal integrated $p\text{CO}_2$ values less than $300 \mu\text{atm}$, and the NN flux (USGS data) was averaged from one and two month in advance to the month of $p\text{CO}_2$ values. The correlation coefficient was high ($R^2 = 0.80$) for those alongshore plume (black dots).

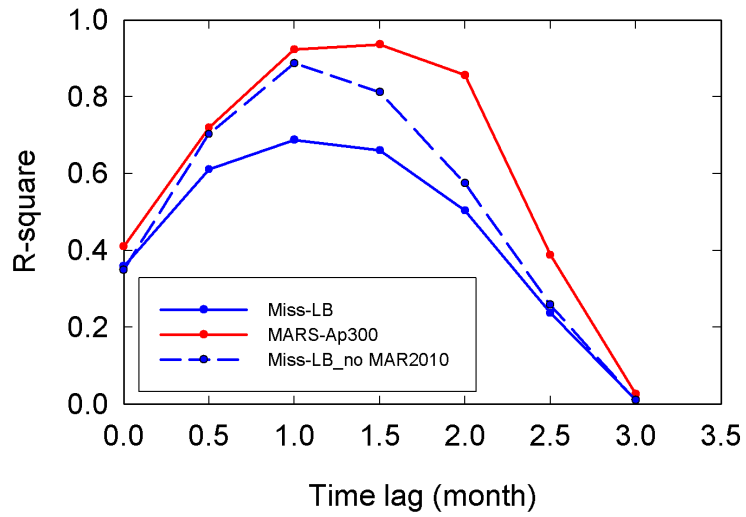


Figure 4.13. The relationship between the lag-time to the riverine NN fluxes and the coefficient of determination (R^2). The red line is for the relationship between Mississippi River NN fluxes and air-sea CO_2 fluxes on the LA Bight, and the blue line is for the MARS NN fluxes and the coverage of enhanced PP on the LA shelf.

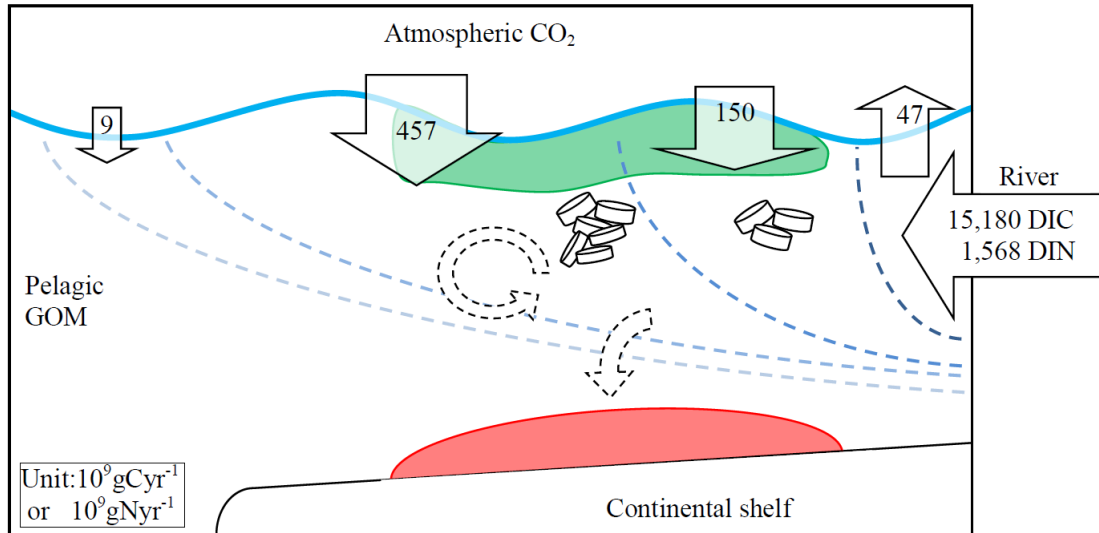


Figure 4.14. The conceptual model. Blue dash lines separate the plume into four salinity divisions: 0-17, 17-25, 25-33, and 33-35. Green area represents enhanced primary production area. (Units are in 10^9 gC yr^{-1} for air-sea CO_2 flux and riverine DIC, and 10^9 g N yr^{-1} for riverine DIN).

CHAPTER 5

THE CARBON DIOXIDE (CO₂) SYSTEM IN THE MISSISSIPPI RIVER DOMINATED
CONTINENTAL SHELF, NORTHERN GULF OF MEXICO—II:
THE DYNAMICS OF SURFACE CO₂ AND OXYGEN¹

¹ Wei-Jen Huang, Wei-Jun Cai, Yongchen Wang, Steven E. Lohrenz, and Patricia L. Yager.

To be submitted to *Journal of Geophysical Research*.

Abstract

Sea surface carbon dioxide (CO_2) is highly dynamic and its controlling factors are complex, especially for a river-dominated continental shelf. We conducted 10 cruises on the lower Mississippi River channel and the Louisiana (LA) shelf, and measured sea surface partial pressure of carbon dioxide ($p\text{CO}_2$), dissolved oxygen (DO), salinity, and temperature with high frequencies. In a companion paper, we report $p\text{CO}_2$ distributions and air-sea CO_2 fluxes. Here, we interpret $p\text{CO}_2$ and DO relationships by simulating three physical and biogeochemical processes: river-ocean mixing, air-sea gas exchange, and biological processes (autotrophy vs. heterotrophy). Our analysis shows that biological CO_2 fixation is generally the most important factor in reducing surface water $p\text{CO}_2$ and increasing DO except for the initial mixing stage ($S < 17$) where mixing is often important in reducing surface water $p\text{CO}_2$. In low salinity waters, mixing is particularly important and biological CO_2 reduction was also important during low discharge seasons. In addition, there are clear spatial and temporal differences in the relative importance of these three processes over the LA shelf. For example, $p\text{CO}_2$ -to-DO relationships suggest autotrophic dominance on the eastern shelf and a transition to heterotrophy when the plume was extended toward Texas in March 2010. Air-sea gas exchange appeared to be important only in November and in some areas in January. Finally, our analysis also reveals a time lag between CO_2 and DO concentrations and the underlying biological processes; i.e. a switch from net autotrophy to net heterotrophy while observed DO was still oversaturated and $p\text{CO}_2$ was under-saturated.

1. Introduction

The continental shelf is an active site of air-sea exchange of carbon dioxide (CO₂) and is an important part of the global carbon cycle [Borges, 2011; Cai, 2011; Cai *et al.*, 2006; Chen and Borges, 2009; Ducklow and McCallister, 2005; Mackenzie *et al.*, 2004]. A thorough understanding of the dynamics of *p*CO₂ variations on the continental shelf is necessary for the estimate of the global carbon budget and for predicting the system response to global climate change. Previous studies have shown that river discharges of freshwater and nutrients are often important in controlling the partial pressure of CO₂ (*p*CO₂) variations in its plume and surrounding areas [Cai, 2003; Cooley *et al.*, 2007; Kortzinger, 2003; TERNON *et al.*, 2000; Tseng *et al.*, 2011; Tsunogai *et al.*, 1997; Zhai and Dai, 2009; Zhai *et al.*, 2007], mostly through biological activities in the river plumes [Borges and Gypens, 2010; Cai *et al.*, 2011; Chou *et al.*, 2011]. However, as most of these studies have focused on limited spatial or time scales, a shelf-wide survey of the dynamics of *p*CO₂ variations over annual time scales is still needed for large river-dominated shelves.

The Louisiana (LA) shelf receives a large amount of freshwater discharge from the Mississippi and Atchafalaya River system (MARS) and experiences intense mixing processes [Dinnel and Wiseman, 1986; Zhang *et al.*, 2012]. In addition, enhanced primary production and complicated biological activities are also observed in the Mississippi River plume [Lehrter *et al.*, 2009; Lohrenz *et al.*, 1997]. Previous studies have suggested that mixing and biological activities are two important variables for *p*CO₂ variations in a limited region of the Mississippi River plume [Cai, 2003; Lohrenz and Cai, 2006; Lohrenz *et al.*, 2010]. John *et al.* [2007] also have shown that the relationship between the diatom/pelagophyte productivity was largely responsible for a large CO₂ drawdown in the Mississippi River plume. As the biological activities are highly

dynamic in the Mississippi River plume, *Dagg and Breed* [2003] have proposed a conceptual model to demonstrate the transition of trophic status: autotrophic activities reached maximum in near-field to mid-field, and heterotrophic activities reached maximum later, from mid-field to far-field. But how various plume-associated processes affect the variation of sea surface $p\text{CO}_2$ is still not clear.

In addition to biologically induced CO_2 variations, the role of air-sea CO_2 exchanges in water carbonate systems have been considered along with air-sea oxygen exchange [*Carrillo et al.*, 2004; *DeGrandpre et al.*, 1998; *Zhai et al.*, 2009]. *Zhai et al.* [2009] have associated the surface $p\text{CO}_2$ and DO relationship by coupling them with the Redfield ratio [*Redfield*, 1958] and the Revelle factor in a coastal plume and upwelling system. In addition, *DeGrandpre et al.* [1998] have suggested that oxygen air-sea reequilibration was quicker than CO_2 reequilibration and suggests this characteristic has significant impact on the $p\text{CO}_2$ -to-DO relationship. *Carrillo et al.* [2004] have demonstrated the importance of air-sea gas exchanges solely through this characteristic and also discuss effects from photosynthesis/respiration and cooling/heating, separately. However, their examples were from systems where mixing is not as important as in a river-ocean mixing case. Thus a dynamic model considering the combinatorial effects of simultaneous interactions between biological and air-sea gas exchanges on $p\text{CO}_2$ -to-DO relationship under the mixing scheme is needed to explain the complicated plume system.

In this study, we first present sea surface $p\text{CO}_2$ and DO relationships from ten cruises over the LA shelf from four seasons. We further consider the transition of trophic status (from autotrophy to heterotrophy) and air-sea gas exchanges simultaneously, and simulate the dynamic $p\text{CO}_2$ and DO relationship to discuss the controlling factor of $p\text{CO}_2$ over the LA shelf. This study follows our companion paper entitled “The Carbon dioxide (CO_2) system in the Mississippi

River dominated continental shelf, northern Gulf of Mexico--I: the distribution and air-sea fluxes” (referred to as “study Part I” here).

2. Methods

Ten cruises were conducted on the LA shelf and its surrounding area (Table 5.1) including three shelf-wide cruises in 2006 and 2007, five other larger shelf-wide cruises in 2009-2010, one cruise was conducted on the LA Bight in 2004, and the other one on the middle LA shelf in July 2008 (Fig. 5.1).

During all cruises, seawater was continuously pumped from underway system from a depth of about 1 to 2 m. Surface seawater $p\text{CO}_2$ was measured through an underway $p\text{CO}_2$ analyzer installed in the shipboard laboratory. For the $p\text{CO}_2$ measurements, see study Part I for technical details. Sea surface salinity (SSS) and temperature (SST) were measured by a Seabird SBE-45 flow through thermo-salinograph. Sea surface oxygen was measured by a Yellow Springs Instrument meter (YSI) from 2006 to 2007 and was measured by an Aanderaa DO sensor from 2008 to 2010. Both DO sensors were calibrated against discrete samples measured by the Winkler method. DO samples for the Winkler methods were taken from the Go-Flow bottles installed with a SEACAT thermosalinograph system (CTD) at surface depth (1 to 2 m).

3. Results

3.1. Distribution of sea surface salinity, $p\text{CO}_2$, and DO

Detailed descriptions for the SSS and $p\text{CO}_2$ were presented in Part I of our study [*Chapter 4*] with the results summarized below. Based on the distribution of sea surface salinity, the freshwater distributions were alongshore toward Texas and were confined to north of 28°N for

most of the cruises, except in March 2010 and in July 2009. For these alongshore plumes, $p\text{CO}_2$ values were usually under-saturated with respect to the atmosphere on the inner shelf. In addition, under-saturated $p\text{CO}_2$ values were mostly observed along the MARS plume trajectory. When the plume trajectory was affected by wind forcing, the distribution of under-saturated $p\text{CO}_2$ also changed correspondingly. For example, under-saturated concentrations of $p\text{CO}_2$ were observed in a wide MARS plume to the south of 28°N in March 2010. This was observed when the MARS plume was confined to the eastern LA shelf due to an unusual shelf circulation in July 2009.

Distributions of DO also showed strong spatial variations and were related to the distribution of freshwater sources. DO saturation displayed contrasting distributions with export from freshwater sources to the shelf, i.e. waters were under-saturated in the Mississippi River mouth and the Atchafalaya Bay but were shifted to oversaturated when exported to the shelf (Fig. 5.2). These oversaturated waters gradually transitioned to under-saturated waters when away from these fresh water sources for many months. In September, under-saturated DO waters covered nearly the entire LA shelf except those close to the freshwater sources (Fig. 5.2i). For the widespread plume in March 2010, oversaturated DO waters were also observed in this plume trajectory (Fig. 5.2b). For the MARS plume confined to the eastern shelf in July 2009, the DO distribution was different from the other cruises, showing a contrast between the eastern and west shelves (Fig. 5.2g). In November, oversaturated DO waters largely covered the LA shelf (Fig. 5.2j).

3.2. $p\text{CO}_2$ and DO relationship

Low salinity, middle-to-high salinity, and high salinity waters showed distinctly different $p\text{CO}_2$ and DO relationships. First, low salinity waters ($S < 17$), including the freshwater end-member, were usually characterized with oversaturated $p\text{CO}_2$ and had slightly under-saturated O_2

with respect to the atmospheric saturation values (Fig. 5.3). However, this situation changed from May to July: more under-saturated $p\text{CO}_2$ were observed, while their corresponding DO concentrations were oversaturated in the low salinity plume. During this productive and high river discharge season, the DO saturation often went as high as 150-200% while $p\text{CO}_2\%$ dropped to half of the atmospheric value. In later summer and fall, high DO% was no longer observed in low salinity waters.

For the middle-to-high salinity waters ($17 < S < 35$), most were characterized with highly oversaturated DO and under-saturated $p\text{CO}_2$ from January to September (Fig. 5.4). The highest DO% and lowest $p\text{CO}_2\%$ waters were also observed from these months, e.g., DO% was 250% in July 2009 and $p\text{CO}_2\%$ was close to 20% in May 2007 and Jun 2006. However, these waters showed different $p\text{CO}_2$ and DO characteristics in November, i.e., DO% varying from 150% to 100% while the variation of $p\text{CO}_2\%$ was rather small (Fig. 5.4j). Finally, high salinity ($S > 35$) waters also showed different characteristics from those of low-to-middle waters, being usually distributed close to equilibrium with the atmosphere on the $p\text{CO}_2$ and DO diagram (Fig. 5.5).

3.3. Distributions of Quadrants from $p\text{CO}_2$ and DO diagram

Following *Carrillo et al.* [2004], we identified the characteristic quadrants for waters with various $p\text{CO}_2$ and DO saturation values, and they showed clear and consistent spatial and seasonal variability (Fig. 5.6). Data from quadrant I with high DO% and low $p\text{CO}_2\%$ were widely distributed along the LA shelf throughout the year. Data from quadrant two, i.e., high $p\text{CO}_2$ and oversaturated DO or low salinity waters, were only important in January, June, July, and November. Data from quadrant III with high $p\text{CO}_2$ and slightly lower DO% were usually observed on or close to the freshwater sources throughout every month, but they were also observed offshore in June and September. Data from quadrant IV with DO% and low $p\text{CO}_2\%$

covered spotty areas for most of the year and only covered continuous areas in March 2010 and in September 2009.

4. Discussion

4.1. Effect of mixing in low salinity sub-region

The $p\text{CO}_2$ and DO relationship in low salinity sub-region ($S < 17$) demonstrated a characteristic different from the other salinity sub-regions, i.e., high $p\text{CO}_2\%$ in the river end-member (usually higher than 200%). We estimated the conservative mixing lines between freshwater and seawater end-members on the $p\text{CO}_2$ and DO diagram by converting from conservative mixing of dissolved inorganic carbon (DIC) and total alkalinity (TA) to $p\text{CO}_2$. Both oversaturated and under-saturated DO conditions in the freshwater end-members are used for the simulation (Fig. 5.3k). Observed $p\text{CO}_2$ and DO data from low salinity waters showed that these waters were consistent with this mixing-controlled mechanism from January to April and August to November (Fig. 5.3). *Lohrenz et al.* [2010] used the Principle Component Analysis and also suggested that the same conclusion for waters with salinity less than 18 in April and August. The water was not significantly affected by air-sea gas exchange because the water transportation time was short (about two days) for the low salinity waters [*Green et al.*, 2006].

However, for low salinity waters during May to September, while some data were still consistent with the modeled mixing curve, more often the low salinity waters deviated from this conservative mixing curve, suggesting factors other than mixing affected those waters with oversaturated DO and/or under-saturated $p\text{CO}_2$. We suggest that biological activities were also important in low salinity waters from May to July and September (see Section 4.3 for further discussion of this point).

4.2. Effect of trophic transition and air-sea gas exchanges during spring and summer

We combined the concept of trophic status transition and air-sea gas exchanges to develop a dynamic $p\text{CO}_2$ and DO model, and discussed their effect on spatial and seasonal variations of $p\text{CO}_2$ on the $p\text{CO}_2$ and DO diagram.

4.2.1. Model structure

We assumed DIC concentration in a water mass was affected by net community production (NCP) and air-sea CO_2 exchanges, resulting in a new DIC as in Eq. 1:

$$DIC_{new} = DIC_{initial} + NCP_C + F_{CO_2} \times t/h \quad (1)$$

where DIC_{new} is the newly generated DIC concentration, $DIC_{initial}$ is the initial DIC concentration, NCP_C is the NCP in DIC unit, F_{CO_2} is the air-sea CO_2 flux, t represents time, and h represents mixing layer depth. Assuming TA was constant ($2400 \mu\text{mol kg}^{-1}$), this new DIC concentration and TA is used to calculate a new water $p\text{CO}_2$ value through the CO2SYS (Matlab version). This new water $p\text{CO}_2$ therefore created new air-sea CO_2 flux by Eq. 2:

$$F_{CO_2} = Kt \times S_{CO_2} \times (pCO_{2w} - pCO_{2a}) \quad (2)$$

where Kt is the gas exchange coefficient which we adopted from the equation given by Wanninkhof [1992], S_{CO_2} is the CO_2 solubility adopted from Weiss [1974], $p\text{CO}_{2w}$ is the water $p\text{CO}_2$, and $p\text{CO}_{2a}$ is the atmospheric CO_2 . Wind speed of 7.5 m s^{-1} was set for general simulation and the other boundary conditions can be found in Table 5.2. Thus, this new air-sea CO_2 flux resulted in another new DIC (Eq. 1) and therefore changed the air-sea CO_2 fluxes again. This effect of air-sea interaction and NCP on the DIC can be summarized as the following equation:

$$\frac{dDIC}{dt} = NCP_C + \frac{F_{CO_2}}{h} \quad (3)$$

Air-sea gas exchange and effect of NCP were also applied to DO concentration by the following equation:

$$DO_{new} = DO_{initial} + NCP_{O_2} + F_{O_2} \times t/h \quad (4)$$

where DO_{new} is the new DO concentration, $DO_{initial}$ is the initial DO concentration, NCP_{O_2} is the NCP in O_2 unit, and F_{O_2} is the air-sea O_2 fluxes. This new water DO therefore results in a new air-sea O_2 flux by Eq. 5:

$$F_{O_2} = Kt \times S_{O_2} \times (pO_{2w} - pO_{2a}) \quad (5)$$

where S_{O_2} is the solubility adopted from *Weiss* [1974], pO_{2w} is the water O_2 pressure and pO_{2a} is the atmospheric O_2 pressure. This O_2 flux therefore results in a new DO concentration through Eq. (4). This dynamic process between air-sea gas exchanges and NCP is summarized as Eq. 6:

$$\frac{dO_2}{dt} = NCP_{O_2} + \frac{F_{O_2}}{h} \quad (6)$$

Finally, NCP_C and NCP_{O_2} were coupled by the Redfield ratio [*Redfield*, 1958]:

$$NCP_C = C/O_{Redfield} \times NCP_{O_2} \quad (7)$$

The initial DO, TA, DIC, pCO_2 values are listed in Table 5.2. This dynamic process is simulated in 0.1- to 0.2-day intervals. The atmospheric pCO_2 value is set to 390 μatm .

4.2.2. Under auto-to-hetero-trophy processes and gas exchanges

To simplify the conceptual model of trophic transition given by *Dagg and Breed* [2003], we assume a water mass with positive NCP (net community production) in the first N days. This positive NCP (autotrophy) transits to negative NCP (heterotrophy) on day N and maintains this negative NCP for the remaining days. This assumption implies that autotrophy in the first N days is in the near-field, and heterotrophy is in the far-field.

As a result, the O_2 saturation status ($O_2\%$) increased over time in the first N day (autotrophy) and then kept decreasing for the remaining days (heterotrophy) (Fig. 5.7a); the pCO_2 saturation with respect to the atmosphere value ($pCO_2\%$) decreased over time in the first N days (autotrophy) and kept increasing for the remaining days (heterotrophy) (Fig. 5.7b). When

we plotted DO% against $p\text{CO}_2\%$, autotrophic sections and heterotrophic sections composed an “inverted V-shape”: the upper/right section was during autotrophy and the bottom/left section was during heterotrophy (Fig. 5.7c). Under a higher NCP, the transition point had a higher DO% and lower $p\text{CO}_2\%$; in other words, a larger V-shape was developed (Fig. 5.7d).

Furthermore, when biological activities with varied NCP developed simultaneously, the snapshot for the $p\text{CO}_2$ and DO concentrations from various “inverted V shapes” composed a linear relationship (one of the blue line Fig. 5.7d). This synchronistic $p\text{CO}_2$ -to-DO relationship with various NCP changed its slope during the transition of trophic status, i.e. increasing over time. In addition, we simulated the above model with salinity ranging from 25 to 35 (Fig. 5.7e) and found the effect of salinity variation on this simulation was minor. Since the TA in the river end-member was close to the sea end-member, the impact of TA on salinity variation was also minor.

4.2.3. Example in March 2010, when an alongshore plume became wider

An alongshore plume became wider due to northerly winds in March 2010 and showed enhanced primary production and provided a good example of the effect of trophic status transition and air-sea gas exchanges on the $p\text{CO}_2$ and DO relationship. While this wide plume drifted westward to Texas [*Chapter 2*], the $p\text{CO}_2\%$ and DO% relationship on each transect revealed this transition of trophic status from net autotrophic on the eastern shelf to net heterotrophic on the western LA shelf (Fig. 5.8). In the near-field transect at the 90.4°W transect line, the $p\text{CO}_2$ and DO relationship suggests strong positive NCP, especially for those middle-to-high salinity waters (Fig. 5.8a). When following the plume trajectory westward to transects at 91.0°W and 91.7°W , the $p\text{CO}_2$ and DO relationships suggest stronger NCP than in 90.4°W (Fig. 5.8b). For transects from 91.7°W to 93.0°W (Fig. 5.8c,d,e), although the lowest $p\text{CO}_2\%$

remained around 40 to 50%, the slope of $p\text{CO}_2$ and DO relationship increased at 92.4°W and decreased at 93.0°W . This variation in slope may be explained by the joining of the Atchafalaya River plume to the Mississippi River plume [Hetland and DiMarco, 2008]. The $p\text{CO}_2$ and DO relationship at 93.0°W also suggests a transition from autotrophy to heterotrophy. Finally, the slope of DO% and $p\text{CO}_2\%$ was steepest in the 93.7°W transect, reflecting that the plume was on the late stage of the trophic transition (Fig. 5.8f).

Furthermore, a pattern of the $p\text{CO}_2$ and DO relationship similar to that observed in 93.7°W was also observed on the northern South China Sea [Zhai *et al.*, 2009] and was suggested to be dominated by photosynthesis/respiration. The slope of this relationship was also suggested to be influenced by the effect of air-sea gas exchanges proposed by Carrillo *et al.* [2004]. This showed that our simulation had the potential to be applied to other plume systems when survey transects were properly distributed on the plume area.

4.2.4. Example in July 2009, under a different plume path

The MARS plume was confined to the eastern shelf in July 2009 [Zhang *et al.*, 2012][Chapter 3] and demonstrated the ability to distinguish the difference between plume and pelagic water using the $p\text{CO}_2\%$ and DO% relationship (Fig. 5.9). On the eastern shelf, the $p\text{CO}_2$ and DO relationship suggests strong signals of plume net production process (Fig. 5.9a,b). In contrast, on the western LA shelf where high sea surface salinity waters were observed (see Part 1), the DO% and $p\text{CO}_2\%$ relationship suggests relatively weak NCP (Fig. 5.14e,f) (Fig. 5.9e,f). In the region between the eastern and western shelf, the $p\text{CO}_2$ and DO relationship showed a moderate plume signal between these two contrasting signals (Fig. 5.9c,d).

In the above two examples, we demonstrated the model simulation with constant salinity and temperature and neglected the day-night variation, tidal variation, and cooling/heating

effects. However, temperature only affected 4% of the variation of $p\text{CO}_2$ [Carrillo *et al.*, 2004] and had a minor effect on $p\text{CO}_2$ compared to the biological activities. Model results also showed that the effect of salinity variation was minor in middle to high salinity waters (Fig. 5.7e). We found no other factors that could explain the $p\text{CO}_2$ -to-DO relationship displayed in the examples. The trophic transition and the accompanied air-sea compensation still dominated $p\text{CO}_2$ and O_2 variations on the LA shelf.

On the $p\text{CO}_2$ -to-DO diagram, the biological activities resulted in lots of water located on the quadrant I for each month, and data from Quadrant I largely enclosed the LA shelf in spring and summer (Fig. 5.6). Thus, we suggest that biological activities during the trophic transition were also responsible for the spatial $p\text{CO}_2$ variations on the LA shelf from March to September.

4.3. Effect of long water residence times

4.3.1. Changed location for auto- and hetero-trophy

Continued from Section 4.1, the fact that the low salinity data deviated from the conservative mixing line in July and September were consistent with the autotrophic section of this inverted V-shape signal. In other words, this autotrophic section migrated from the shelf/bight (spring to early summer) to on/close to the river channel/bay (July and September) (Fig. 5.3). In particular, the autotrophic signal was observed even when $p\text{CO}_2$ was oversaturated in the river channel/bay.

For example, in September, the low-to-middle salinity waters on the LA bight and the Mississippi River channel demonstrated a $p\text{CO}_2$ -to-DO relationship suggesting strong autotrophic signal and might result in the transition point with high DO% (Fig. 5.10a,b). After the transition point, the $p\text{CO}_2$ -to DO relationship followed previous simulations, i.e., combined effect of air-sea gas exchanges and respiration. In particular, the slope of $p\text{CO}_2$ to DO

relationship for the bottom section of the inverted V-shape was much steeper than in March or July, implying a faster rate of respiration plus gas exchange. This migration of auto-and heterotrophies was probably due to slower discharge and longer water residence (about 3 to 6 months) in the LA shelf during late summer and fall [Zhang *et al.*, 2012].

4.3.2. Comparison with short residence time

Although heterotrophic signals were observed on $p\text{CO}_2$ -to-DO diagrams in both March 2010 and September 2006, they appeared in different patterns. In March 2010, the $p\text{CO}_2$ -to-DO relationship on the western shelf suggests synchronistic signals from various NCP. Such a relationship in one transect (200 km) also implies the trophic transition were synchronistic in a large stable water mass when discharge was high and water residence time was short (two months) [Zhang *et al.*, 2012]. In contrast, in September 2006, $p\text{CO}_2$ -to-DO relationships in each transect (Fig. 5.10 c,d) showed several heterotrophic sections of the inverted V-shape and each section suggests a stable NCP during the time period (estimated to be 2 to 15 days). These varying NCP signals over two transects suggest there were several non-synchronistic biological activities; and they distributed scattered on these two transects when the water discharge was low and water residence time was long (two to six months). Such suggested biological distribution is consistent with circulation characteristics, i.e. small gyres might be observed under such long residence times [Zhang *et al.*, 2012].

While the $p\text{CO}_2$ -to-DO relationship suggests more heterotrophic signals in September, it suggests more autotrophic signals in March. Therefore, we compare the areal-integrated $p\text{CO}_2$ values to average Chlorophyll-a (Chl-a) concentrations, which were measured in the same cruise with $p\text{CO}_2$ during 2006-2007 [Lehrter *et al.*, 2009]. The $p\text{CO}_2$ and average Chl-a in the euphotic layer was negatively correlated in April and June (though non-linear, Fig. 5.11a) but was not in

August and September (Fig. 5.11b). This comparison implies that the photosynthesis was weaker in fall than in spring, and also implies that likely changing of microorganism species and/or varied species from region to region in fall. For example, it can be caused by more heterotrophic biological activities or more species with relatively poor carbon concentration mechanisms, such as *Prochlorococcus* [John et al., 2007]. Such non-correlated $p\text{CO}_2$ -to-Chl-a relationship is consistent with the spotty biological activities reflected by the $p\text{CO}_2$ -to-DO relationships.

4.4. The effect of air-sea gas exchanges

The $p\text{CO}_2$ -to-DO relationship in November (Fig. 5.12) suggests the waters were controlled mostly by the air-sea gas exchange during the late stage of transition from autotrophy to heterotrophy. For those $p\text{CO}_2$ to DO relationships quickly equilibrated with the atmosphere, the heterotrophy might be even weak or close to zero. These signals of re-equilibration may come from regions and/or time periods that we did not survey or regions already past the autotrophic section. Such characteristics can be observed on the western shelf in July 2009 (Fig. 5.9c,d) and off-shore in January 2009 (Fig. 5.13a). Since the biological activities were weak, the effect of temperature was observed on the $p\text{CO}_2$ to DO relationship, i.e. higher temperatures showed more oversaturated $p\text{CO}_2$ than those in lower temperatures (Fig. 5.12).

Finally, a clear contrast of dominant factors between the northern and southern LA shelf was observed in January. The patterns of the DO% and $p\text{CO}_2$ % relationship on the southern LA shelf to south of 28.5°N was similar to the ones in November, showing strong gas exchanges and weak biological activities (Fig. 5.13a,b). In contrast, on the LA shelf to the north of 29.0°N, the data distribution on the DO% and $p\text{CO}_2$ % was close to the model prediction under strong plume biological production and the impact of gas exchanges (Fig. 5.13c,d).

4.5. Strong buffer capacity for carbonate system

The lower gas exchange rate for the carbonate system is not only due to slower gas exchange rate for $p\text{CO}_2$ than DO [Cai *et al.*, 1999; DeGrandpre *et al.*, 1998] but also to the strong buffer capacity of the carbonate system; in other words, the small aquatic CO_2 pool is buffered or sustained by the much greater HCO_3^- and CO_3^{2-} pool. As DIC inventory is about 5 to 10 times that of the DO in water (i.e., 1000-2000 $\mu\text{mol kg}^{-1}$ vs. 200 $\mu\text{mol kg}^{-1}$), it takes about 5-10 times longer to alter the estuarine and marine DIC pool than that of the DO pool during the exchange with the atmosphere. Similarly, Zhai *et al.* [2009] used a Revell factor of 9 to 17 from the inner shelf to outer shelves to explain the nature of disparate aeration time in CO_2 and DO on the northern South China Sea, as the Revelle factor showed spatial variation (8 to 16) over the world [Sarmiento and Gruber, 2006]. Carrillo *et al.* [2004] modeled the air-sea CO_2 exchange by a Revell factor of 15 on the Antarctic Ocean (here low RF is due to low temperature). TA and DIC values were both above 1800 to 2000 μM from the river end-member of the MARS [Cai *et al.*, 2010; Cai *et al.*, 2008; Guo *et al.*, 2012; Huang *et al.*, 2012; Wang *et al.*, 2013], and the MARS plume was also characterized with high carbonate buffer ability. Therefore, these large river plumes in high TA and DIC might respond to the exchange with the atmospheric CO_2 slower than other low buffer capacity systems.

4.6. The implication on heterotrophy and autotrophy

Previous studies have suggested that autotrophy corresponded to under-saturated $p\text{CO}_2$ or oversaturated DO; and heterotrophy corresponded to oversaturated $p\text{CO}_2$ or under-saturated DO. However, under the dynamic trophic transition, we suggest that net autotrophy might already have occurred in oversaturated $p\text{CO}_2$ waters and led the $p\text{CO}_2/\text{DO}$ saturation toward under-saturation/oversaturation, respectively; net heterotrophy might already have happened in under-

saturated DO waters and led the $p\text{CO}_2$ and DO saturation toward oversaturation/under-saturation, respectively.

More and more evidence has been gathered to support the concept of transition from autotrophy to heterotrophy described by *Dagg and Breed* [2003]. In our study Part I, we noticed that a good correlation between riverine nitrate plus nitrite (NN) fluxes and CO_2 fluxes was observed on the eastern shelf (the LA Bight) but was not observed over the LA shelf. In another study, *Murrell et al.* [2013] also suggested heterotrophy on the western shelf by the same cruises as this study during 2006 to 2007. The evidence is consistent with the dynamic analysis in this study, which suggests a transition from net autotrophy to net heterotrophy on the MARS plume, arbitrarily separated by 91.5 to 92.5°W.

5. Summary

We considered the transition of trophic status and the effect of air-sea gas exchanges on the $p\text{CO}_2$ variation to simulate the $p\text{CO}_2$ -to-DO relationship in a large river plume. The wide plume in March 2010 revealed coherent spatial and temporal variations on the $p\text{CO}_2$ -to-DO relationship, showing more net autotrophic signals on the eastern LA shelf, and more net heterotrophic signals on the western LA shelf. Based on this theoretical $p\text{CO}_2$ -to-DO relationship, we suggest that $p\text{CO}_2$ variations on the LA shelf were dominated by a dynamic transition from auto- to hetero-trophy which was accompanied with air-sea CO_2 exchanges and mixing processes. These two factors varied spatially and temporally: mixing dominated low salinity water from January to May, and was less important from June to September. Biological activities were observed in the inner shelf in January and observed over the shelf from March to September. Signals of autotrophy were observed in middle salinity waters from January to May and were

observed in low salinity waters from July to September. More heterotrophic signals were observed over the LA shelf in September. In November, signals of air-sea gas exchanges observed in middle-to-high salinity water largely covered the LA shelf and signals of biological activities were weak. Overall, based on the time scale and the spatial coverage, we suggest that the transition of auto-to-hetero-trophic activities and accompanied air-sea gas compensation were largely responsible for the variation of $p\text{CO}_2$ values on the LA shelf.

References

- Borges, A. V. (2011), Present day carbon dioxide fluxes in the coastal ocean and possible feedbacks under global change oceans and the atmospheric carbon content, edited by P. Duarte and J. M. Santana-Casiano, pp. 47-77, Springer Netherlands.
- Borges, A. V., and N. Gypens (2010), Carbonate chemistry in the coastal zone responds more strongly to eutrophication than to ocean acidification, *Limnology and Oceanography*, 55(1), 346-353.
- Cai, W.-J. (2003), Riverine inorganic carbon flux and rate of biological uptake in the Mississippi River plume, *Geophysical Research Letters*, 30(2), 1032.
- Cai, W.-J. (2011), Estuarine and coastal ocean carbon paradox: CO₂ sinks or sites of terrestrial carbon incineration?, *Annual Review of Marine Science*, 3(1), 123-145.
- Cai, W.-J., M. Dai, and Y. C. Wang (2006), Air-sea exchange of carbon dioxide in ocean margins: A province-based synthesis, *Geophysical Research Letters*, 33(12), L12603.
- Cai, W.-J., L. R. Pomeroy, M. A. Moran, and Y. Wang (1999), Oxygen and carbon dioxide mass balance for the estuarine-intertidal marsh complex of five rivers in the southeastern U.S., *Limnology and Oceanography*, 44(3), 639-649.
- Cai, W.-J., X. Hu, W.-J. Huang, L.-Q. Jiang, Y. Wang, T.-H. Peng, and X. Zhang (2010), Alkalinity distribution in the western North Atlantic Ocean margins, *Journal of Geophysical Research*, 115(C8), C08014.
- Cai, W.-J., X. Guo, C.-T. A. Chen, M. Dai, L. Zhang, W. Zhai, S. E. Lohrenz, K. Yin, P. J. Harrison, and Y. Wang (2008), A comparative overview of weathering intensity and HCO₃⁻ flux in the world's major rivers with emphasis on the Changjiang, Huanghe, Zhujiang (Pearl) and Mississippi Rivers, *Continental Shelf Research*, 28(12), 1538-1549.

- Cai, W.-J., et al. (2011), Acidification of subsurface coastal waters enhanced by eutrophication, *Nature Geosci*, 4(11), 766-770.
- Carrillo, C. J., R. C. Smith, and D. M. Karl (2004), Processes regulating oxygen and carbon dioxide in surface waters west of the Antarctic Peninsula, *Marine Chemistry*, 84(3-4), 161-179.
- Chen, C.-T. A., and A. V. Borges (2009), Reconciling opposing views on carbon cycling in the coastal ocean: Continental shelves as sinks and near-shore ecosystems as sources of atmospheric CO₂, *Deep Sea Research Part II: Topical Studies in Oceanography*, 56(8-10), 578-590.
- Chou, W.-C., G.-C. Gong, C.-M. Tseng, D. D. Sheu, C.-C. Hung, L.-P. Chang, and L.-W. Wang (2011), The carbonate system in the East China Sea in winter, *Marine Chemistry*, 123(1-4), 44-55.
- Cooley, S. R., V. J. Coles, A. Subramaniam, and P. L. Yager (2007), Seasonal variations in the Amazon plume-related atmospheric carbon sink, *Global Biogeochem. Cycles*, 21(3), GB3014.
- Dagg, M. J., and G. A. Breed (2003), Biological effects of Mississippi River nitrogen on the northern Gulf of Mexico—a review and synthesis, *Journal of Marine Systems*, 43(3/4), 133.
- DeGrandpre, M. D., T. R. Hammar, and C. D. Wirick (1998), Short-term pCO₂ and O₂ dynamics in California coastal waters, *Deep Sea Research Part II: Topical Studies in Oceanography*, 45(8-9), 1557-1575.
- Dinnel, S. P., and J. W. J. Wiseman (1986), Fresh water on the Louisiana and Texas shelf, *Continental Shelf Research*, 6(6), 765-784.

- Ducklow, H. W., and S. L. McCallister (2005), The biogeochemistry of carbon dioxide in the coastal oceans, in *The global coastal ocean. Multiscale interdisciplinary processes. The sea: ideas and observations on progress in the study of the seas.*, edited by A. R. Robinson and K. H. Brink, pp. 269-315, Harvard University Press, Cambridge, MA.
- Green, R. E., T. S. Bianchi, M. J. Dagg, N. D. Walker, and G. A. Breed (2006), An organic carbon budget for the Mississippi River turbidity plume and plume contributions to air-sea CO₂ fluxes and bottom water hypoxia, *Estuaries and Coasts*, 29(4), 579-597.
- Guo, X., et al. (2012), Carbon dynamics and community production in the Mississippi River plume, *Limnology and Oceanography*, 57(1), 1-17.
- Hetland, R. D., and S. F. DiMarco (2008), How does the character of oxygen demand control the structure of hypoxia on the Texas-Louisiana continental shelf?, *Journal of Marine Systems*, 70(1-2), 49-62.
- Huang, W.-J., W.-J. Cai, R. T. Powell, S. E. Lohrenz, Y. Wang, L. Q. Jiang, and C. S. Hopkinson (2012), The stoichiometry of inorganic carbon and nutrient removal in the Mississippi River plume and adjacent continental shelf, *Biogeosciences*, 9(7), 2781-2792.
- Jiang, L.-Q., W.-J. Cai, Y. Wang, R. Wanninkhof, and H. Lüger (2008), Air-sea CO₂ fluxes on the U.S. South Atlantic Bight: Spatial and seasonal variability, *J. Geophys. Res.*, 113, C07019.
- John, D. E., Z. A. Wang, X. Liu, R. H. Byrne, J. E. Corredor, J. M. Lopez, A. Cabrera, D. A. Bronk, F. R. Tabita, and J. H. Paul (2007), Phytoplankton carbon fixation gene (RuBisCO) transcripts and air-sea CO₂ flux in the Mississippi River plume, *ISME J*, 1(6), 517-531.

- Kortzinger, A. (2003), A significant CO₂ sink in the tropical Atlantic Ocean associated with the Amazon River plume, *Geophysical Research Letters*, 30(24), 4.
- Lehrter, J. C., M. C. Murrell, and J. C. Kurtz (2009), Interactions between freshwater input, light, and phytoplankton dynamics on the Louisiana continental shelf, *Continental Shelf Research*, 29(15), 1861-1872.
- Lohrenz, S. E., and W.-J. Cai (2006), Satellite ocean color assessment of air-sea fluxes of CO₂ in a river-dominated coastal margin, *Geophysical Research Letters*, 33(1), L01601.
- Lohrenz, S. E., W.-J. Cai, F. Chen, X. Chen, and M. Tuel (2010), Seasonal variability in air-sea fluxes of CO₂ in a river-influenced coastal margin, *J. Geophys. Res.*, 115(C10), C10034.
- Lohrenz, S. E., G. L. Fahnenstiel, D. G. Redalje, G. A. Lang, X. Chen, and M. J. Dagg (1997), Variations in primary production of northern Gulf of Mexico continental shelf waters linked to nutrient inputs from the Mississippi River, *Marine Ecology Progress Series*, 155, 45-54.
- Mackenzie, F. T., A. Lerman, and A. J. Andersson (2004), Past and present of sediment and carbon biogeochemical cycling models, *Biogeosciences*, 1(1).
- Murrell, M. C., R. S. Stanley, J. C. Lehrter, and J. D. Hagy III (2013), Plankton community respiration, net ecosystem metabolism, and oxygen dynamics on the Louisiana continental shelf: Implications for hypoxia, *Continental Shelf Research*, 52(0), 27-38.
- Redfield, A. C. (1958), The biological control of chemical factors in the environment, *American Scientist*, 46, 205-221.
- Sarmiento, J. L., and N. Gruber (2006), *Ocean biogeochemical dynamics*, Princeton University Press, New Jersey.

- Ternon, J. F., C. Oudot, A. Dessier, and D. Diverres (2000), A seasonal tropical sink for atmospheric CO₂ in the Atlantic ocean: the role of the Amazon River discharge, *Marine Chemistry*, 68(3), 183-201.
- Tseng, C.-M., K. K. Liu, G. C. Gong, P. Y. Shen, and W. J. Cai (2011), CO₂ uptake in the East China Sea relying on Changjiang runoff is prone to change, *Geophys. Res. Lett.*, 38(24), L24609.
- Tsunogai, S., S. Watanabe, J. Nakamura, T. Ono, and T. Sato (1997), A preliminary study of carbon system in the East China Sea, *Journal of Oceanography*, 53(1), 9-17.
- Wang, Z. A., R. Wanninkhof, W.-J. Cai, R. H. Byrne, X. Hu, T.-H. Peng, and W.-J. Huang (2013), The marine inorganic carbon system along the Gulf of Mexico and Atlantic coasts of the United States: Insights from a transregional coastal carbon study, *Limnology and Oceanography*, 58(1), 325-342.
- Wanninkhof, R. (1992), Relationship between wind speed and gas exchange over the ocean, *Journal of Geophysical Research*, 97(C5), 7373-7382.
- Weiss, R. F. (1974), Carbon dioxide in water and seawater: the solubility of a non-ideal gas, *Marine Chemistry*, 2(3), 203-215.
- Zhai, W., and M. Dai (2009), On the seasonal variation of air - sea CO₂ fluxes in the outer Changjiang (Yangtze River) Estuary, East China Sea, *Marine Chemistry*, 117(1-4), 2-10.
- Zhai, W., M. Dai, and X. Guo (2007), Carbonate system and CO₂ degassing fluxes in the inner estuary of Changjiang (Yangtze) River, China, *Marine Chemistry*, 107(3), 342-356.
- Zhai, W., M. Dai, and W.-J. Cai (2009), Coupling of surface pCO₂ and dissolved oxygen in the northern South China Sea: impacts of contrasting coastal processes, *Biogeosciences*, 6(11), 2589-2598.

Zhang, X., R. D. Hetland, M. Marta-Almeida, and S. F. DiMarco (2012), A numerical investigation of the Mississippi and Atchafalaya freshwater transport, filling and flushing times on the Texas-Louisiana Shelf, *J. Geophys. Res.*, *117*(C11), C11009.

Table 5.1. Summary of the cruises information

	Season	Date, Year	Boat	Survey Region	Note for plume
1	Spring	5/2- 7, 2007	OSV Bold	LA shelf	Alongshore
2	Spring	4/20-5/1, 2009	Cape Hetterass	LA shelf	Alongshore
3	Spring	3/9-21, 2010	Cape Hetterass	LA shelf	Wide,alongshore
4	Summer	6/6-11, 2006	OSV Bold	LA shelf	Alongshore
5	Summer	7/17-20, 2008	R/V Pelican	Center shelf	Alongshore
6	Summer	7/19-29, 2009	Cape Hetterass	LA shelf	Confined to East
7	Summer	8/9-12, 2004	R/V Pelican	LA Bight	None
8	Fall	9/6-11, 2006	OSV Bold	LA shelf	Alongshore
9	Fall	10/28-11/7, 2009	Sharp	LA shelf	Alongshore
10	Winter	1/9-20, 2009	Cape Hetterass	LA shelf	Alongshore

Table 5.2. Initial conditions for each simulation

Month	Fig.#	T °C	Sal	Wind m s ⁻¹	h m	Kt for DO	TA μmol kg ⁻¹	pCO ₂ %	DO%	NCP g C m ⁻² d ⁻¹	shifting day
January	13	15	28	8	8	2.91	2400	1	1	0, 0.5, 2	5.5
March	8	18	28	7	10	2.6	2400	1	1	0.2, 0.4, 1.8	10
September	10a,b	30	25	4.5	4.5	2.6	2400	1	1	3	12
September	10c,d	29.3	30	4.5	5.5	2.6	2400	1	1	0, 0.15, 0.75	8

“h” is the mixing layer depth, Kt for DO is from Weiss (1974), the numbers for NCP are in the sequences of “starting value, adding value, final value”; “shifting day” is the day that transited from autotrophy to heterotrophy.

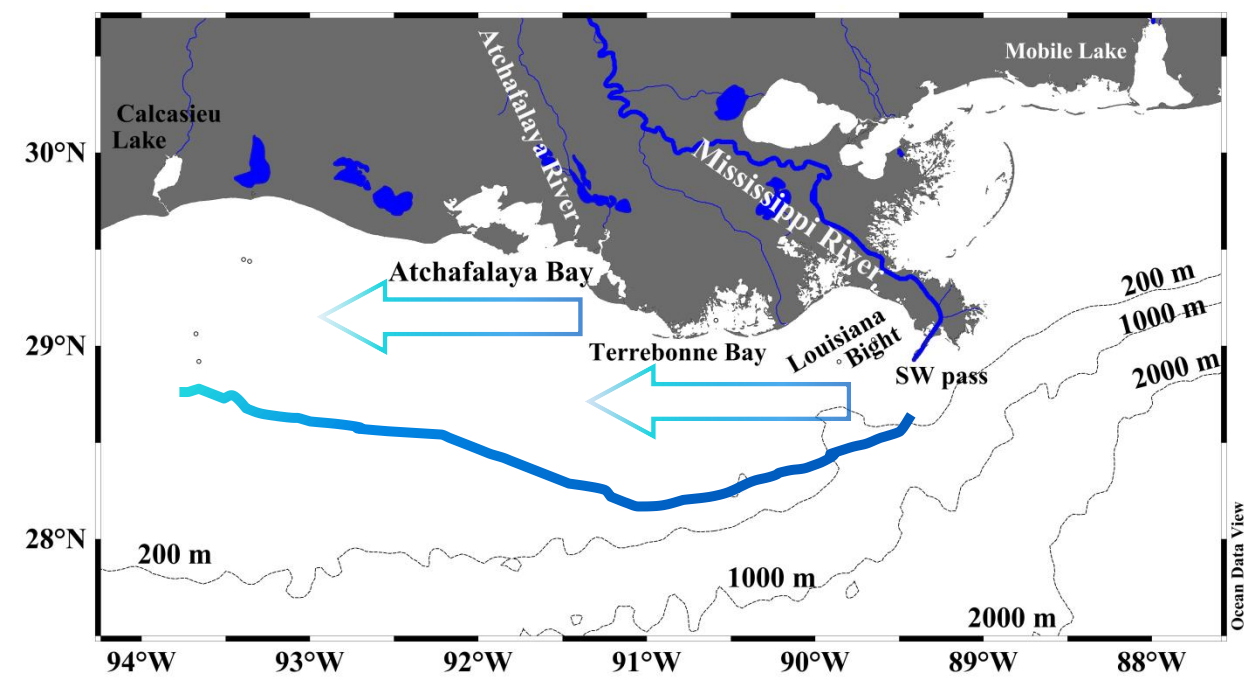


Figure 5.1. Site maps. Shelf-wide area (until 200 m isobaths) was surveyed for three cruises during June 2006 to 2007, and cross-shelf area was surveyed for five cruises during 2009 to 2010. LA Bight was surveyed during August 2004 and the area off the Atchafalaya Bay was surveyed during July 2008. Detail cruise tracks for each cruise were shown on the DO distribution (Fig. 2). The Mississippi and Atchafalaya River system (MARS) plume was usually confined to the north of 28°N on the LA shelf (the blue line is an arbitrary boundary) and drifted alongshore toward Texas (blue arrows).

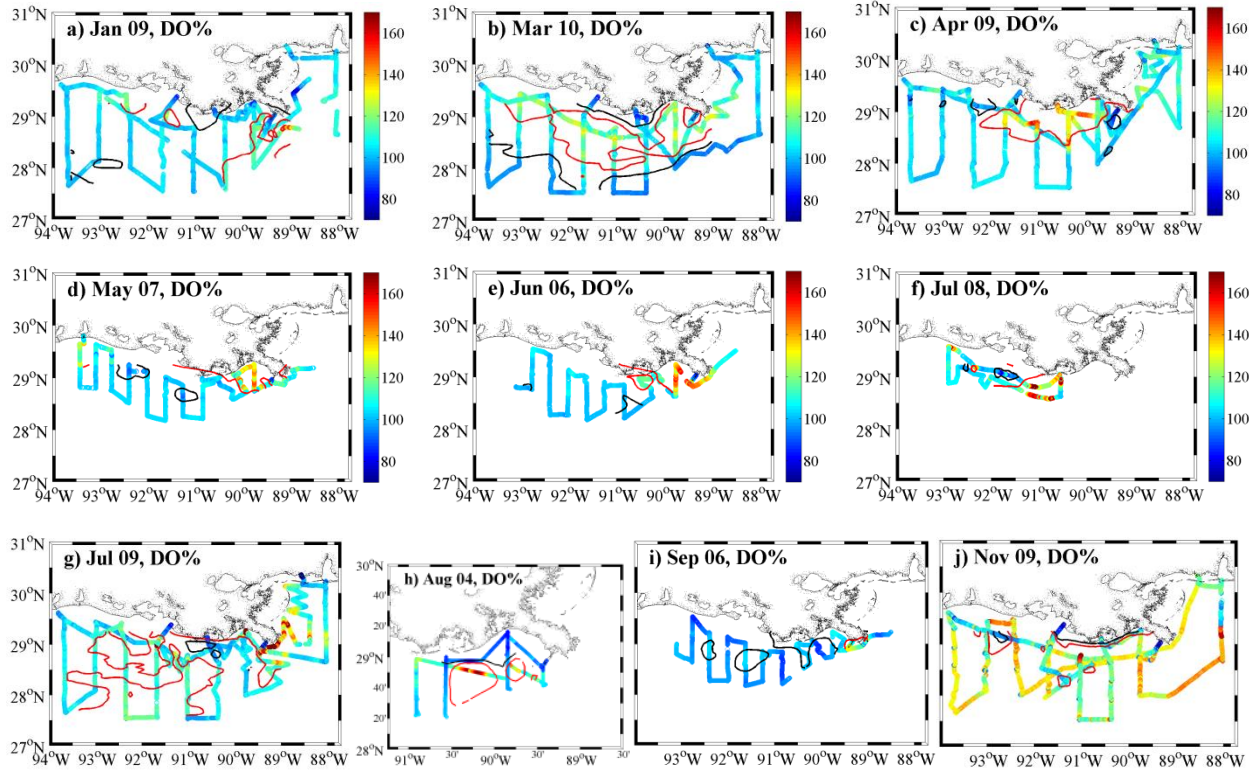


Figure 5.2. The distribution of sea surface dissolved oxygen (DO). Jan 2010 (a), Mar 2010 (b), Apr 2009 (c), May 2007 (d), Jun 2006 (e), Jul 2008 (f), Jul 2009 (g), Aug 2004 (h), Sep. 2006 (i), and Nov 2010 (j). Detail cruise tracks of each cruise are also demonstrated. Panel g) to j) share the same color bar as a) to f).

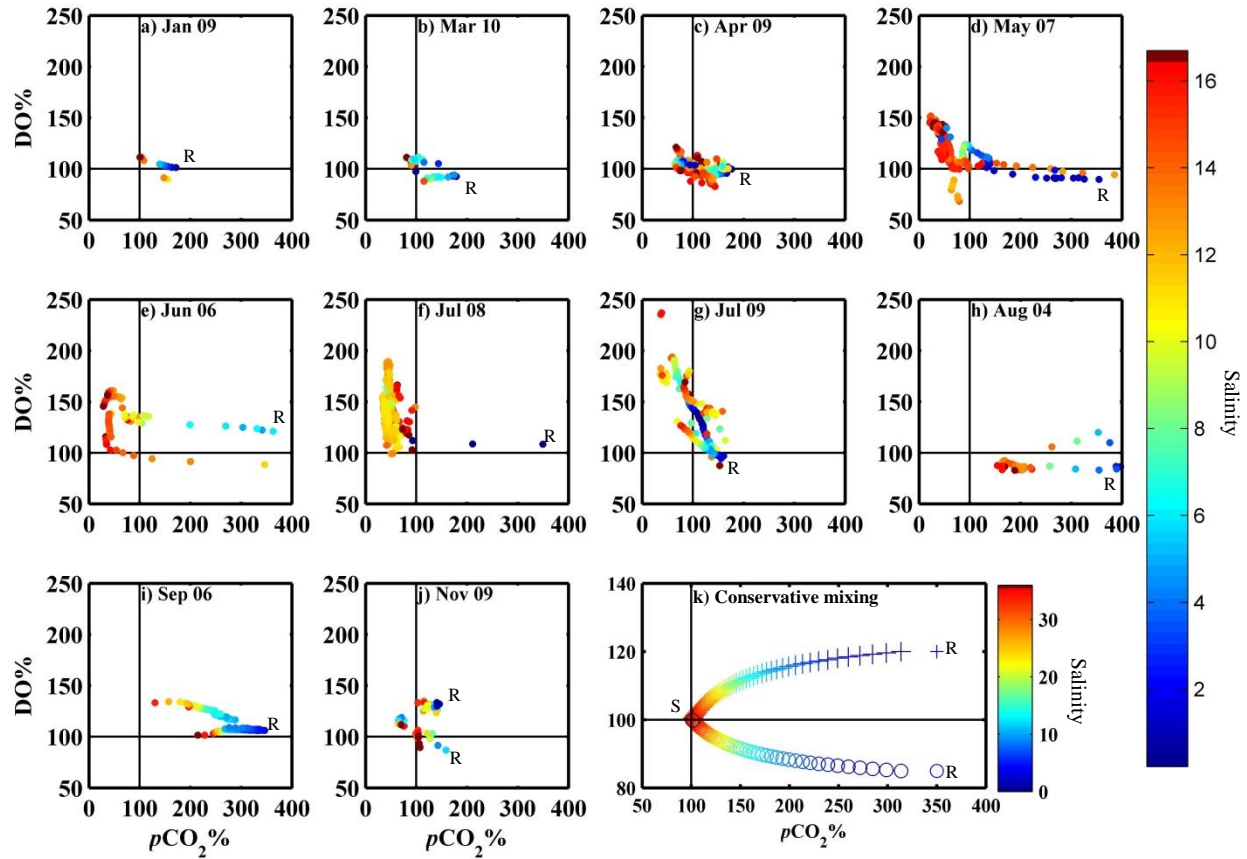


Figure 5.3. $p\text{CO}_2$ -to-DO relationship for low salinity ($S < 17$) waters. Jan 2010 (a), Mar 2010 (b), Apr 2009 (c), May 2007 (d), Jun 2006 (e), Jul 2008 (f), Jul 2009 (g), Aug 2004 (h), Sep. 2006 (i), and Nov 2010 (j). Panel k) displayed two conservative mixing lines: as $p\text{CO}_2$ was oversaturated $p\text{CO}_2\%$, one started from under-saturated DO and the other started from oversaturated DO. “R” is the abbreviation of river end-member. Color variation in each panel refers to the salinity variation as the color bars.

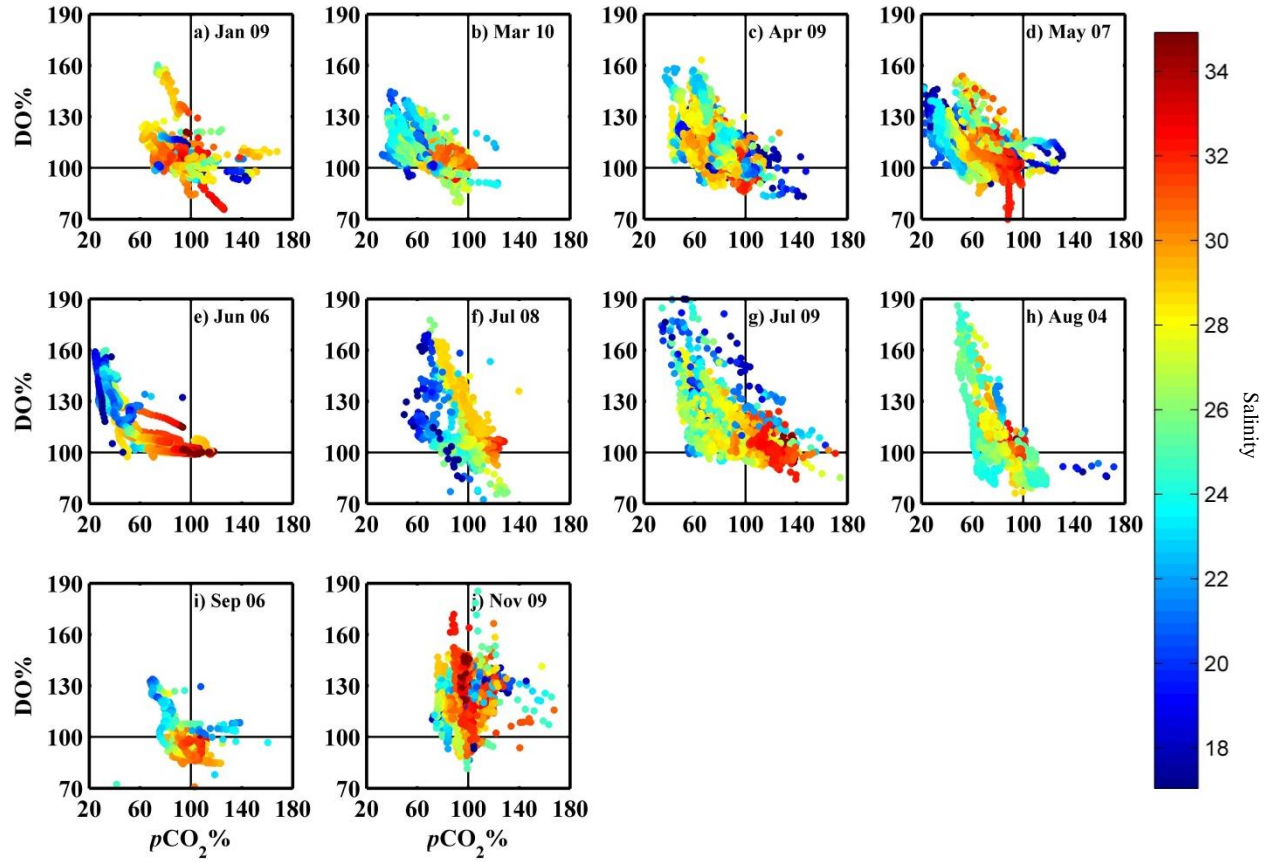


Figure 5.4. $p\text{CO}_2$ -to-DO relationship for water among salinity 17 to 35. Jan 2010 (a), Mar 2010 (b), Apr 2009 (c), May 2007 (d), Jun 2006 (e), Jul 2008 (f), Jul 2009 (g), Aug 2004 (h), Sep. 2006 (i), and Nov 2010 (j). The color of data points represents its salinity.

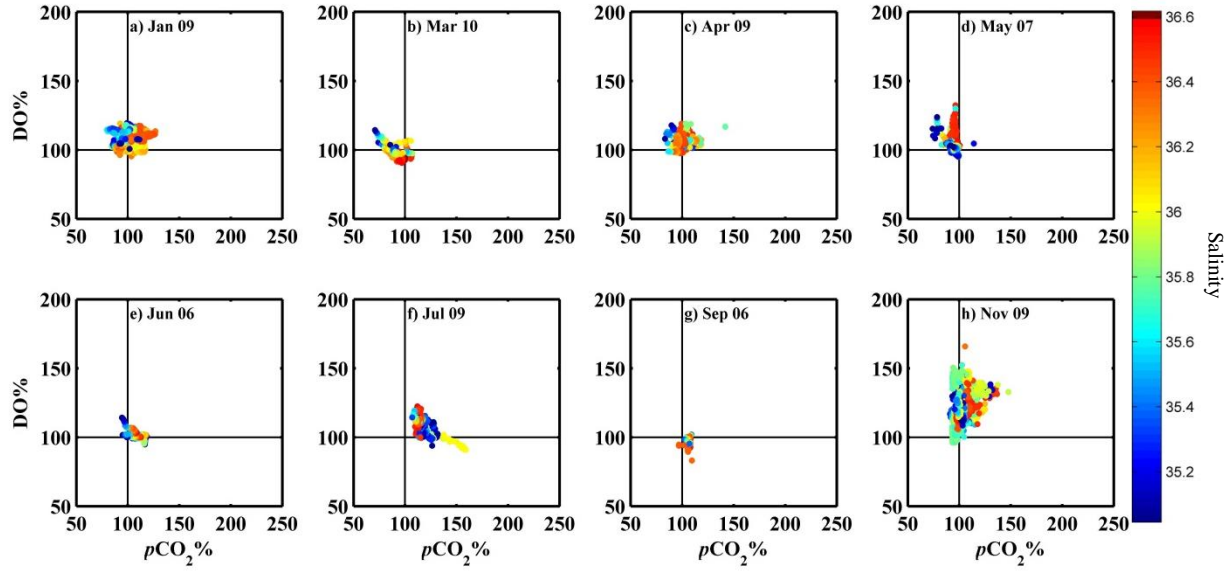


Figure 5.5. $p\text{CO}_2$ -to-DO relationship for high salinity ($S > 35$) waters. The color represents corresponding salinity.

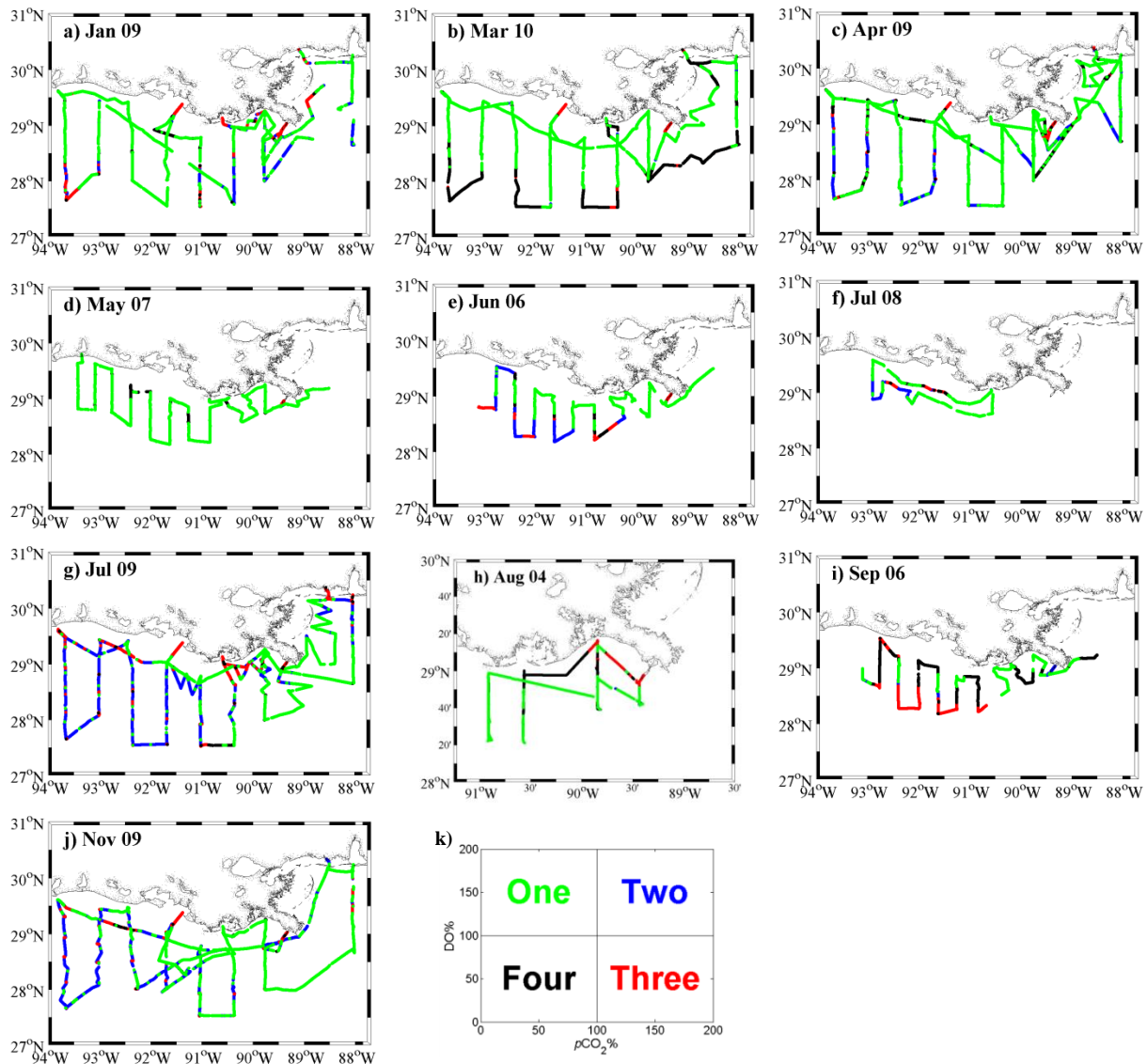


Figure 5.6. Distributions of Quadrants of DO% and $p\text{CO}_2\%$ in Jan. 2010 (a), Mar. 2010 (b), Apr. 2009 (c), May 2007 (d), Jun. 2006 (e), Jul. 2008 (f), Jul. 2009 (g), Aug. 2004 (h), Sep. 2006 (i), and Nov. 2010 (j). Green, blue, red, and black colors represented Quadrants one to four on the $p\text{CO}_2$ -to-DO diagram, respectively (k).

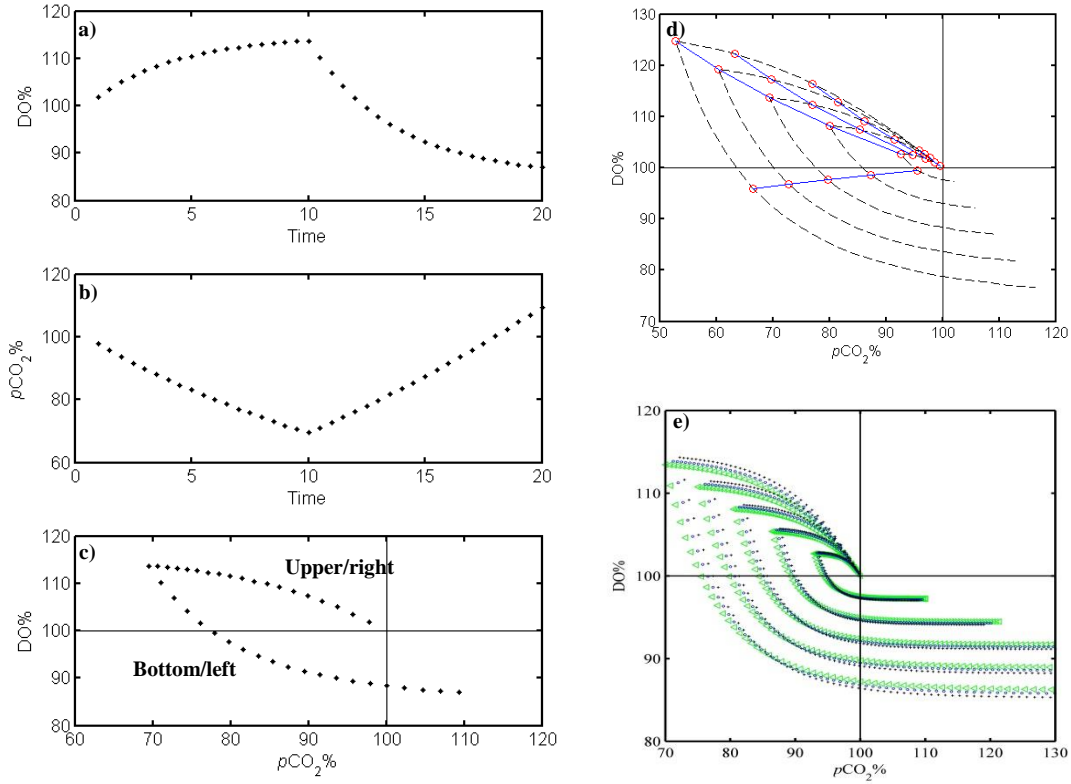


Figure 5.7. Theoretical $p\text{CO}_2$ -to-DO relationship under plume processes. In the first 10 days, net autotrophy (positive NCP) increased DO% (a) and decreased $p\text{CO}_2\%$ (b); after day 10, net autotrophy transits to net heterotrophy (negative NCP), which decreased DO% (a) and increased $p\text{CO}_2\%$ (b). Therefore, the $p\text{CO}_2$ -to-DO relationship during this time period showed an “inversed V-shape” tilted to the left (c): the upper/right section was net autotrophy and the bottom/left section was net heterotroph. When the absolute value of the $\pm\text{NCP}$ was larger, this “inversed V-shape” was larger (d). When various NCP developed simultaneously, the $p\text{CO}_2$ -to-DO relationship is a linear in a specific time (the blue line in panel d); and its slope increases with increasing time. Panel e) showed the effect of salinity variations from 25 to 35. The simulation was under three kinds of salinity, 25 (green triangle), 30 (blue circle), and 35 (black cross). The result showed that the effect of salinity change was minor comparing to the effect of NCP. The other initial condition was the same as the one for September.

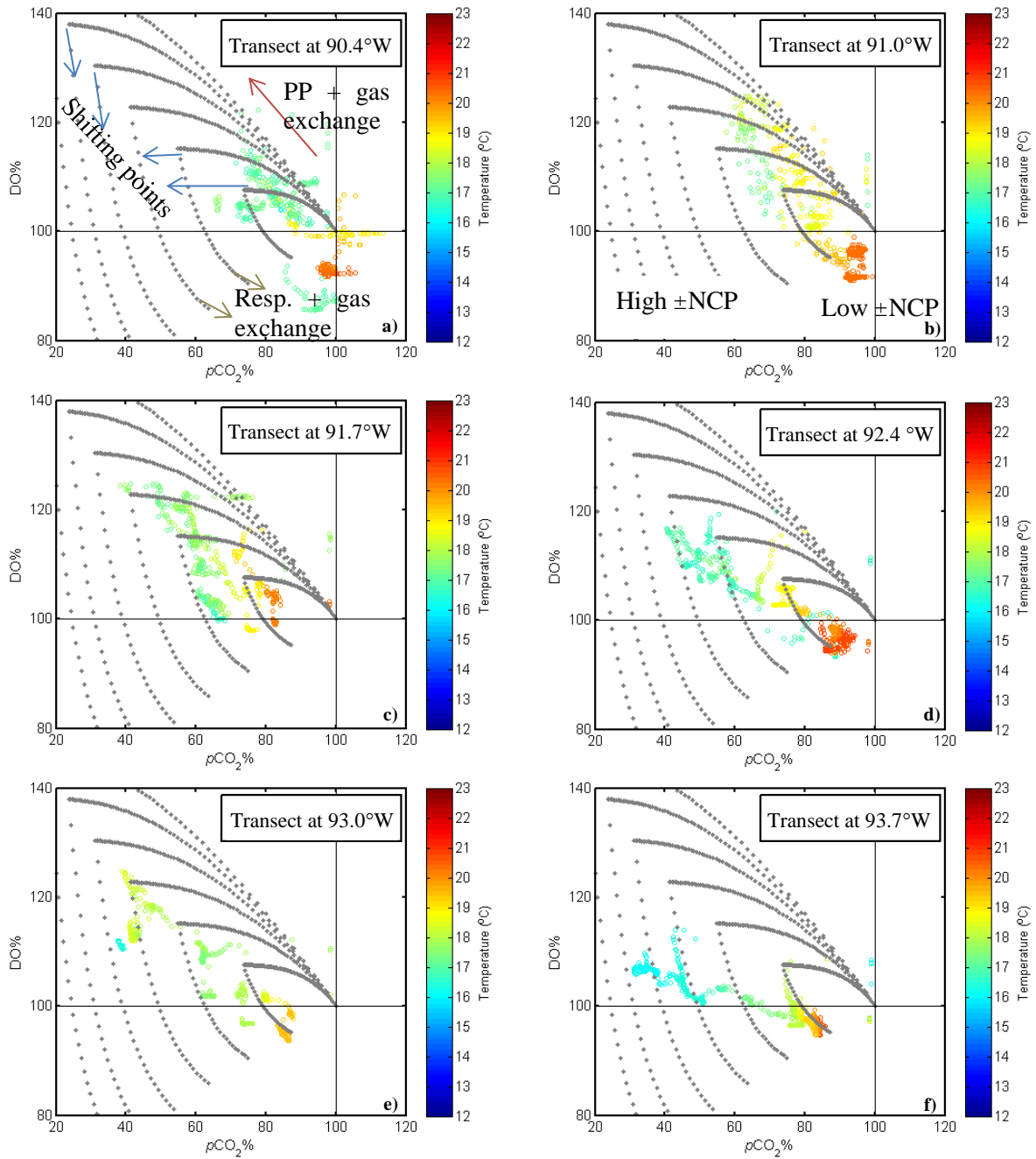


Figure 5.8. $p\text{CO}_2$ -to-DO relationship in March 2010. This wide plume provided a good example to show the plume processes alongshore toward Texas. As this plume became “old” westward, this relationship suggests more signals close to early stage during the plume processes on the eastern shelf (a,b) and transit to more heterotrophic signals from middle shelf (c,d) to the western shelf (e,f). Gray dots displayed the theoretical simulation with initial values in Table 5.2.

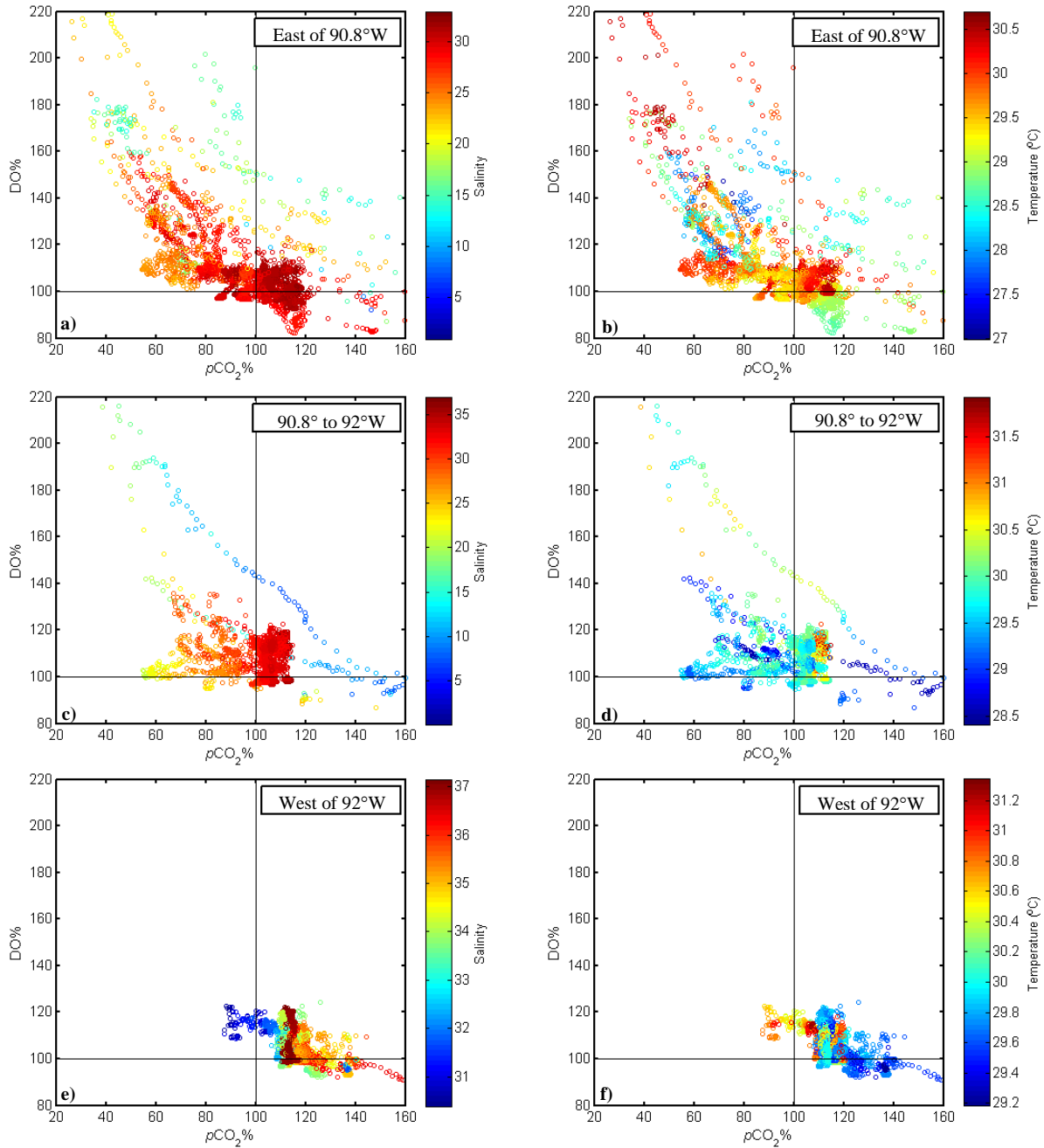


Figure 5.9. $p\text{CO}_2$ -to- DO relationship in July 2009. Due to the shelf circulation, the MARS plume was confined to the eastern shelf and high salinity waters was observed on the western shelf in July 2009. This relationship also suggests strong signals of plume processes on the eastern shelf (a,b), less signal was observed on the middle shelf (c,d), and weaker photosynthesis signals on the western shelf (e,f).

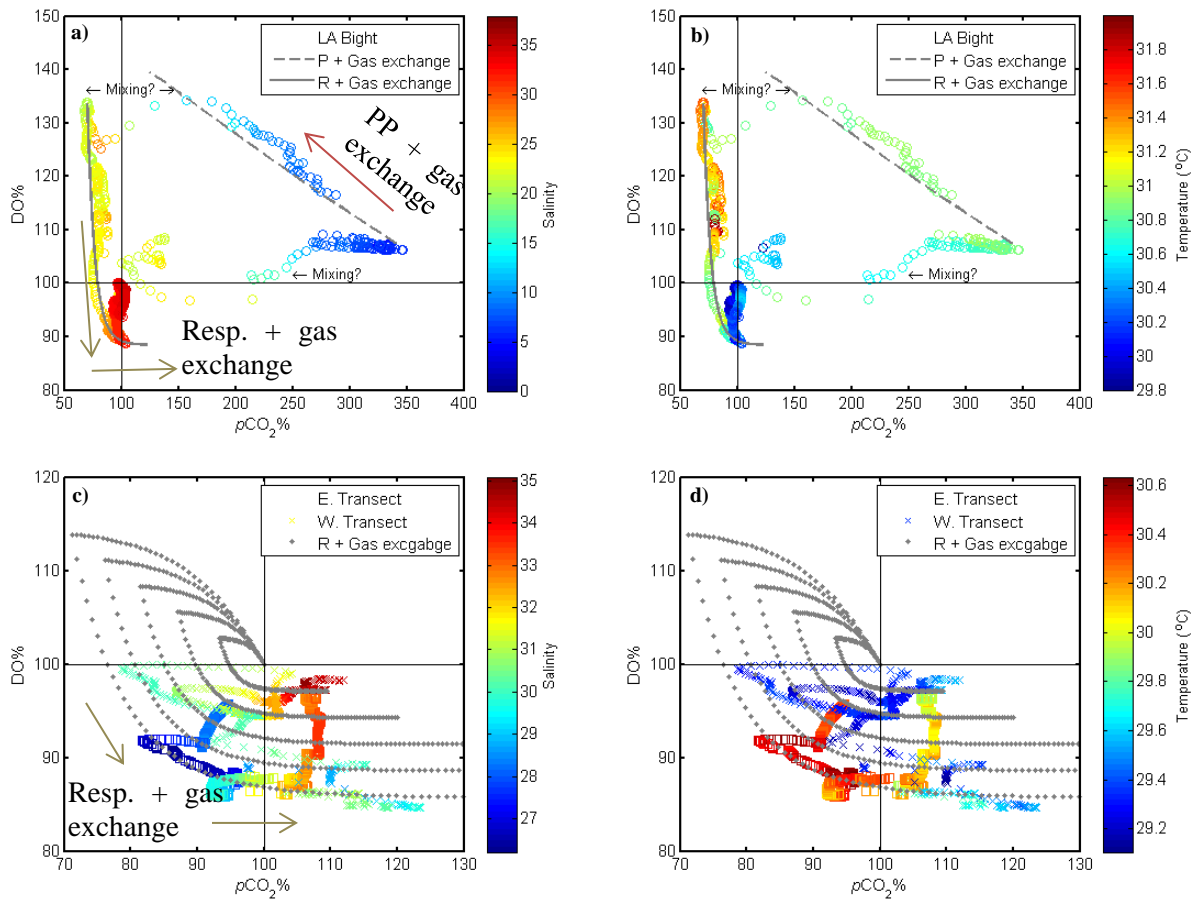


Figure 5.10. $p\text{CO}_2$ -to- DO relationship in September 2006. The autotrophic section of plume processes was in the Mississippi River channel, and autotrophic section was on the LA Bight (a,b). Both eastern and western shelf showed respiration plus air-sea gas exchanges signals (c, d).

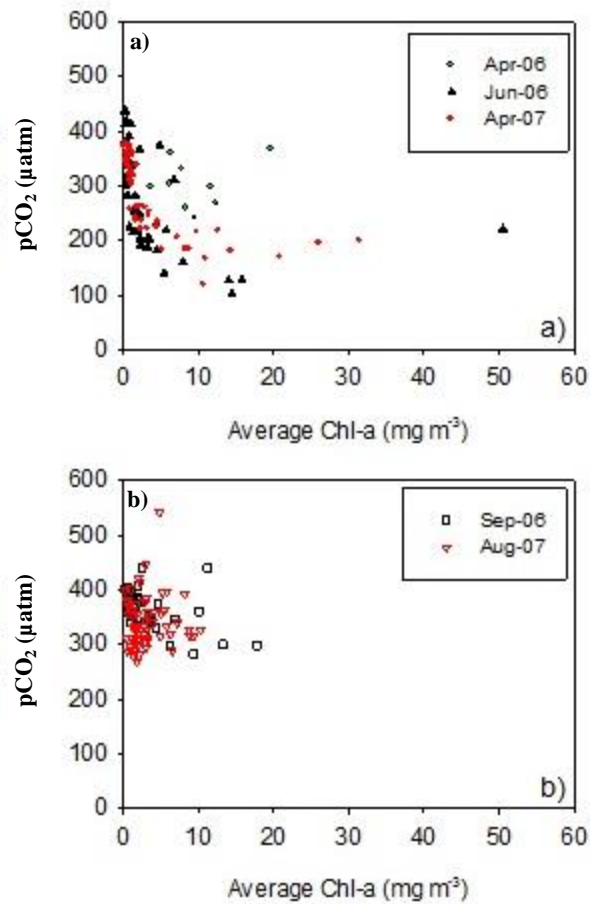


Figure 5.11. $p\text{CO}_2$ -to-Chl-a relationship during 2006 and 2007. $p\text{CO}_2$ decreased to below 200 μatm as Chl-a concentration increased in Spring and early summer, but did not decrease to below 250 μatm in August and September.

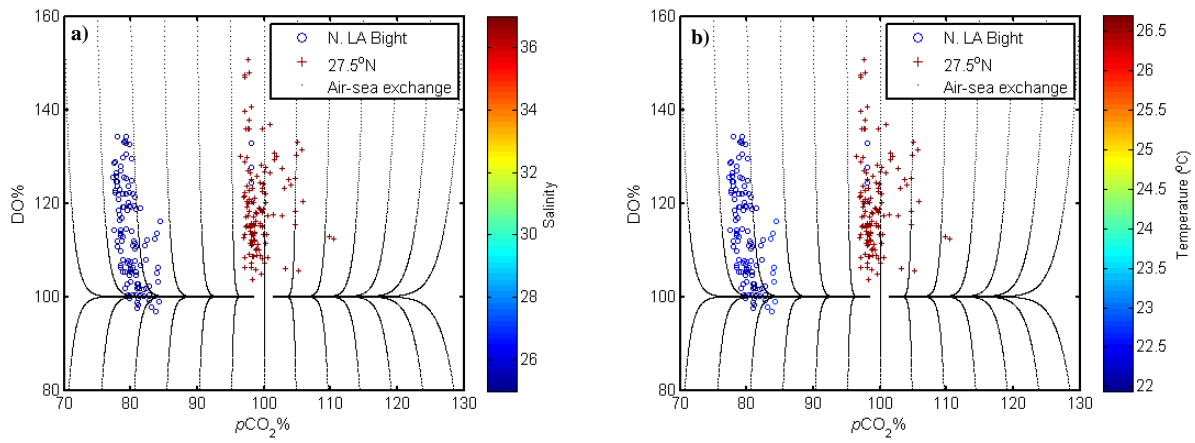


Figure 5.12. $p\text{CO}_2$ -to-DO relationship in November 2009. This relationship suggested that northern LA Bight was dominated by respiration and gas exchange, and the southern region showed signals from pelagic waters.

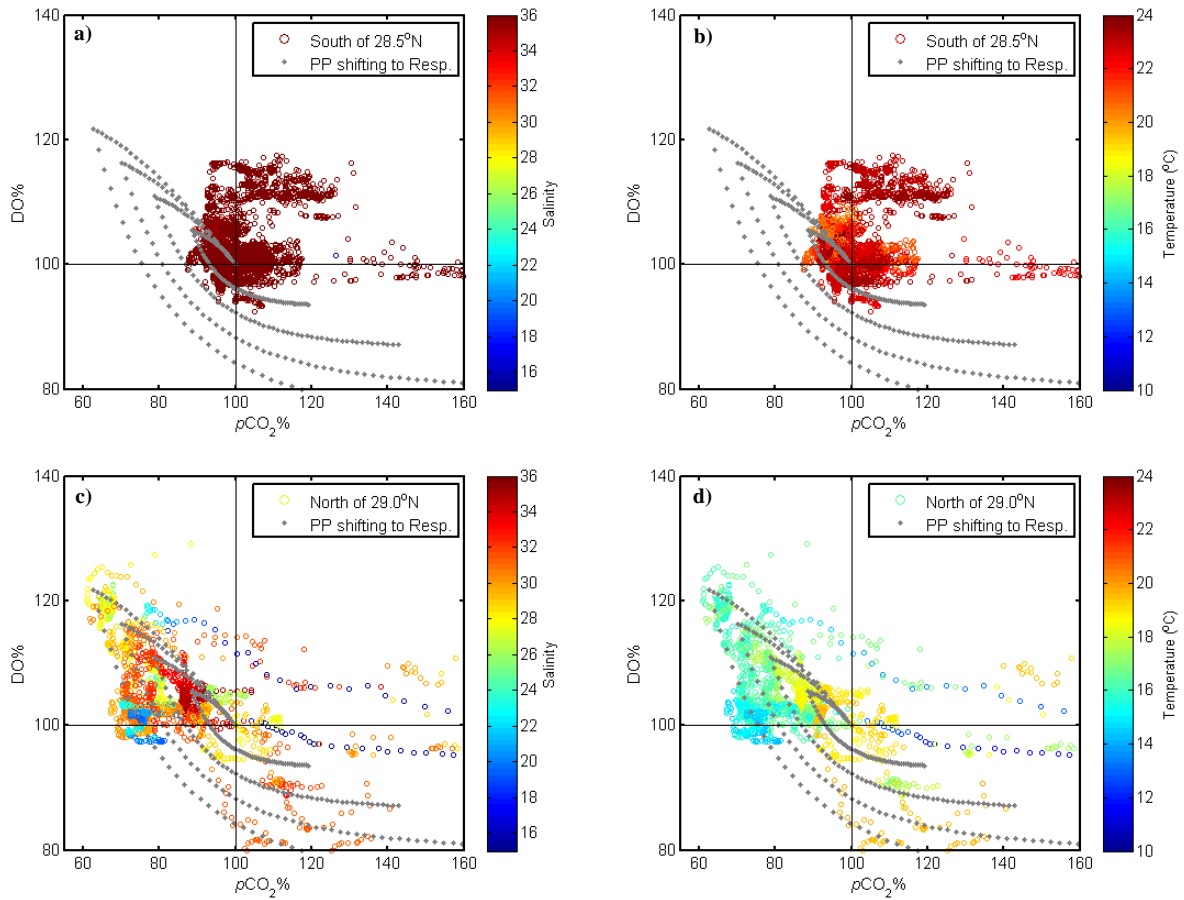


Figure 5.13. $p\text{CO}_2$ -to- DO relationship in January 2009. This relationship suggested the signals of plume processes to the north of 29°N and signals on the southern region still showed pelagic waters.

CHAPTER 6

SUMMARY

This dissertation focuses on sea surface $p\text{CO}_2$ distribution and dynamics on the LA shelf. In the previous chapters, I have demonstrated the response of $p\text{CO}_2$ distribution to wind forcing under unusual weather on the LA shelf in Chapter 2 and 3. I have also quantified the response of surface $p\text{CO}_2$ to riverine nitrogen fluxes in Chapter 4. Moreover, I modeled the response of $p\text{CO}_2$ to the combination effect of biological uptake/release and air-sea CO_2 exchanges in Chapter 5. Additionally, DIC, TA, and pH in the water column have also been systematically measured. Only few of these water column properties are used in this dissertation but they play an important role when discussing the biogeochemical processes in the bottom water in Chapter 3; and also as the river and seawater end-members for the models in Chapter 4 and 5. Here I synthesize these impacts from wind forcing, river inputs, biological activities, and air-sea gas exchanges to show an integrated concept for the $p\text{CO}_2$ variation in the LA shelf.

1. Spatial and temporal variations of $p\text{CO}_2$ distribution and dynamics

The surface water $p\text{CO}_2$ distribution showed both seasonal and spatial variations on the LA shelf. The average of the areal-integrated $p\text{CO}_2$ values was under-saturated in spring, close to atmospheric CO_2 values in summer, oversaturated in fall, and close to the atmosphere again in winter. The inner to middle shelf usually acted as a sink of atmospheric CO_2 and the outer shelf acted as a weak source. The eastern LA shelf, especially in the LA Bight, acted as a stronger sink

than the western LA shelf. In an annual average, the LA shelf acted as a sink of atmospheric CO₂ (-0.963 mol C m⁻² yr⁻¹).

It is important to discuss the *p*CO₂ variation based on the distribution of the MARS plume as the LA shelf is a river-dominated shelf. The MARS plume was distributed alongshore and confined to the shelf under normal weather conditions (Fig. 6.1a), evident from satellite information and measured sea surface salinity. In this salinity defined river plume (salinity less than 35), *p*CO₂ values showed a bimodal relationship with the salinity, i.e. *p*CO₂ values were oversaturated in waters of salinity 0 to 17, were under-saturated in waters of salinity 17 to 33; and were close to the atmosphere values in waters of salinity 33 to 35. Thus, a sink of the atmosphere CO₂ was usually observed on the shelf and the degree of the sink varied among the salinity regions (Fig. 6.1b). Furthermore, this bimodal relationship between *p*CO₂ and salinity was suggested to be highly dominated by biological NO₃-removal involved mixing processes.

We further suggest that these two factors, abiotic mixing and biotic processes, varied spatially and temporally based on the *p*CO₂-to-DO relationships: mixing dominated low salinity water from January to May, and was less important from June to September. Enhanced biological activities in the plume was observed on the inner shelf in January and observed over the shelf from March to September. These suggestions were based on the comparisons between measured and simulated *p*CO₂-to-DO relationship when the later considered the effects of trophic status transition (from autotrophy to heterotrophy) and the air-sea gas exchanges. The comparison also suggests that trophic status varies seasonally and spatially: signals of net autotrophy were observed in middle salinity waters from January to May when the river discharge was high, and were observed in low salinity waters from July to September when the river discharge was low. More heterotrophic signals were observed over the LA shelf in

September. In November, signal of air-sea gas exchanges from middle-to-high salinity water largely covered the LA shelf and signal of biological activities was weak. These spatial variations of trophic status were likely due to variations of water residence time. Overall, we suggest that biological activities during the plume processes and corresponding air-sea gas compensation were largely responsible for the variation of $p\text{CO}_2$ values as these activities were largely dominant over time scale and the spatial coverage on the LA shelf. Mixing however plays a very important role in low salinity waters.

2. The CO_2 dynamics under unusual weather conditions

We suggest that the spatial $p\text{CO}_2$ variation on this shelf is highly related to the distribution of shelf circulations. When the local wind forcing was different from the mean condition on the LA shelf, the trajectory of this MARS plume is relocated to different distributions. The under-saturated CO_2 water with respect to the atmosphere also varied its location corresponding to the freshwater plume. This study provided two examples in March 2010 and July 2009, respectively, to illustrate the importance of such wind-drive circulation patterns on CO_2 and O_2 biogeochemistry.

In March 2010, a large extension of the MARS plume cross the shelf to the pelagic Gulf of Mexico was observed (Fig. 6.1c, blue color) and was most likely induced by the combination of high MARS river discharge and northerly winds driven by a large low-pressure system over the North America continent. The wide plume in March 2010 displayed high Chl-a concentrations and low $p\text{CO}_2$ values on and cross the LA shelf. As a result, this MARS plume acted as a strong sink of CO_2 with respect to the atmosphere. Its extensive area replaced the pelagic region that was usually neutral to the air-sea CO_2 flux with a strong CO_2 sink with

respect to the atmosphere. Furthermore, we also compare the measured and simulated $p\text{CO}_2$ -to-DO relationships by considering effects from biological activities and the following compensation from gas exchanges with a quantitative model. These results also suggest the coherent correspondence between biological transitions on plume trajectory: the biological transition was from net autotrophy to net heterotrophy while the MARS plume trajectory was from eastern to western shelf.

During July 2009, the MARS plume was confined to the eastern Louisiana shelf (Fig. 6.1c, red color), where the cross-shelf component was promoted. This relocation of MARS plume was mostly due to the altered shelf circulation when more southerly winds were observed in July 2009. The comparison results from measured and modeled $p\text{CO}_2$ -to-DO relationships were consistent with this shelf circulation, suggesting more plume associated signals on the eastern shelf and less biological activities on the western shelf. As a result, the LA shelf was shifted from a neutral status to a weak CO_2 source. Additionally, shelf circulations not only affect surface waters but also bottom waters. Bottom brackish waters (salinity lower than 35) and high salinity waters (salinity higher than 35) both were distributed alongshore and were separated by a zone between isobath 10 and 20 m under normal plume distribution in August 2007. But these two water masses were identified to be limited on the eastern shelf in July 2009. The stratification area was also reduced to on the eastern shelf. Therefore, we suggest that the fact that altered shelf circulation relocated of the MARS plume trajectory and reduced the overlap between hypoxia potential and stratification envelope was the major reason that the bottom water hypoxic coverage was much smaller than predicted in July 2009.

3. Association between riverine nitrogen and surface $p\text{CO}_2$ or CO_2 fluxes

The $p\text{CO}_2$ values responded differently to the riverine nitrogen fluxes between in a limited region (the LA Bight) and in a larger region (the LA shelf). The relationship between the air-sea CO_2 fluxes on the LA Bight and the Mississippi riverine NN fluxes were quantified to be with a one-month time lag. This quantitative correlation was not observed over the larger LA shelf, though air-sea CO_2 fluxes was on the coverage of enhanced PP on the LA shelf (area with $p\text{CO}_2$ less than $300 \mu\text{atm}$) and was correlated to MARS NN fluxes with a 1- to 1.5-month lag. These two relationships were observed when the MARS plumes were distributed alongshore to the north of 28°N . This different response of $p\text{CO}_2$ variation was consistent with our previous interpretation of the $p\text{CO}_2$ -to-DO relationship over the LA shelf, indicating more autotrophy on the eastern shelf and more heterotrophy on the western shelf. The complex CO_2 drawdown/release controlled by biological activities thus reduces the correlation between nitrogen flux and its induced low $p\text{CO}_2$ values. Furthermore, the effect of the compensation of air-sea gas exchange became more important when the response time of the $p\text{CO}_2$ to the nitrogen flux was increased, i.e. on the “downstream” western shelf or called “far-field.”

When the MARS plume was relocated to other type of distribution, they behaved differently from those alongshore plume in responding to riverine nitrogen fluxes, such as in March 2010, July 2009, and October 2005. Based on the importance of freshwater distribution and riverine nitrogen fluxes in CO_2 variations over the LA shelf, we suggested that air-sea CO_2 fluxes on large-river dominated shelves were largely related to anthropogenic nitrogen exports and regional weather events.

4. Integration of the interactions between river-to-sea and air-to-sea fluxes

To draw conclusions on the physical and biogeochemical controls on sea surface CO₂ dynamics and distribution on a large river-dominated shelf: first, the river-to-sea associated processes, mostly mixing and biological activities, dominated the *p*CO₂ variation along the salinity gradient while air-sea gas exchanges compensate this *p*CO₂ variation. Second, the coverage of river plume controlled *p*CO₂ spatial variation while local wind forcing largely controlled the distribution of this river plume. We proposed a conceptual model to show the integrated interactions (Fig. 6.1). When the MARS plume was narrow-alongshore distribution, the riverine nitrogen flux was negatively correlated to the surface *p*CO₂ values in the autotrophic activities dominated region of the plume (Fig. 6.1d). But such positively correlated relationship was changed when the distributions of MARS plume was different from narrow-alongshore distribution. When the plume covered a wider area on the LA shelf, the LA shelf acted as a stronger sink (Fig. 6.1c). But when the plume drifted southeastward and covered less area on the LA shelf, the LA shelf acted as a weaker sink or even a source of CO₂ (Fig. 6.1c). We suggest that regional weather might affect the efficiency of this relationship between riverine nitrogen flux and CO₂ fluxes in autotrophic region on the LA shelf, i.e., weaken or enhanced the effect of the riverine nitrogen flux on the LA shelf. Through the effects of wind forcing on shelf circulations, regional climate change might be important to the distribution of coastal biogeochemical process.

Future studies could focus on the following topics: first, the effect of physical exchange and the associated biogeochemical processes on water column CO₂ dynamics 1) between bays and shelf and 2) between shelf and pelagic gulf; second, the effect of climate change through local wind forcing and the plume trajectory on biogeochemical processes on the shelves.

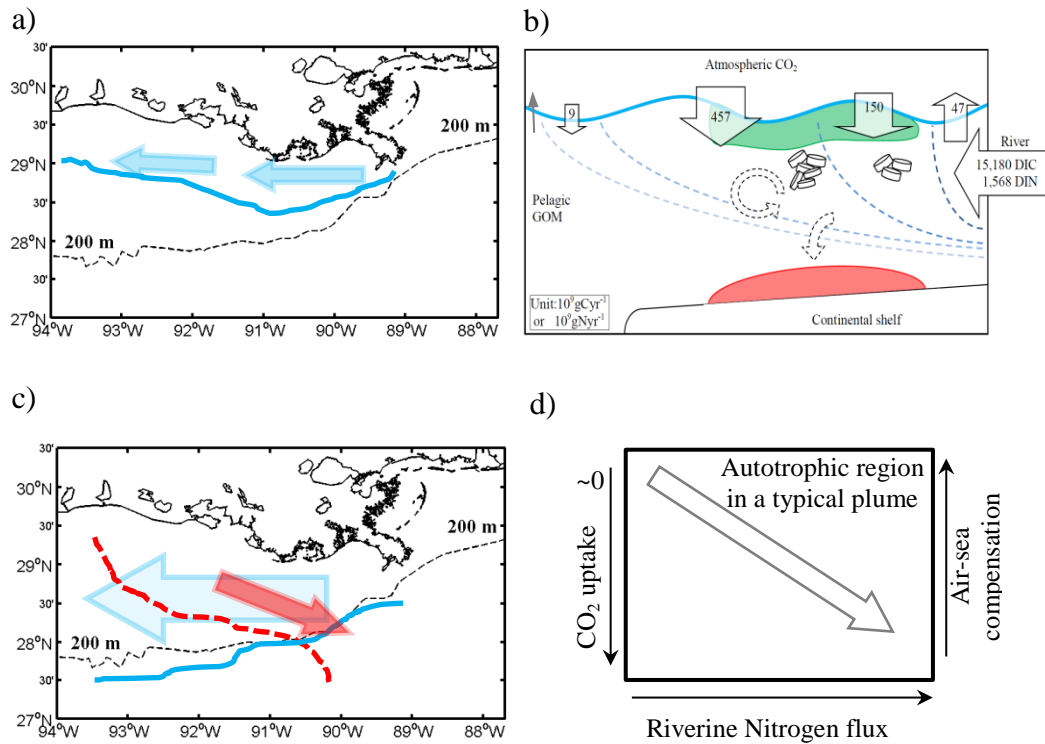


Figure 6.1. Conceptual model synthesizing the interactions between river-to-sea and air-to-sea related processes. a) The plume distribution under mean weather condition, easterly wind forcing, the blue arrows and lines demonstrate the drifting direction and boundary, respectively; b) the conceptual model for the river-to-sea processes, c) the plume distribution under southerly (red color) or northerly (blue) wind forcing, and d) the conceptual relationship between the riverine nitrogen flux and the $p\text{CO}_2$ values in the autotrophic biological activities dominated region in a typical large river plume (i.e., alongshore for the MARS plume).

APPENDIX A

ASSESSMENT OF SAMPLE STORAGE TECHNIQUES FOR TOTAL ALKALINITY AND
DISSOLVED INORGANIC CARBON IN SEAWATER¹

¹ Wei-Jen Huang, Yongchen Wang, and Wei-Jun Cai. 2012. *Limnology and Oceanography: Methods*. 10: 711-717.

Reprinted here with permission of the publisher.

Abstract

The borosilicate glass bottle sealed with a ground stopper and vacuum grease is a high quality container for preserving seawater samples for total alkalinity (TA) and dissolved inorganic carbon (DIC); it is recommended in the standard methods, even though this bottle is expensive and hard-to-handle. As there is an increased demand for sample storage and transportation by laboratories involved in biological and ocean acidification research, we explore alternative sample storage techniques by testing four types of containers. The results demonstrated that over a period of 47 days, TA values from seawater samples stored in polypropylene (PP) bottles and high density polyethylene (HDPE) bottles were not statistically different from those stored in the benchmark borosilicate glass bottles, both at room or refrigerated temperatures. In addition, DIC concentrations from a seawater sample stored in soda-lime glass bottles and small volume borosilicate glass vials with screw caps were not statistically different from those stored in the borosilicate glass bottles over at least 148 days. However, the TA value of seawater stored in soda-lime glass bottles increased significantly with increasing storage time, indicating that this type of soft glass bottle is not suitable for TA sample storage. Therefore, we suggest that PP or HDPE bottles can be used for TA sample storage and small volume borosilicate glass vials with screw caps can be used for DIC sample storage for a period of at least 1.5 months. These storage containers provide economical and easy-to-transport alternatives to the recommended high-quality borosilicate glass bottles.

Introduction

Total alkalinity (TA) and dissolved inorganic carbon (DIC) are two important parameters in oceanic carbon cycle research (Broecker and Peng 1982; Cai et al. 2010; Chen and Pytkowicz 1979; Dickson 1981; Dickson 1992; Lee et al. 2006). TA of a natural water is defined as the number of mole of hydrogen ion equivalent to the excess of proton acceptors (bases formed from weak acid with a dissociation constant $K \leq 10^{-4.5}$ at 25 °C and zero ionic strength) over proton donors (acids with $K > 10^{-4.5}$) in one kilogram of sample (Dickson, 1981) and is commonly expressed as:

$$\text{TA} = [\text{HCO}_3^-] + 2[\text{CO}_3^{2-}] + [\text{B}(\text{OH})_4^-] + [\text{OH}^-] + [\text{HPO}_4^{2-}] + 2[\text{PO}_4^{3-}] + [\text{SiO}(\text{OH})_3^-] + [\text{NH}_3] + [\text{HS}^-] - [\text{H}^+] - [\text{HSO}_4^-] - [\text{HF}] - [\text{H}_3\text{PO}_4]$$

And DIC is defined as:

$$\text{DIC} = [\text{CO}_2^*] + [\text{HCO}_3^-] + [\text{CO}_3^{2-}]$$

where CO_2^* includes all forms of molecular carbon dioxide.

TA is quantified with a Gran titration (Gran 1952) and has been modified for an open cell titration method quantified with nonlinear least-squares calculation (Dickson et al. 2003). DIC is commonly measured by acidifying a known volume of water to release CO_2 which is then absorbed into an organic base solution and titrated with a colorimetric detector (Johnson et al. 1987), or which is quantified with an infrared detector (DOE 1994; Goyet and Snover 1993). In order to control the quality of TA and DIC analysis worldwide, certified reference materials (CRMs) have been developed (Dickson et al. 2003) and stored in high-quality borosilicate narrow-neck ground-stopper glass bottles that are sealed by high quality vacuum grease (Apiezon , L-Grease). The borosilicate bottle has also been used for preserving “Tris”

(tris[hydroxymethyl]aminomethane) buffers (Nemzer and Dickson 2005) and has been suggested to be the best container for TA and DIC sample storage (Dickson et al. 2007).

Seawater TA and DIC samples usually need to be preserved and stored for later analysis for two reasons. First, due to limitations on research vessels, in particular on small boats, water samples are often preserved onboard and returned home for later analysis. Second, due to increased research needs in coastal carbon cycle and ocean acidification studies, water samples are often collected by researchers with various backgrounds and shipped to laboratories with appropriate expertise to be analyzed. However, the recommended borosilicate bottles are expensive and need to be packed well for transportation. The ground-glass stopper requires being sealed with high quality vacuum grease and fixed with a rubber band and a hose clamp. Although high density polyethylene (HDPE) bottles have been also suggested as a container for TA samples during earlier work (Schock and Schock 1982), no comparison between these two types of bottles has been documented. Therefore, the purposes of this paper are: 1) to find convenient and low-cost alternatives to the borosilicate bottle for TA and DIC sample storage by comparing the difference of TA and DIC values of seawater stored in various types of containers to that in borosilicate glass bottles, and 2) to examine whether refrigerated conditions help the storage of TA samples.

Materials and Procedures

To examine storage effects on seawater TA and DIC values, we compared four types of containers to the borosilicate glass bottle recommended in the best practices report over time (DOE 1994). The benchmark container was the recommended narrow-neck, borosilicate glass bottle (Corning Pyrex 7789, Fisher catalog # 02-940C, 250 ml, USP Type 1 borosilicate glass,

ASTM glass Type 1, low expansion coefficient) with a ground-glass stopper (Table 1). Grease (Apiezon , L-Grease) was applied to the surface of the ground-glass stopper to ensure an air-tight seal (DOE 1994); a plastic hose clamp (Cole-Parmer , 2.36 cm × 2.72 cm) and a rubber band (Alliance , 5.9 cm long × 2.5 cm wide) were used to fasten this stopper to the bottle body. The four types of bottles to be evaluated were (Table 1): narrow-mouth soda-lime glass bottles with screw caps (Wheaton 800 glass, 250 ml, USP Type III soda-lime glass), polypropylene (PP) bottles (Fisher catalog # 02-925C, 125 ml), HDPE bottles (Fisher catalog # 02-924-5A, 125 ml), and borosilicate glass vials (60 ml) with screw caps (Teflon PTFE-lined). Although PP and HDPE bottles are CO₂ permeable, air-water CO₂ exchange did not affect TA values (Dickson 1981) as long as it did not lead to CaCO₃ precipitation. The glass bottles were prepared by burning off organic carbon in a 500 °C muffle furnace for 30 minutes, then rinsing with deionized (DI) water and drying at room temperature. PP and HDPE bottles were cleaned by a method similar to the cleaning of sampling bottles for inorganic nutrients; i.e., they were rinsed with DI water, soaked in a 1 N HCl solution for ~24 hrs, rinsed and soaked again in DI water for another 24 hrs, and then dried in cool air (Dore et al. 1996).

These TA and DIC sample-storage comparison experiments followed the same sampling procedure: seawater was transferred from a Niskin bottle to a 20 L carboy (Nalgene , a HDPE container with a PP screw cap). After shaking the carboy thoroughly, the seawater was sampled into the test bottles by the procedure described in DOE (1994). 100 or 50 µl saturated HgCl₂ solution was added into each test bottle in this study (250 or 120 ml, respectively). The air-tight seals of the ground-glass stoppers were checked by visual examinations; air-tight seals of screw caps were checked with extra care. In the following paragraphs, we describe storage comparison experiments separately for TA and DIC.

The TA storage comparison included three experiments. The first TA experiment (TA Exp. 1) compared the TA variation of samples stored in soda-lime glass bottles to those stored in borosilicate glass bottles. We used 12 bottles of each kind (total 24 samples) to store surface seawater collected from the northern Gulf of Mexico. This surface water of salinity 36 was not filtered because filtration is not necessary when measuring high salinity TA seawater samples (Chanson and Millero 2007). For each type of bottle, we analyzed duplicate samples on the first and 38th days and single samples on other days, separated by 3- to 8-day intervals over the first 38 days (Fig. A.1). After each measurement, samples were stored in a refrigerator (5-9 °C) until the 48th day. Six of these 12 bottles were relocated to a dark box at room temperature (20- 2 °C) while the others remained in the refrigerator. These bottles, which were at least half filled, were measured for a second time on different days over intervals of 12-25 days from the 48th day to the 95th day of the experiment (Fig. A.1).

TA experiment two (TA Exp. 2) was similar to the first 38 days of TA Exp. 1 (Fig. A.1), but it used salinity 29.0 seawater from the northern Gulf of Mexico that was filtered with a capsule filter (Whatman catalog # 6714-6004, 0.45 µm). The third TA storage experiment (TA Exp. 3) compared PP and HDPE bottles with borosilicate glass bottles filled with seawater (salinity of 34.8) from the South Atlantic Bight. TA Exp. 3 also compared the TA values of seawater in bottles stored in a refrigerator (5-9 °C) with those in a dark box at room temperature (20- 24 °C). We analyzed duplicate samples on the first and 47th day, and measured other samples in PP or HDPE bottles and in borosilicate glass bottles on different days as shown in Fig. A.1 over this period.

TA was measured by the Gran titration (Gran 1952) using the open cell method with a semi-automatic titration system (AS-ALK2, Apollo Scitech), consisting of two KloehnTM syringe

pumps (module #50300) of 1 mL and 25 mL respectively, a pH meter (AR15, Accumet Research), and a ROSS combination pH glass electrode (Orion 8102BN, Thermo Scientific). Throughout the entire experiment, the TA samples, the HCl solution, and the syringes of the KloehnTM pumps were all water-jacketed at 25 ± 0.1 °C maintained by a thermal bath (VWR Scientific Product). Tygon tubing (R-3603) was used to transfer solutions between these containers. For each measurement, 25 ml of TA sample was titrated with an HCl solution (0.1 M HCl and 0.5 M NaCl). This TA titration system has a precision of better than 0.1 % (Cai et al. 2010). All the TA values were directly measured with reference to two batches of CRMs (#99 and 104). Opened CRM bottles were stored in the refrigerator and the solutions were discarded after a half month to ensure the quality of CRMs. We also adopted two measurements to ensure the stability and reproducibility of the TA analysis over these time periods. First, opened and stored bottles from these three batches of CRMs (#92, 99 and 104) were crosschecked for accuracy and stability by referencing to other newly opened CRMs (accuracy < 0.1 %). As our purpose is to compare the difference between varying types of bottles, these CRMs provided a robust reference to achieve this goal. Second, by repeat analysis of seawater samples stored in the borosilicate bottles over a long period, the reproducibility of the analytical method was ensured.

The DIC storage experiment compared soda-lime glass bottles and screw-capped small borosilicate glass vials (60 mL) with the benchmark borosilicate glass bottles. Seawater was sampled from the South Atlantic Bight and the sampling method was the same as in the TA storage experiments. All DIC samples were stored in a refrigerator before analysis. On the day of measurement, DIC samples were allowed to warm up at room temperature which was also monitored and recorded during the measuring process. DIC was measured using a DIC analyzer

(AS-C2, Apollo Scitech), consisting of a KloehnTM syringe pump (module #50300) with a 2.5 mL syringe. Seawater samples (0.5 mL) were acidified by adding 0.5 mL 10 % H₃PO₄, and the released CO₂ was subsequently quantified by a nondispersive infrared CO₂ detector (LI-COR , LI-6262). The method has a precision of 0.1 %. All DIC values were directly measured with reference to CRMs (#99, 104, and 106). A newly opened CRM was used on each day of DIC measurement and was stored in the refrigerator after the measurement. This stored bottle of CRM was used to crosscheck the accuracy of measurements by comparing with other newly opened bottles thereafter. The accuracy of the DIC analysis was assessed with the difference between the measured CRM value and the certified CRM value. Therefore, the measurement accuracy was determined using one or more bottles of CRMs from different batches. Again, this approach serves our purpose of evaluating the difference between varying types of sample storage vessels sufficiently.

In each experiment, the mean TA or DIC value from samples stored in the borosilicate glass bottles during this period of time was treated as the benchmark value. Therefore, we evaluated the change of TA or DIC (ΔC) by subtracting this benchmark value from each TA or DIC value of a test sample. For each type of test bottles, its mean ΔC and standard deviation over course of the study were also calculated from each experiment. Finally, we compared the mean ΔC of the test bottles to the one from the borosilicate glass bottles by the statistical method described in SOP 23 of DOE (1994).

Results and Assessment

TA sample storage

These three sets of storage experiments in the borosilicate glass bottles generated the same standard deviation of ΔTA of $2.2 \mu\text{mol kg}^{-1}$ from 18 measurements during TA Exp. 1 (95 days), 12 measurements during TA Exp. 2 (38 days), and 6 measurements during TA Exp. 3 (47 days), respectively. These results confirmed that the borosilicate glass bottles have no noticeable effect on seawater sample storage for TA analysis and also reflected the high precision and reproducibility of this TA analysis method over these time periods (Fig. A.2, Table 2). However, the difference in TA values between seawater samples stored in all soda-lime glass bottles and those in borosilicate glass bottles increased with time (Fig. A.3, Table 2), yielding a statistically significant difference in the mean ΔTA (*t*-test, $t = 2.000$, $df = 58$, $p > 0.05$). According to the manufacturer's description, the soda-lime glass contained lower silicate and higher Na_2O and K_2O , and had a lower soft point than the borosilicate glass. Such different glass composition and properties of the soda-lime glass might cause the increase of samples' TA values over time. This increasing TA result was consistent with the finding of a leached glass layer depleted in Na on the inner surface of an empty soda-lime glass bottle after being stored for 12 months (Chopin et al. 2008; Verit et al. 2009).

The mean ΔTA values were 0.9 ± 2.3 and $1.3 \pm 2.6 \mu\text{mol kg}^{-1}$ in seawater samples stored in the HDPE and PP bottles in the refrigerator ($5\text{-}9^\circ\text{C}$), respectively, while they were -0.3 ± 3.7 and $0.7 \pm 2.9 \mu\text{mol kg}^{-1}$ from samples stored in the HDPE and PP bottles at room temperature (20 to 24°C) over 47 days (Fig. A.4, Table 2). There was no statistical difference in mean ΔTA between samples stored in the plastic bottles and in the benchmark borosilicate glass bottles (for PP or HDPE samples in the refrigerator, *t*-test, $t = 2.120$, $df = 16$, $p < 0.05$; for PP or HDPE in

the room, t -test, $t = 2.306$, $df = 8$, $p < 0.05$), nor was there a statistical difference between samples stored in the refrigerator and at room temperature (for PP or HDPE, t -test, $t = 2.145$, $df = 14$, $p < 0.05$).

DIC sample storage

The standard deviation of seven Δ DIC values of samples stored in borosilicate glass bottles was $1.5 \mu\text{mol kg}^{-1}$ over 148 days except for one outlier on the first day (Fig. A.5, Table 3). This result confirmed that the borosilicate glass bottles had no effect on seawater DIC sample storage, and it also reflected the high precision and reproducibility of this DIC analytical method during this time period. The difference in DIC concentrations between seawater samples stored in the small borosilicate glass vials and in the benchmark borosilicate glass bottles yielded a mean Δ DIC of $-0.5 \pm 0.8 \mu\text{mol kg}^{-1}$; the difference between samples stored in the soda-lime glass bottles and in the borosilicate glass bottles yielded a mean Δ DIC of $-0.3 \pm 1.2 \mu\text{mol kg}^{-1}$ (Table 3). These results indicated that there was no statistically significant difference for Δ DIC among the samples stored in these three glass containers over 148 days (for soda-lime and borosilicate bottles, t -test, $t = 2.160$, $df = 13$, $p < 0.05$; for borosilicate vials and bottles, t -test, $t = 2.179$, $df = 12$, $p < 0.05$). This result excluded two outliers on the first day (the borosilicate glass bottle) and 21st day (the borosilicate glass vial), which were probably caused by contamination during the sampling or measuring process (Fig. A.5).

Comments and recommendations

The results of this study indicate that there was no difference in TA value between samples stored in HDPE (and PP) bottles and borosilicate glass bottles over a period of at least 47 days. The results also showed no difference between TA samples stored at room temperature

and in a refrigerator. In contrast, TA samples stored in soda-lime glass bottles could be compromised (i.e. 10-20 $\mu\text{mol kg}^{-1}$ higher). In addition, this study illustrated that there was no difference in DIC concentration between samples stored in borosilicate glass vials (also soda-lime glass bottles) and samples stored in the benchmark borosilicate glass bottles over a period of 148 days.

To properly apply these results, five caveats should be taken into consideration. First, as displayed in the results, the preservation time of these samples was limited. Second, this study was analyzed with a stable reproducibility of precision of 0.1 %. Third, the samples were stored in less disturbed environments (such as in dark boxes or refrigerators). Fourth, the air-tight between the cap and the bottle was critical to ensure data quality. Finally, this study was directly referenced to CRMs preserved in borosilicate glass bottles for CRMs have been broadly adopted (Dickson et al. 2003) and borosilicate glass bottles are recommended by the SOP of DOE (1994).

Among various carbon cycling research, including method developments (Chanson and Millero 2007; Dickson et al. 2003; Martz et al. 2006) and field work studies (Cai et al. 2010; Feely et al. 2001; Watanabe et al. 2006), borosilicate glass bottles have provided stable storage for both TA and DIC samples, but these bottles are expensive and are less convenient to handle and transport (i.e., the ground stopper needs to be greased and held in place with a rubber band and a hose clamp; the bottles also need a custom packing box for transportation). It would be advantageous to use PP, HDPE, and small borosilicate glass vials when the caveats are taken into consideration because these containers are inexpensive and easy to handle. Additionally, considering packing convenience when the containers need to be shipped, the PP and HDPE bottles are more suitable. The small volume (60 ml) vial also saves storage space and shipping cost. Therefore, our laboratory regularly uses small glass vials (30 ml) for DIC sample collection

in estuarine and coastal waters and during incubation experiments (Jiang et al. 2008). To ensure data quality, we also recommend that TA and DIC measurements should be completed as soon as possible when using this kind of storage method. Consequently, this study suggests that this combination of borosilicate glass vials for DIC and HDPE or PP bottles for TA samples could provide an economical alternative to borosilicate glass bottles.

References

- Broecker, W. S., and T.-H. Peng. 1982. Tracers in the Sea. Lamont-Doherty Geological Observatory.
- Cai, W.-J. and others 2010. Alkalinity distribution in the western North Atlantic Ocean margins. *J. Geophys. Res.* 115: C08014 [doi:10.1029/2009jc005482].
- , and Y. Wang. 1998. The chemistry, fluxes, and sources of carbon dioxide in the estuarine waters of the Satilla and Altamaha Rivers, Georgia. *Limnol. Oceanogr.* 43: 657-668 [doi:10.4319/lo.1998.43.4.0657].
- Chanson, M., and F. J. Millero. 2007. Effect of filtration on the total alkalinity of open-ocean seawater. *Limnol. Oceanogr. Meth.* 5: 293-295 [doi:10.4319/lom.2007.5.293].
- Chen, C.-T. A., and R. M. Pytkowicz. 1979. On the total CO₂-titration alkalinity-oxygen system in the Pacific Ocean. *Nature* 281: 362-365 [doi:10.1038/281362a0].
- Chopinot, M.-H. and others 2008. Soda-lime-silica glass containers: chemical durability and weathering products. *Adv. Mat. Res.* 39-40: 305-310 [doi:10.4028/www.scientific.net/AMR.39-40.305].
- Dickson, A. G. 1981. An exact definition of total alkalinity and a procedure for the estimation of alkalinity and total inorganic carbon from titration data. *Deep-Sea Res.* 28, No.6: 609-623 [doi:10.1016/0198-0149(81)90121-7].
- . 1992. The development of the alkalinity concept in marine chemistry. *Mar. Chem.* **40**: 49-63 [doi:10.1016/0304-4203(92)90047-E].
- , A. G., J. D. Afghan, and G. C. Anderson. 2003. Reference materials for oceanic CO₂ analysis: a method for the certification of total alkalinity. *Mar. Chem.* 80: 185-197 [doi:10.1016/S0304-4203(02)00133-0].

- , A. G., C. L. Sabine, and J. R. Christian. 2007. Guide to best practices for ocean CO₂ measurements. North Pacific Marine Science Organization.
- DOE. 1994. *Handbook of methods for the analysis of the various parameters of the carbon dioxide system in sea water; version 2*. In A. G. Dickson and C. Goyet [eds.].
- Dore, J. E., T. Houlihan, D. V. Hebel, G. Tien, L. Tupas, and D. M. Karl. 1996. Freezing as a method of sample preservation for the analysis of dissolved inorganic nutrients in seawater. *Mar. Chem.* 53: 173-185 [doi:10.1016/0304-4203(96)00004-7].
- Feely, R.A., C.L. Sabine, T. Takahashi, and R. Wanninkhof. 2001. Uptake and storage of carbon dioxide in the ocean: The global CO₂ survey. *Oceanography* 14(4): 18-32 [doi:10.5670/oceanog.2001.03].
- Goyet, C., and A. K. Snover. 1993. High-accuracy measurements of total dissolved inorganic carbon in the ocean: comparison of alternate detection methods. *Mar. Chem.* 44: 235-242 [doi:10.1016/0304-4203(93)90205-3].
- Gran, G. 1952. Determination of the equivalence point in potentiometric titrations. Part II. *Analyst* 77: 661-671 [doi:10.1039/AN9527700661].
- Jiang, L.-Q., W.-J. Cai, and Y. Wang. 2008. A comparative study of carbon dioxide degassing in river- and marine-dominated estuaries. *Limnol. Oceanogr.* 53: 2603-2615 [doi:10.4319/lo.2008.53.6.2603].
- Johnson, K. M., J. M. Sieburth, P. J. L. Williams, and L. Brändström. 1987. Coulometric total carbon dioxide analysis for marine studies: Automation and calibration. *Mar. Chem.* 21: 117-133 [doi:10.1016/0304-4203(87)90033-8].

- Lee, K. and others 2006. Global relationships of total alkalinity with salinity and temperature in surface waters of the world's oceans. *Geophys. Res. Lett.* **33**: L19605 [doi:10.1029/2006gl027207].
- Martz, T. R., A. G. Dickson, and M. D. Degrandpre. 2006. Tracer monitored titrations: Measurement of total alkalinity. *Anal. Chem.* **78**: 1817-1826 [doi: 10.1021/ac0516133].
- Nemzer, B. V., and A. G. Dickson. 2005. The stability and reproducibility of Tris buffers in synthetic seawater. *Mar. Chem.* **96**: 237-242 [doi:10.1016/j.marchem.2005.01.004].
- Schock, M. R., and S. C. Schock. 1982. Effect of container type on pH and alkalinity stability. *Water Res.* **16**: 1455-1464 [doi:10.1016/0043-1354(82)90244-5].
- Verit, M., R. Falcone, G. Sommariva, M. H. Chopinet, and P. Lehu. 2009. Weathering of the inner surface of soda-lime-silica glass containers exposed to the atmosphere. *Glass Technol. - Part A* **50**: 65-70.
- Watanabe, A. and others 2006. Analysis of the seawater CO₂ system in the barrier reef-lagoon system of Palau using total alkalinity-dissolved inorganic carbon diagrams. *Limnol. Oceanogr.* **51**: 1614-1628 [doi:10.4319/lo.2006.51.4.1614].

Table A.1. Summary of the five types of containers.

Type of containers	Borosilicate glass bottle	Soda-lime glass bottle	High density polyethylene bottle	Polypropylene bottle	Borosilicate glass vial
Abbreviation	BG	SG	HDPE	PP	Vial
Brand	Corning 7789	Wheaton 800	Fisher	Fisher	Fisher
Expansion coeff.	32.5×10^{-7} cm cm ⁻¹ °C ⁻¹	88×10^{-7} cm cm ⁻¹ °C ⁻¹	-	-	32.5×10^{-7} cm cm ⁻¹ °C ⁻¹
strain point	510 °C	507 °C	-	-	510 °C
anneal point	560 °C	546 °C	-	-	560 °C
soft point	815 °C	727 °C	-	-	815 °C
Permeability*	-	-	280	90	-
Volume	250 ml	120 ml	120 ml	120 ml	60 ml
Exp. Used	TA, DIC	TA, DIC	TA	TA	DIC
Type and material of caps	Ground-glass stopper	Screw cap lined with Teflon	HDPE screw cap	PP screw cap	Screw cap lined with PTFE (Polytetrafluoro ethylene)

*Unit of permeability at 25 °C: cc-mm s⁻¹ cm⁻² cmHg⁻¹ 10⁻¹⁰

Table A.2. Mean Δ TA for each type of bottle over time in each experiment (units: $\mu\text{mol kg}^{-1}$).

Abbreviation	Salinity	Mean Δ TA	SD	n	days	Exp. #	Storage Location
BG1	36.0	0	2.2	18	95	Exp. 1	Refrigerator
BG2	29.0	0	2.2	12	38	Exp. 2	Refrigerator
BG3	34.8	0	2.2	6	47	Exp. 3	Refrigerator
SG1	36.0	11.6	6.7	18	95	Exp. 1	Refrigerator
SG2	29.0	6.1	2.7	12	38	Exp. 2	Refrigerator
HDPE	34.8	0.9	2.3	12	47	Exp. 3	Refrigerator
HDPE_rm	34.8	-0.3	3.7	4	47	Exp. 3	Room
PP	34.8	1.3	2.6	12	47	Exp. 3	Refrigerator
PP_rm	34.8	0.7	2.9	4	47	Exp. 3	Room

”SD” means standard deviation. “n” represents the number of the TA measurements. Temperature in the refrigerator was ~5 to 9 °C and in the room was ~20 to 24 °C.

Table A.3. Mean Δ DIC concentration and its standard deviation (SD) for each type of containers over 148 day (unit: $\mu\text{mol kg}^{-1}$)

Bottles	Salinity	mean Δ DIC	SD	n
BG_250ml	31.3	0	1.5	8
SG_120ml	31.3	-0.5	0.8	7
Vial_60ml	31.3	-0.3	1.2	6

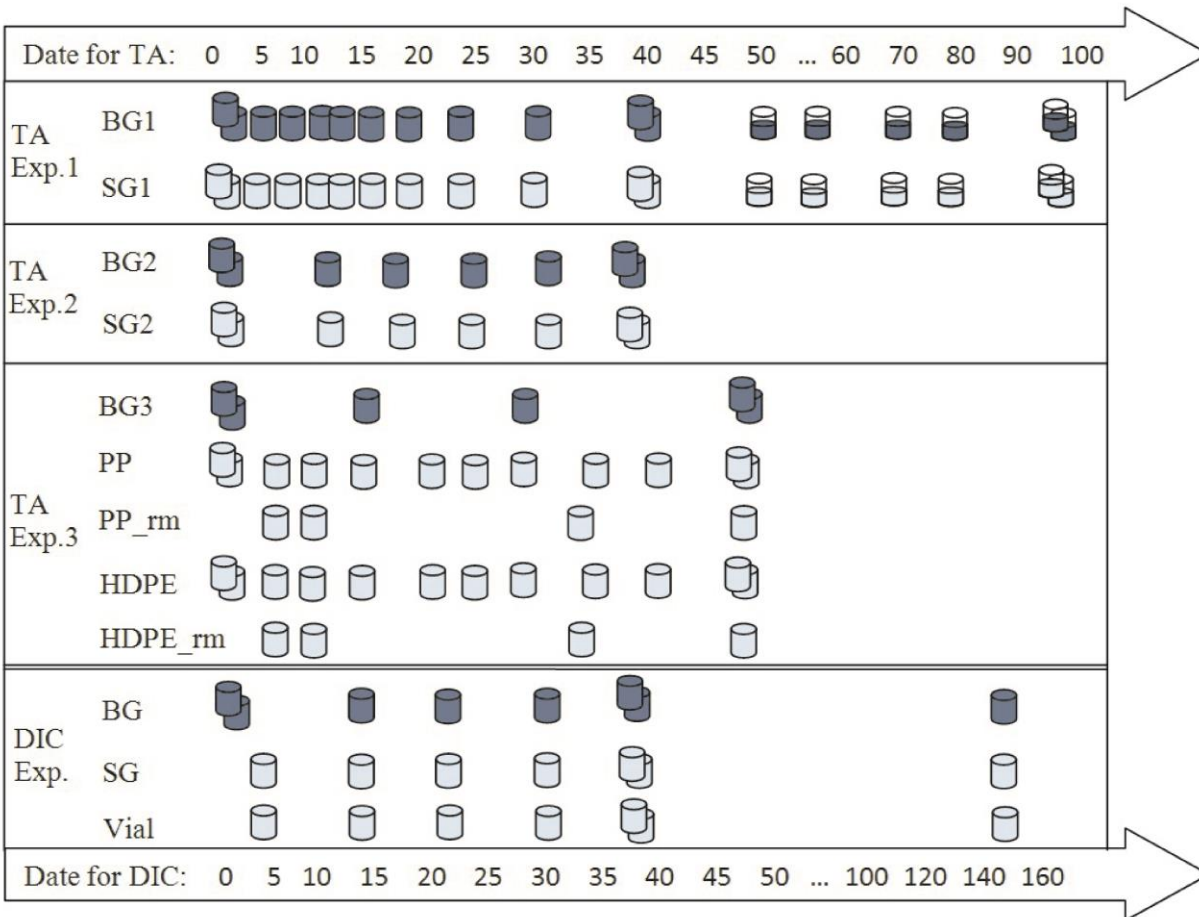


Figure A.1. Summary of measurements for TA and DIC during each experiment along the timeline. Each cylinder symbol represents a TA or DIC measurement on that day. The cylinder with half blank represents the bottle is half filled. “BG” represents the borosilicate glass bottle, “SG” is the soda-lime glass bottle, “PP” is the PP bottle, “HDPE” means the HDPE bottle, and “Vial” is the borosilicate glass vial. The number following each abbreviation indicates the label number of the TA experiment. Samples were stored in a refrigerator (5-9 °C) except that samples of abbreviations ending with “_rm” were stored at room temperature (20-24 °C).

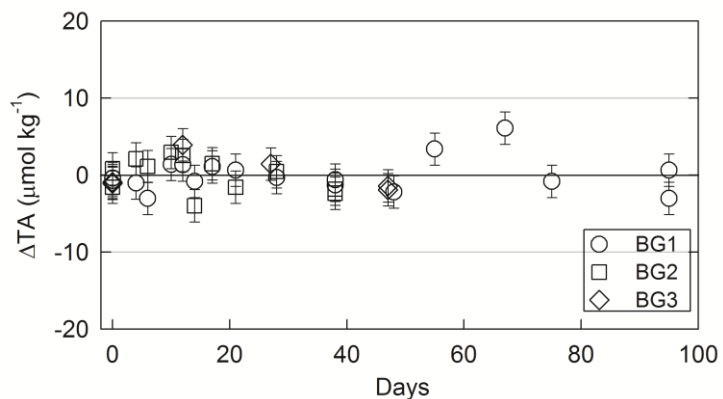


Figure A.2. ΔTA variations for the borosilicate glass bottle samples in TA Exp. 1, 2, and 3 over 95 days. ΔTA is the difference in TA between each tested value and its corresponding mean value (i.e. 2315.3, 2215.2, and 2309.3 $\mu\text{mol kg}^{-1}$ in TA Exp. 1, 2, and 3, respectively.) Open circles (BG1) represent ΔTA of samples stored in the refrigerator in TA Exp. 1. Open squares (BG2) represent samples from TA Exp. 2 and open rhombuses (BG3) are samples from TA Exp. 3. Each error bar shows $\pm 2.3 \mu\text{mol kg}^{-1}$.

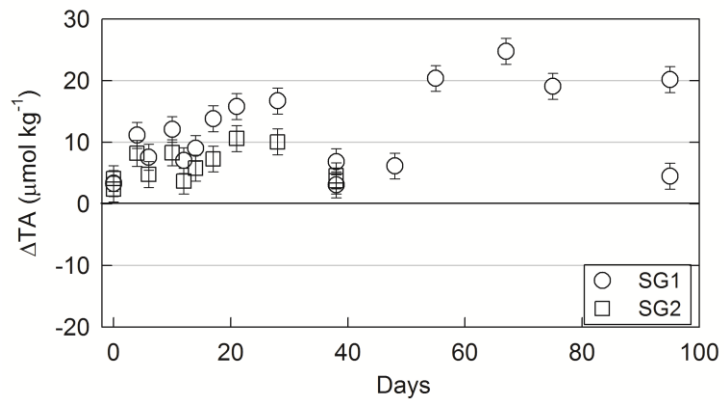


Figure A.3. Δ TA variations for the soda-lime glass bottles used in TA Exp. 1 and 2 over 95 days. Δ TA is the difference in TA between each value from the soda-lime glass bottles and their benchmark value (i.e. mean TA of BG1 or BG2). Open circle (SG1) are samples with salinity 36 in TA Exp. 1. Open squares (SG2) are samples with salinity 29 in TA Exp. 2. Each error bar shows $\pm 2.3 \mu\text{mol kg}^{-1}$.

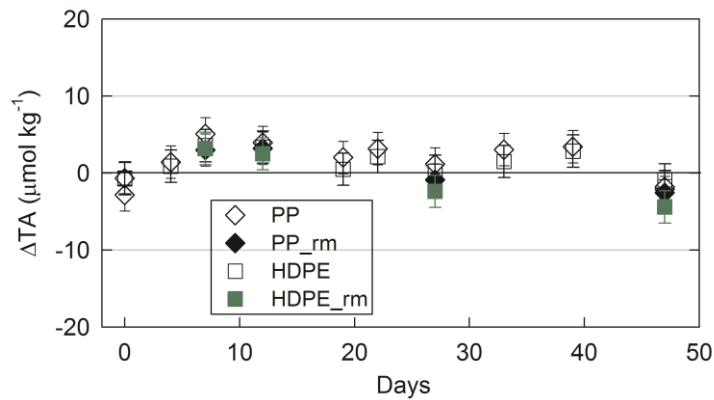


Figure A.4. Δ TA variation for the PP or HDPE bottles in TA Exp. 3 over 47 days. Δ TA is the difference in TA between values from samples stored in HDPE (or PP) bottles and their benchmark value (i.e. mean TA of BG3). Open rhombuses are samples stored in PP bottles and solid rhombuses (PP_rm) are samples stored in PP bottles at room temperature. Open squares (HDPE) are samples stored in HDPE bottles and solid squares (HDPE_rm) are samples stored in HDPE bottles at room temperature. Each error bar shows $\pm 2.3 \mu\text{mol kg}^{-1}$.

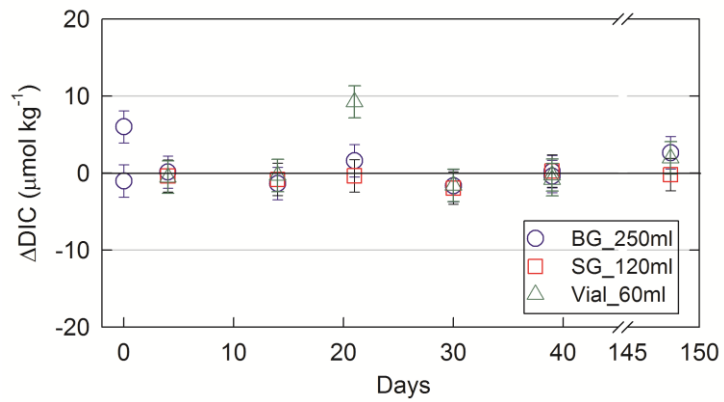


Figure A.5. Δ DIC variations for borosilicate glass bottles, soda-lime glass bottles, and the small volume borosilicate glass vials over 148 days. Δ DIC is the difference in DIC between the values from test bottles and the mean concentration from the borosilicate glass bottles ($2064.2 \mu\text{mol kg}^{-1}$). Each error bar shows $\pm 2.1 \mu\text{mol kg}^{-1}$.